Thermal Management and Humidity Based Prognostics of High-Power LED Packages

Law Thong Kok

Submitted in fulfilment of the requirements for the

Degree of Doctor of Philosophy

School of Engineering
College of Science and Engineering
University of Glasgow

Acknowledgement

I would like to thank the following people for their invaluable help and contributions to this research project, whose support and encouragement in all aspects of this research I could not have done without:

Associate Professor Fannon Lim, University of Glasgow, for his tutorship and providing direction and clarity to the research.

Dr Ronnie Teo, Agency for Science and Technology A*STAR, for his expertise and technical guidance without which this research would not have been accomplished.

The Management of Nanyang Polytechnic, for logistical and financial resources, and giving me this opportunity to embark on this journey of learning.

My family, whose undying patience and support provided me the strength to persevere through the years.

Author's Declaration

I hereby declare that this dissertation is the result of my own work. No part of this dissertation has been submitted for any other degree, diploma or qualification.

.....

Law Thong Kok

June 2019

Abstract

While Light Emitting Diodes (LEDs) hold much potential as the future of lighting, the high junction temperatures generated during usage result in higher than expected degradation rates and premature failures ahead of the expected lifetime. This problem is especially under-addressed under conditions of high humidity, where there has been limited studies and standards to manage humidity based usage. This research provides an analysis of the factors that contribute to high junction temperatures and suggests prognostic techniques to aid in LED thermal management, specifically under humidity stress.

First, this research investigates the effects of current, temperature and humidity on the electrical-optical-thermal (EOT) properties. Temperature rises within an LED because of input stressors which cause heat to build up: the input current, the operating and ambient temperature, and the relative humidity of the environment. Not only is there an accumulation of heat due to these factors that alter the thermal properties, but the electrical and optical characteristics are changed as well. By uncovering specific configurations causing the EOT performance to degrade under stress, better thermal management techniques can be employed.

Second, this research proceeds to quantitatively link the EOT performance degradation to the humidity causal factor. The recent proliferation of LED usage in regions with high humidity has not corresponded with sufficient studies and standards governing LED test and usage under the humidity stressor. This has led to indeterminate use and consequentially, a lack of understanding of humidity based failures. A novel humidity based degradation model (HBDM) is successfully developed to gauge the impact of the humidity stressor by means of an index which is shown to be an effective predictor of colour degradation. This prognostication of the colour shift by the HBDM provides both academia and industry not only with an indicator of the physical degradation but also an assessment of the LED yellow-blue colour rendering stability, a critical application criterion. Using the HBDM parameters as indicators of the state of the LED, the degradation study is expanded in the development of a Distance Measure approach to isolate degraded samples exceeding a specified multivariate boundary. The HBDM and Distance Measure approach serve as powerful prognostic techniques in overall LED thermal management.

Table of Contents

Nomenclature

Greek Symbols

α	Degradation Rate
α_{stress}	Degradation Rate under the Stress Humidity Conditions
α_{use}	Degradation Rate under the Initial Humidity Conditions
ϵ	Capture Cross Section of the Active Layer
μ	Mean
λ	Wavelength
Φ	Luminous Flux Output
Φ_e	Radiant Flux Output
ψ_H	Humidity Index
σ	Standard Deviation
η	Efficiency
η_{conv}	Ratio of the Emitted Power of Light by the LED package to the Power of Light Emitted by the LED Chip
γ	Carrier Density
θ	Humidity Constant

Acronyms

Al	Aluminum
AlN	Aluminum Nitride
A_H	Humidity Acceleration Factor
ANN	Artificial Neural Network
ASME	American Society of Mechanical Engineers
a.u.	Arbitrary Unit

B	Initial Degradation Constant
B_{rad}	Radiative Recombination Coefficient
C	Conventional
CCT	Colour Correlated Temperature
CIE	International Commission on Illumination
COB	Chip-on-Board
CRI	Colour Rendering Index
C-V	Capacitance-Voltage
D	Squared Mahalanobis Distance
DAQ	Data Acquisition
ED	Euclidean Distance
EOT	Electrical-Optical-Thermal
EPTC	Electronics Packaging and Technology Conference
FC	Flip-chip
e	Unit Elementary Charge
d	Thickness of Active Layer
H	Humidity Expression
h	Thickness of Phosphor
HBDM	Humidity Based Degradation Model
IEEE	Institute of Electrical and Electronics Engineers
IES	Illuminating Engineering Society
InGaN	Indium Gallium Nitride
I-V	Current-Voltage
J_D	Electron Current Density
JEDEC	Joint Electron Device Engineering Council

K	Humidity Constant
K_m	Maximum Spectral Luminous Efficacy Normalization Factor
KF	Kalman Filter
L_e	Photon Emission Rate
L_p	Lumen Maintenance Life based on the Percentage of the Initial Lumen Output Maintained p
LED	Light Emitting Diode
Lu	Lutetium
MD	Mahalanobis Distance
MTTF	Mean Time to Failure
N_d	Defect Density
O	Oxygen
P	Power
p	Percentage of the Initial Lumen Output Maintained
pcLED	Phosphor-converted Light Emitting Diode
POF	Physics of Failure
q	Pearson Correlation Variable
r	Pearson Correlation Coefficient
R_s	Series Resistance
RH	Relative Humidity
R_{stress}	Testing Relative Humidity Level
R_{use}	Reference Relative Humidity Level
R_{th}	Thermal Resistance
SEM-EDX	Scanning Electron Microscopy with Energy Dispersive X-ray Spectrometry
SPD	Spectral Power Distribution

SRH	Shockley–Read–Hall
T	Absolute Temperature in Kelvin
t	T-test Statistic
TDMA	Trivariate Distance Measure Approach
TEC	Thermoelectric Cooler
T_{env}	Control Temperature of the Thermoelectric Cooler TEC
TIR	Total Internal Reflection
T_j	Junction Temperature
T_{rise}	Rise in Junction Temperature
V_F	Forward Voltage
$V(\lambda)$	Spectral Luminous Efficiency Function for Photopic Vision
v_{th}	Thermal Velocity of Electrons
YAG:Ce	Yttrium Aluminum Garnet: Cerium
YBR	Yellow-Blue Ratio

List of Figures

List of Tables

Chapter 1

Introduction

1.1 Research Motivation

According to the U.S. Department of Energy, the average energy consumption of Light Emitting Diodes (LEDs) over its life cycle is about one quarter of the incandescent lamp energy consumption [8], which makes it an exciting potential as lighting source of the future. However, LED degradation due to high junction temperatures is the main limiting factor to its widespread adoption [9], and remains a major challenge to be addressed by researchers [10].

The main factors responsible for the degradation of LEDs are the electrical stress, the temperature at which it operates, and the relative humidity of the environment [11], all of which cause a build-up of heat and lead to subsequent damage. The number of humidity related studies are significantly low [11], but with the advent of LED usage in harsher environmental conditions and environments, this is an area of research that should not be overlooked, considering that one fifth of electronic device failures are attributable to humidity [12]. In addition, current test standards do not include the humidity factor, which is particularly crucial for countries with high relative humidity.

The degradation of the LED is primarily categorised into 2 kinds: lumen depreciation and colour shift, both of which result from the inherently high amount of heat accumulation [13]. The colour shift is closely related to lumen depreciation of the LED and is a critical indicator of overall degradation. Additionally, the colour shift is an important attribute where the evaluation depends on the chromaticity maintenance either for the same LED in various applications or various LEDs for the same application. Most literature treat these two characteristics individually [14] even though they should be studied together. The motivation

behind this research is the need to quantitatively link this degradation to its input stressor so as to provide a practical tool for overall thermal management. Accordingly, a humidity based degradation model (HBDM) is developed that indicates the impact of humidity based on a comprehensive study of the effect of all 3 input factors on the electrical, optical and thermal characteristics of the LED. This model is shown to be an effective predictor of colour degradation, providing system integrators, manufacturers and consumers alike not only an indicator of the physical degradation but also an assessment of the LED yellow-blue colour rendering stability. Besides reliability prediction, an approach to issue advance failure warnings via early anomaly detection capability would help to improve future designs and aid in evidence based scheduled maintenance. This need would be fulfilled by a deterministic model based on the performance of key features of the LED. The methodology prescribed offers a cost-effective alternative to the resource-consuming component or functional testing currently used in industry. Used together with the HBDM, the methodology provides effective overall thermal management of LEDs, which may be used also to complement existing solutions to provide LEDs with higher reliability.

1.2 Objectives and Overview

The primary objective of this research is to develop an approach to quantitatively link the degradation of LEDs to the input stressors which induce heat accumulation by comprehensive analyses of the impact of input stressors on the electrical-optical-thermal performance. In the development of a model to serve this purpose, the following objectives are identified to achieve this goal.

1. Develop proper measurement procedures to derive the electrical-optical-thermal (EOT) performance characteristics of the LED, in particular with regard to the temperature control during measurement (Chapter 3).

2. Establish how the inputs of current and temperature affect the EOT performance of LEDs of different Correlated Colour Temperatures (CCT) and packaging architectures, not only to ascertain critical thermal management principles but also to develop a platform upon which the parameters of the model will be based (Chapter 4).

3. Establish how humidity affects the EOT performance of different LEDs and their degradation mechanisms, to provide the failure characteristics in the development of the model (Chapter 5).

4. Develop a humidity based degradation model with the capability to quantitatively indicate the level of moisture incursion and the associated degradation of the correlated colour shift (Chapter 6).

5. Enhance the degradation model with the development of a method to detect LED degradation outliers using key interrelated features to provide the capability of early failure prediction (Chapter 6).

Fig. 1.1 presents an overview of the research plan which is delineated into primarily 3 phases to encompass the above objectives.

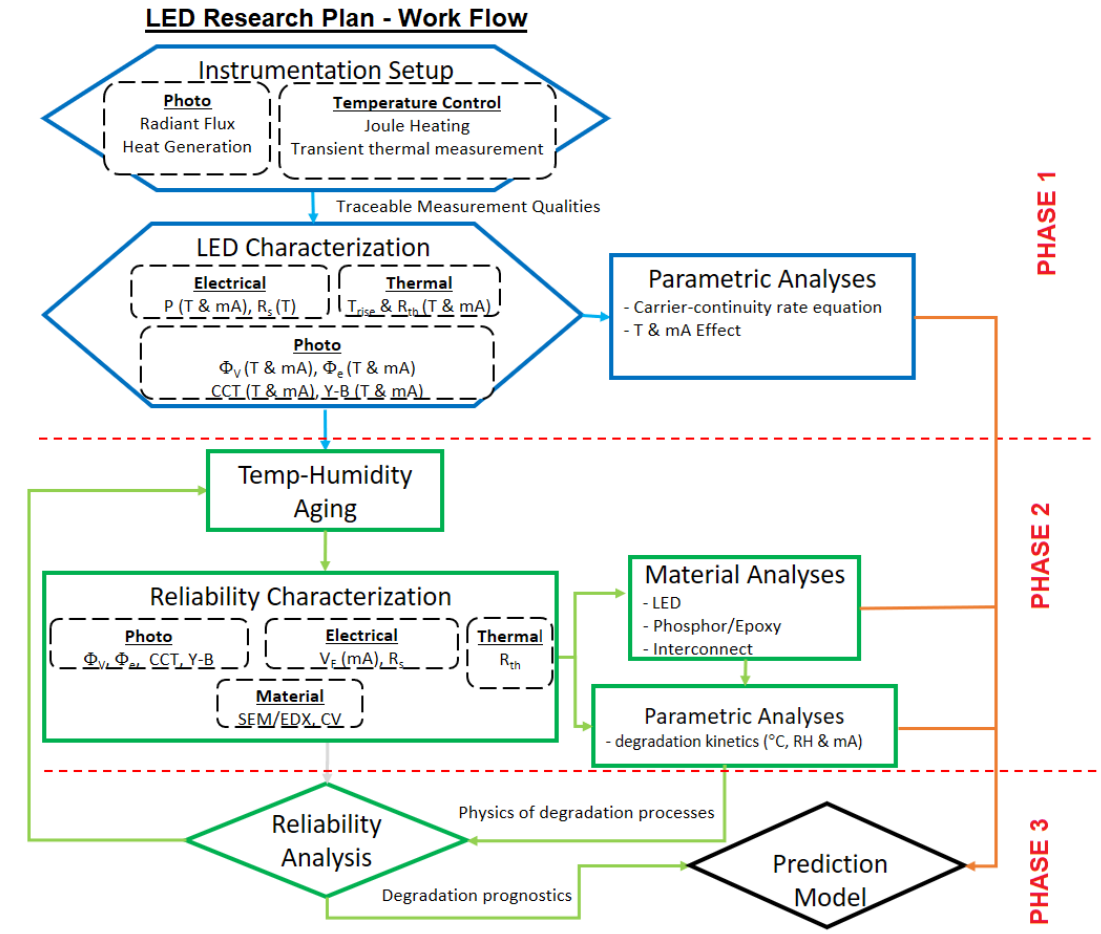

Fig. 1.1. Overview of Research Plan.

Phase 1 work flow corresponds to Chapter 3 and 4, with the following key processes:

1. Establish baseline parametric measurements and process traceability. As the EOT properties of an LED are interlinked with each other, it is crucial that the equipment setup when measuring these properties under varying temperature control is properly established so that there is consistency in all the results.

2. Conduct EOT characterization to investigate properties and performance of the LEDs under test, serving as the starting point for the research.

3. Identify and isolate anomalies either in the test samples or test methodology not previously identified.

4. Investigate the degradation modes under conditions of high current and/or temperature. As the phosphor layer is a key component of LED degradation, particular attention is paid to the impact of current and temperature on the phosphor layer.

Phase 2 work flow corresponds to Chapter 5, with the following key processes:

1. Evaluate the effect of relative humidity on the EOT characteristics of the LED. Degradation characteristics and data is used directly for the development of the model.

2. Conduct failure analysis to analyze the failure mechanism due to the moisture incursion.

Phase 3 work flow corresponds to Chapter 6, with the following key processes:

1. Develop the humidity based degradation model based on the experimental data derived from the previous 2 phases.

2. Establish the rigour of the model with proper validation.

Table 1.1 provides a summary of the major research proceedings in each phase in terms of their intended quantitative and qualitative objectives. While some procedures are conducted concurrently, the activities in subsequent phases depend on the completion of those in the previous phases so that the desired outcome is achieved.

Table 1.1. Quantitative and Qualitative Objectives of the Research by Phase.

Descriptor	**Quantitative Objectives**	**Qualitative Objectives**
Phase 1		
Instrumentation (Chapter 3)	• Instrumentation setup for traceable measurement quantities • Establish t = 0 baseline parametric EOT quantities for subsequent experiments	• Establish correct EOT methodologies and conditions for parametric measurements • Investigate and identify anomalous test conditions
Thermal (Chapter 4)	• EOT parametric measurements at varying operating temperature and currents for 3 types of LEDs: Electrical: P Optical: Φ, Φ_e, CCT, YBR Thermal: T_{rise}, R_{th} • EOT parametric measurements at different operating temperatures for 1 W LEDs at varying CCT levels	• Investigate the impact of packaging on EOT characteristics • Investigate heat dissipation capabilities of bonding configurations
Phase 2		
Reliability (Chapter 5)	• Accelerated Temperature-Humidity Aging Tests to obtain parametric measurements at varying humidity levels and current @1000h intervals: Electrical: I-V, P, R_s Optical: Φ, Φ_e, CCT, YBR Thermal: T_{rise}, R_{th} • SEM-EDX, Impedance (C-V) verification	• Relate EOT reliability degradation behaviour to corresponding failure mechanisms • Investigate reliability heat dissipation capabilities of different packaging
Phase 3		
Model Development (Chapter 6)	• TM-21 based quantification of reliability results to determine degradation parameters α, B • Degradation based humidity parametric computations to develop a humidity index • ΔYBR and R_{th} based profiling for model development	• Establish degradation pattern of the different LEDs via use of experimental model

1.3 Novelty and Contribution

In the course of the research, a number of unique discoveries and novel developments were made. Some of the main novelties and contributions are:

1. A new approach to indicate the lumen degradation of LEDs due to the effects of humidity from which a humidity index was developed as a practical gauge of moisture incursion. The degree of incursion is related to different failure mechanisms which varies across different types and brands of LEDs [15, 16]. A quantitative indication of the amount of incursion serves an analytical function to aid in the distinguishing of the mode or mechanism of failure. The index also easily translates to remaining lifetime, which provides the user with the linkage between the impact of humidity and the lifespan of different LEDs. While several non-humidity based prognostication options exist for LEDs, in particular for remaining lifetime [17], this approach provides a humidity based model useful to both academia and industry. In the LED manufacturing industry, the humidity index developed allows for sub-binning according to different levels of relative humidity instead of being broadly based at a single relative humidity level, giving a higher level of reliability precision catering for markets in different areas of the world with different relative humidity levels. The index allows for stage checking in the binning process and a fast cost-effective means of ranking the quality of the binned LEDs, which would be useful in particular to LED system integrators. The time-dependent nature of the developed model also gives an extra dimension to the manufacturer to predict the long-term behaviour of the LED under specific humidity environments. Such information provided in testing documentation or datasheets allows both system integrators and consumers alike to understand the range of proper operation for different humidity conditions and make the correct LED selection.

2. A novel way to predict the quantitative colour change in terms of the yellow-blue shift caused by a change in humidity levels.

Although colour shift is an important attribute of LED performance, there are currently no standards governing the colour stability [18]. Colour shift varies for different types of LEDs and fluctuate even within LEDs of the same power class [19]. Furthermore, there are relatively few studies on the impact of humidity on colour shift. This research provides a comprehensive analysis of the effect of relative humidity on the critical parameters of LED performance, and provides a direct and effective approach to predict the colour shift from the lumens degradation based humidity index developed in the model. In LED manufacturing, as lumens based binning is relatively straightforward and cheaper, this approach gives a fast and economical alternative to colour based binning, which can be complex and time-consuming [20]. In addition, the methodology may be used to complement existing component and functional testing of LEDs to improve product reliability. This method presents manufacturers, system integrators and consumers a cost-effective verified colour shift prediction system for environments with different relative humidity.

3. A humidity-specific artificial neural network (ANN) simulation of the degradation model using six key degradation attributes.

LED research methodologies in companies are well entrenched and the risk-benefit ratio of new methods may cause reluctance to their introduction, especially given the success of existing methods [21, 22]. As such LED studies using ANNs are almost non-existent in the public domain, especially given the competitive environment and proprietary nature of LED research and developmental methodologies [23-25]. Using the key attributes from the humidity based model developed, the ANN simulation provides a fast and efficient method to demonstrate the results of the prognostication. It also serves as a platform for further enhancement with the variation of input parameters into the model not just for different types of LED and input conditions.

4. A new Trivariate Distance Measure Approach using three interrelated features which provide good indication of the state of the LED.

The results demonstrate that this approach is a more effective gauge of anomalies than using the usual screen test of one or two variables, which are inconsistent and have a high error rate without supplementary statistical evidence [26]. The method also provides a cheaper alternative to expensive hardware in physically detecting outliers in LED manufacturing and binning processes. Unlike conventional statistical methods, this distance measure approach takes into account the covariance and correlation of the variables involved for greater accuracy in outlier detection. Used together with the humidity based model, the approach provides a powerful tool for overall LED health management.

5. A comprehensive analysis of the impact of current and temperature on the efficiency and colour of LEDs with different CCT levels and package configurations, leading to the establishment of important thermal management principles.

Current thermal studies have largely focussed on individual characteristics of the LED impacted by the stressor, usually driven by piecemeal developments in certain areas [27-33]. The analysis presented provides a comprehensive investigation of the thermal impact by current and temperature stressors on different LED configurations, and also depicts the heat accumulation and dissipation profiles of such configurations by different packaging architectures. The analysis contributes a thorough overall understanding of the linkages between various LED configurations and thermal performance, a critical issue when selecting the right LED for specific applications.

6. Discovery of key discrepancies for different temperature feedback systems utilized during thermal measurements which affect the final results.

The widespread use of electrical sweep and transient thermal measurements in both industry and academia [34, 35] point to the importance of proper instrumental setup to ensure accurate

measurements. Even slight deviation can snowball to possibly catastrophic errors leading to the failure of integrated LED products. This investigation presented uncovers hitherto unreported inconsistencies in the routine temperature control settings used during measurements and details the setting changes required to ensure the correct results. Proper control and procedures for different setups are proposed to prevent erroneous measurements being reported in LED data sheets and documents.

1.4 Thesis Organization

The thesis organization correspond to the phases of the research plan of Fig. 1.1 which represent a logical flow of the research.

Chapter 3 presents key findings during instrumentation set-up and design of methodology during the initial stages of Phase 1. Several anomalies involving temperature control were reported during EOT measurements to be taken into account during the experiments conducted subsequently.

Chapter 4 describes the key research findings during Phase 1 experiments to study the thermal response of LEDs to varying input current and operation temperature. Heat accumulation and dissipation characteristics of LEDs with different package configurations and CCTs were investigated with critical thermal management principles established.

Besides the using of current and operating temperature as stressors in Phase 1, long-term exposure to high levels of humidity also induces thermal related degradation in LEDs, and is therefore an important aspect of thermal management. Chapter 5 investigates the impact of long-term humidity effects on LEDs based on their packaging methods, which is the focus of Phase 2.

Chapter 6 brings together the work done in previous phases and closes out Phase 3 with a humidity based degradation model (HBDM) built upon the characterization data from the

lumens degradation data. A practical estimation method from the degradation behaviour is developed to gauge the moisture incursion by means of a novel humidity index. In addition, a Trivariate Distance Measure approach (TDMA) based on the parameters of the HBDM as LED state indicators is developed to isolate LEDs failing a specified degradation threshold.

1.5 List of Publications

Table 1.2 is a list of publications that have been accepted and published as at present. To date, three journal papers have been published, while two conference papers were presented and published, as shown below.

Table 1.2. List of accepted publications.

Journal/ Conference Name	**Article Title**	**Date Published**	**Volume/Issue/ Page**	**URL**
Journal Publications				
IEEE Photonics Journal	A Practical Degradation Based Method to Predict Long-Term Moisture Incursion and Color Change in High Power LEDs	Oct 2018	10/5/1-14	https://ieeexplore.ieee.org/document/8472891
Journal of Electronic Packaging (American Society of Mechanical Engineers ASME)	Effect of Packaging Architecture on the Optical and Thermal Performances of High-Power LEDs	Feb 2017	139/3/031003-1 to 031003-5	http://electronicpackaging.asmedigitalcollection.asme.org/article.aspx?articleid=2607880
IEEE Transactions on Device and Materials Reliability	Implications of Phosphor Coating on the Thermal Characteristics of Phosphor-Converted White LEDs	Aug 2016	16/4/576-582	http://ieeexplore.ieee.org/document/7557080/?reload=true

Conference Publications				
IEEE 18th Electronics Packaging and Technology Conference (EPTC), 2016	Effects of humidity on the electro-optical-thermal characteristics of high-power LEDs	Feb 2017	2016/18/718-723	http://ieeexplore.ieee.org/document/7861576/
IEEE 17th Electronics Packaging and Technology Conference (EPTC), 2015	Achieving accurate electro-optical-thermal measurements of high-power LEDs	Feb 2016	2015/17/1-14	http://ieeexplore.ieee.org/document/7412321/?reload=true&arnumber=7412321

Chapter 2

Literature Review

2.1 The EOT Thermal-Humidity Model

Advances in Gallium Nitride (GaN) based LED technology have led to widespread adoption of high power LEDs for lighting applications. Because lighting makes up about 20% of energy usage in the world [36], a need arises for emerging lighting inventions to enhance energy utilization and yet simultaneously control carbon production. GaN LEDs have the potential to become the light source of the future due to their high luminous efficacy, long expected lifetime and low overall cost of ownership. The relationship between light output and the factors that influence it is a complicated one exemplified by Poppe and Lasance's "Light depends on everything" model [1] (Fig. 2.1). The relationship shows that light and heat output are dependent upon the input current and the operating temperature, with these factors reliant on each other. However, the electrical-optical-thermal (EOT) characteristics of the LED are also affected by reliability conditions such as humidity, which can invoke different mechanisms resulting in higher temperatures and optical losses.

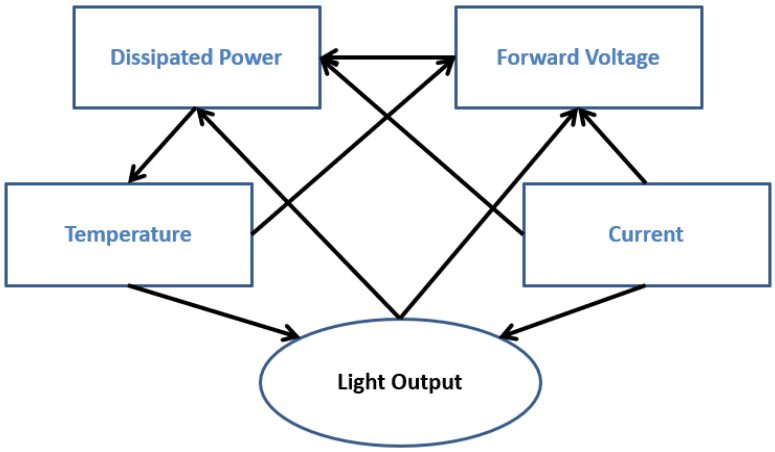

Fig. 2.1. "Light Depends on Everything" Model [1].

Current studies usually separate reliability from thermal research, but for proper thermal management, both thermal and reliability based stressors should be considered. Accordingly, humidity may be treated as a stresssor like temperature and current, with demonstrated interdependence with other parameters in Poppe's model. A model to illustrate the inclusion of humidity as an input factor or stressor to the LED may then be represented in Fig. 2.2.

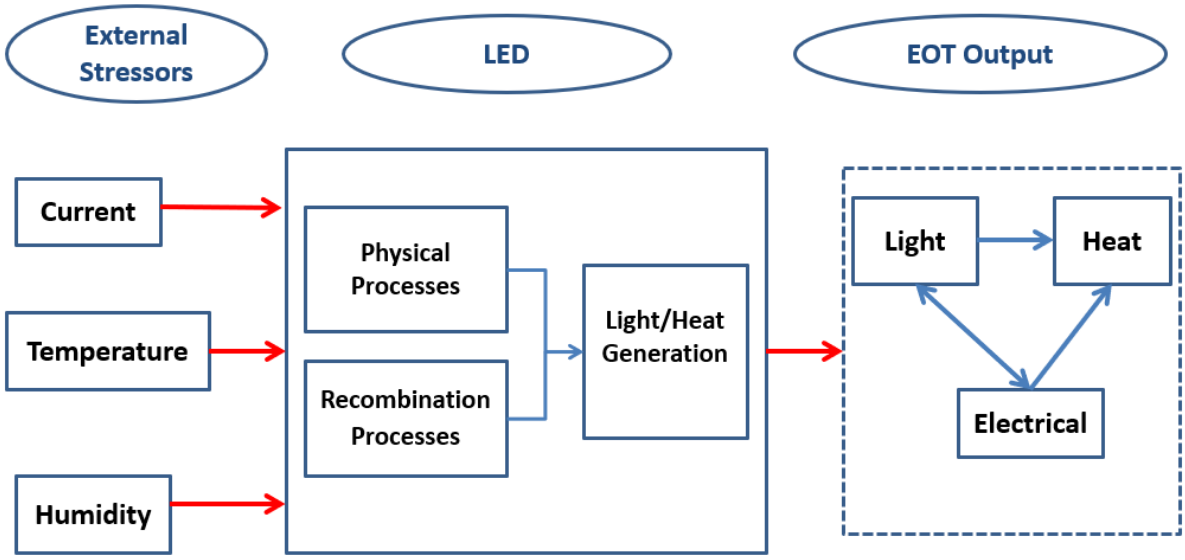

Fig. 2.2. The EOT Thermal-Humidity Model.

The EOT Thermal-Humidity Model (Fig. 2.2) is an input-output based description of the main factors that influence the light output and heat generation in the LED. It is unique as it incorporates the relatively little researched humidity dimension [11] which is not usually included in other thermal models. Along with operating temperature and current, humidity is included as an external stressor to the LED. As the work in Chapter 5 and 6 will show, humidity impacts the EOT output, which can be compared to the time-independent impact of the operating temperature and current (studied in Chapters 3 and 4).

This literature review is organized to address the effect of the stressors of current, temperature and humidity on the LED. Following this, the state of quantitative and qualitative prognosis of LEDs is addressed as a precursor for the HBDM prognostic model presented in Chapter 6.

2.2 Effect of current and temperature

Phosphor converted LEDs (pcLEDs) are manufactured by combining phosphor materials with the chip. As the phosphor medium plays such a key role in determining the electrical, optical and thermal properties of the LED, it is essential to understand its behaviour with different configurations and under different stressors.

The most widely used and commercially available pcLEDs are based on an InGaN LED chip with the Yttrium Aluminum Garnet: Cerium (YAG:Ce) phosphor. The phosphor host emits yellow light (photoluminescence) due to the excitation of blue light (electroluminescence) from the InGaN LED chip, and the mixing of the blue and yellow light produces white light. By altering the properties of the phosphor layer, such as thickness, concentration and location etc, a wide range of CCT (Correlated Colour Temperature) values can be realized. The CCT value is the temperature of a blackbody radiator closest in appearance attempting to use a single number to characterize a full spectrum [2]. In Fig. 2.3, the International Commission on Illumination (CIE) chromaticity diagram depicts the relationship between chromaticity (defined by the xy colour chromaticity coordinate system) and assigned CCT level. This chromaticity system is used extensively as the primary binning scheme by LED manufacturers. The system however does not take into account the impact of variation of input current, operating temperature or relative humidity on colour output, areas that are explored in subsequent chapters, in particular with respect to the role of the phosphor layer (Chapter 4), which is responsible for the colour output of pcLEDs.

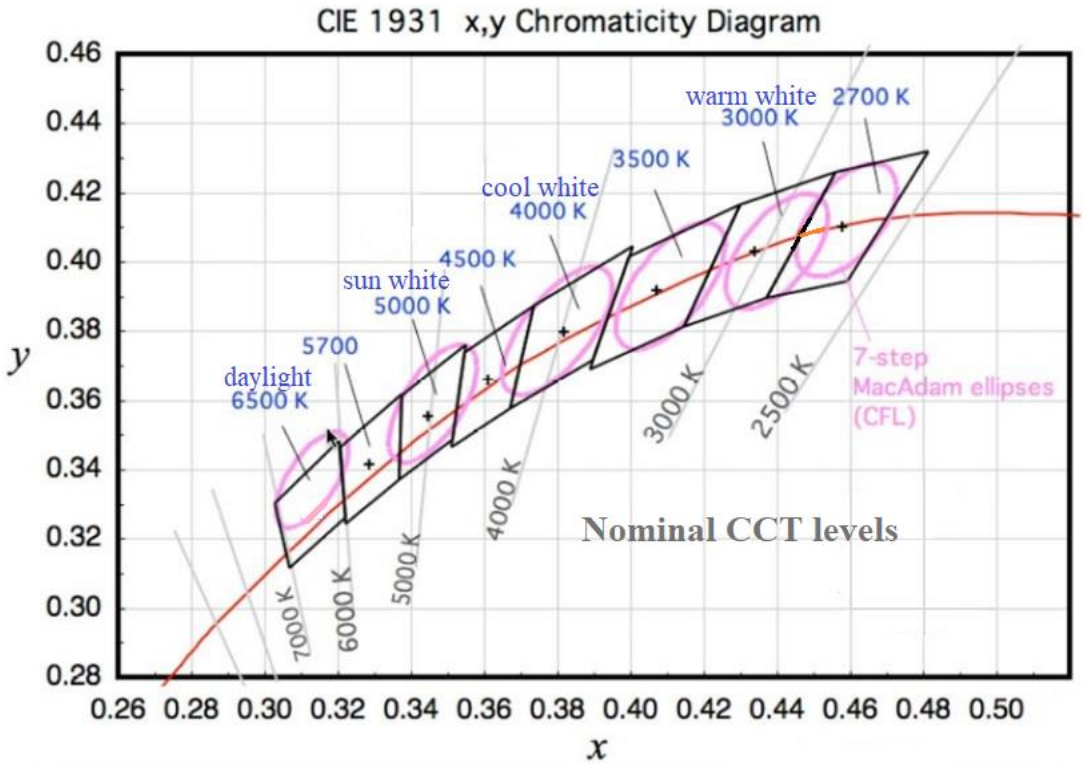

Fig. 2.3. The CIE 1931 Chromaticity Diagram [2] as it relates chromaticity to CCT levels. The x and y coordinate system in this diagram defines the derived parameters for chromaticity in the CIE colour space. The ellipses (MacAdam ellipses) are the regions containing those colours which are indistinguishable to the average human eye from the colour at the center of the ellipse.

The thickness and concentration of the phosphor layer as well as the phosphor particle size are found to strongly influence the luminous efficacy and the colour chromaticity and Colour Rendering Index (CRI) of the light emitted. The CRI is a quantitative measure of the LED's ability to display its colour output in comparison to a given standard. The CRI is calculated from the differences in the chromaticities of eight CIE standard colour samples (CIE 1995 standard) when illuminated by a light source and by a reference illuminant of the same CCT [37]. Tran et al. [3] demonstrated that the lumen output can be improved by regulating the phosphor layer thickness and concentration of the phosphor particles in the phosphor layer. It has been shown that backscattering and back reflection of light within the LED package can

also be minimized by employing optimally sized phosphor particles [4, 38]. With an increase of the phosphor concentration, the CCT output of LED packages decreases because the increased phosphor concentration increases the probability or the amount of blue light being absorbed and correspondingly converted to yellow light, and thus results in a higher yellow-to-blue power ratio and hence lower CCT since yellow light has lower CCT.

As shown in Fig. 2.4(a), the lumen output also decreases with increasing phosphor concentration. As the phosphor concentration increases, there is an associated increase in backscattering and absorption loss by the packaging materials. The absorption loss incurred by this increase in phosphor concentration becomes higher than the positive effect of blue-to-yellow conversion on the luminous efficacy, and the lumen output thus begins to decrease, as demonstrated by Tran et. al [3] .

In terms of phosphor thickness, the package with higher phosphor thickness has higher lumen output than the package with lower phosphor thickness (Fig 2.3(b)). This improvement in lumen output is due to the reduction in optical trapping and an increase in the average distance between the phosphor particles and the LED die. When phosphor thickness increases, the phosphor concentration decreases, thereby obtaining the same CCT value as the package with lower phosphor thickness. Lower phosphor concentration reduces the optical trapping modes of light inside a package by the phosphor particles, especially yellow light, and thus reduces light absorption loss by the packaging materials [39].

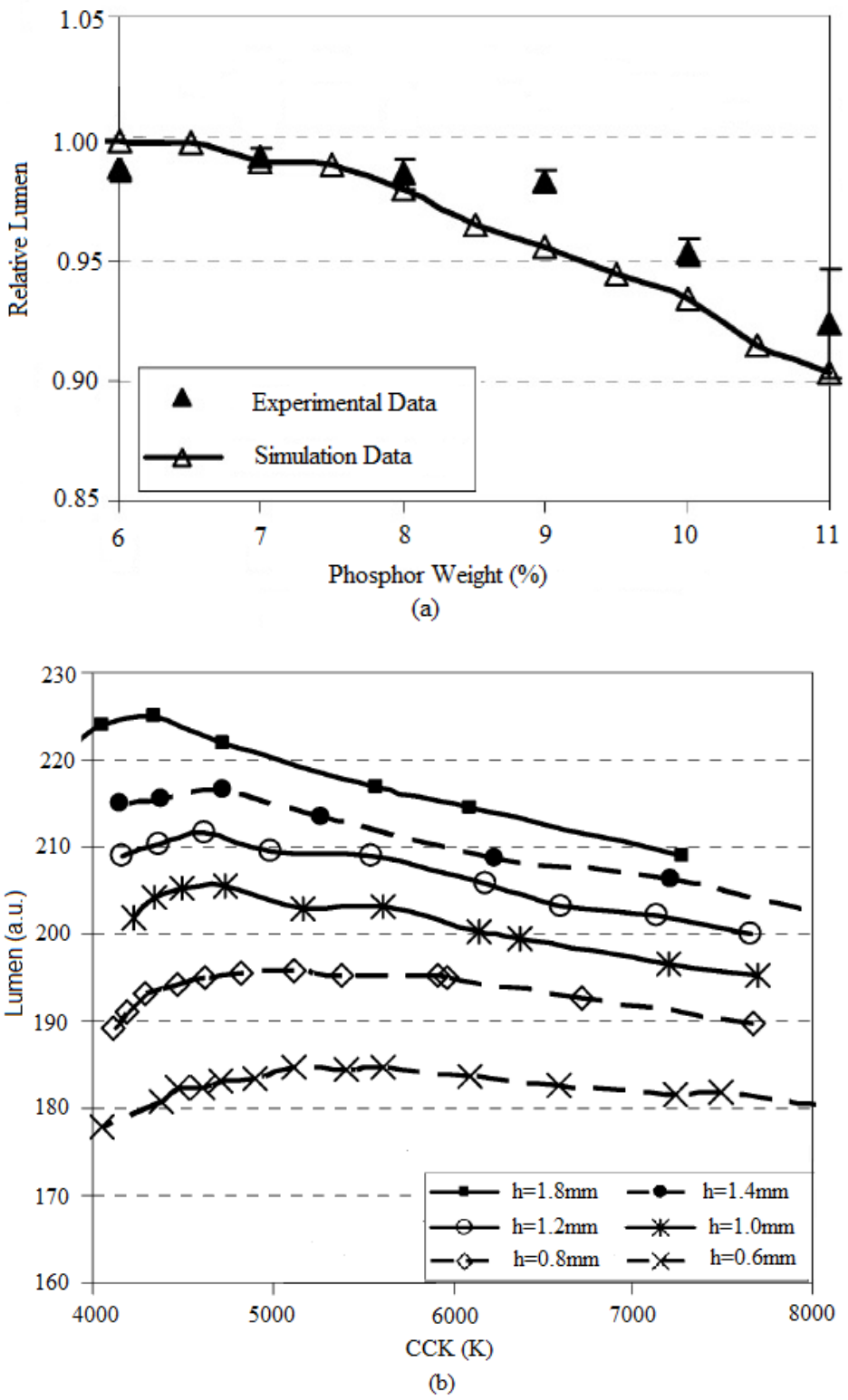

Fig. 2.4. Lumen dependence on (a) phosphor concentration with phosphor thickness h fixed at 0.8 mm, and (b) as a function of CCT and phosphor thickness h [3].

The phosphor particle size affects the scattering intensity and absorption of light within the LED [4]. The scattering intensity distribution of the excitation light and phosphor-emitted light depends on the phase function, which is a function of phosphor size, wavelength, and refractive index of the phosphor particle and the medium. Phosphor particles of different sizes scatter different amount of light with different angular distribution, and a smaller particle size scatters more light than a larger particle size.

As the particle size increases from a nanosize to submicron size, the lumen output decreases. As the particle size continues to increase from the submicron size, the composite becomes more and more transparent to the visible light. The increase in light transparency reduces the trapping efficiency caused by the scattering of particles and the lumen output thus increases as there is more light output and less yellow emission. As shown in Fig. 2.5, the lumen output reaches its maximum value at the particle size of around 20 μm [4].

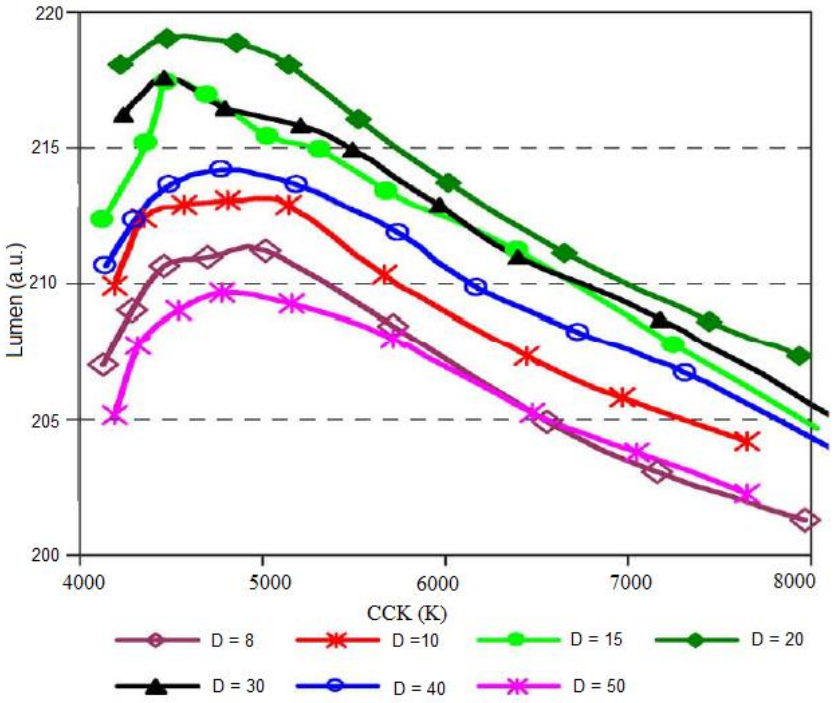

Fig. 2.5. Lumen output of LEDs with different particle sizes [4]. D indicates the diameter of the particles (in μm) only for this figure.

The relative conversion efficiency is the ratio of conversion efficiency to maximum conversion efficiency. The conversion efficiency η_{conv} is defined as the ratio of the emitted power of light by the LED package to the power of light emitted by the LED chip while the maximum conversion efficiency [4] is defined as:

$$\eta_{max\ conv} = \frac{(P_B - P_{Bf}) \times \eta_P + P_{Bf}}{P_B} \tag{2.1}$$

where P_B is the power of light (blue) emitted by the LED chip, P_{Bf} is the power of blue light in the dichromatic white light output of a pc-white LED, and η_P is the conversion efficiency of phosphor material.

To demonstrate this concept in relation to the LEDs used in this thesis, experiments were conducted to extract the relevant parameters under conditions of varying current and temperature for 3 types of LEDs (1 W Philips P1W, 1 W Seoul Semiconductor S1W and 0.3 W Seoul Semiconductor S03W). 5 samples were used for each type of LED to investigate the relative conversion efficiency. Under varying current density, the operating temperature used was 20 °C (Fig. 2.6(a)). Under varying temperature, 350 mA driving input current was applied to both P1W and S1W, while 100 mA driving input current was applied to S03W (Fig. 2.6(b)). The mean relative conversion efficiency $\eta_{conv}/\eta_{max\ conv}$ for all the samples with respect to current density and temperature were computed and plotted in Fig. 2.6. When current is applied to the LED structure, the amount of light emitted from the LED is governed by the carrier continuity model. At a sufficiently high current density where radiative recombination dominates over the non-radiative processes, high external quantum efficiency is observed. As the drive current increases, the accompanying device self-heating effect leads to a higher amount of non-radiative recombination processes. This causes the external quantum efficiency to reduce with current density.

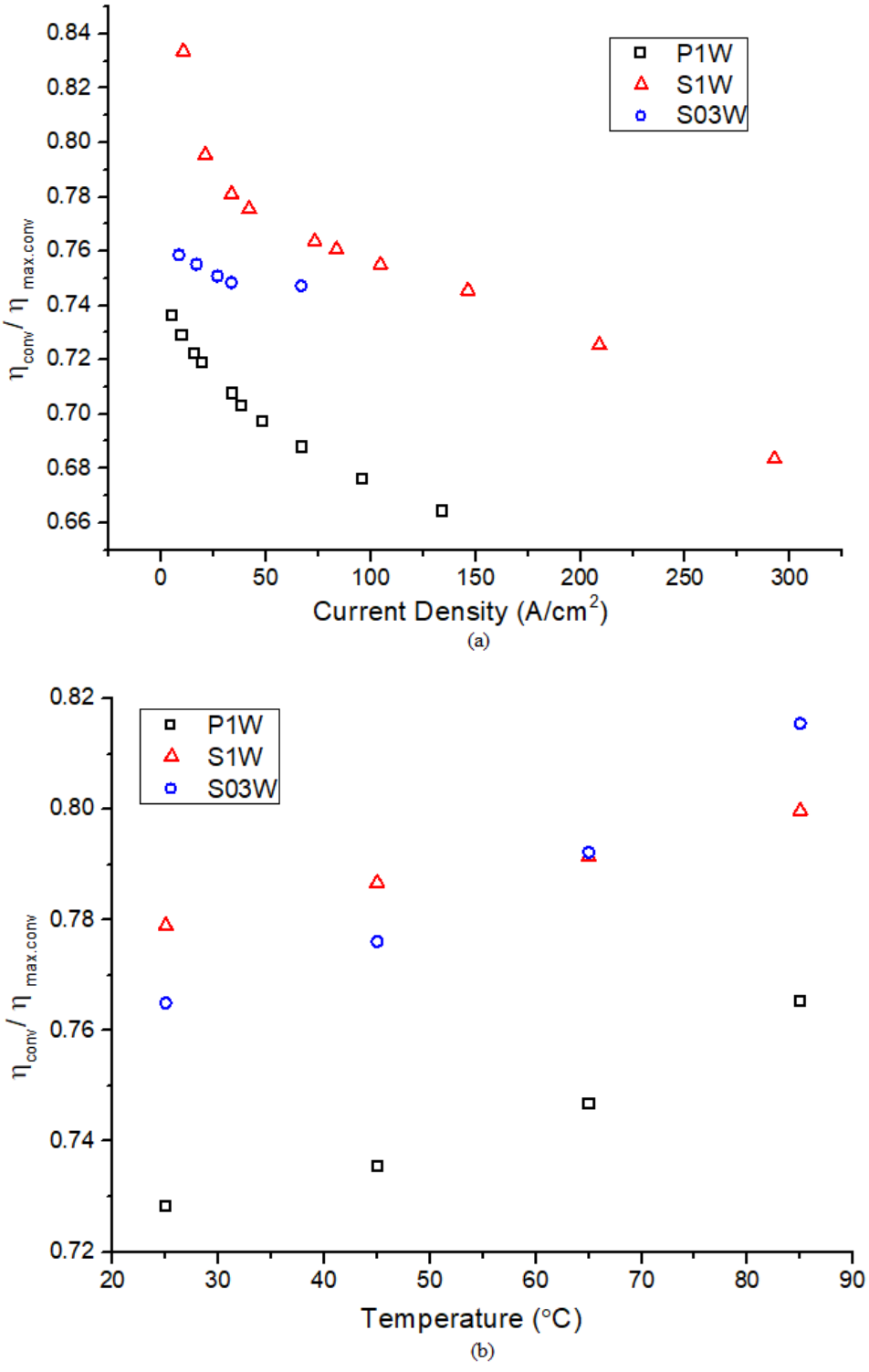

Fig. 2.6. Relative conversion efficiency for P1W, S1W and S03W, (a) as a function of current density and (b) as a function of temperature. Data points represent the average (mean) relative conversion efficiency of all samples tested.

On the other hand, the relative efficiency is seen to increase with higher operating temperature. The radiant flux for all 3 LEDs decreases with increasing temperature but the rate of decrease is less than that of the relative conversion efficiency with temperature. As such, the overall relative efficiency is seen to increase in spite of the reduced phosphor conversion efficiency with temperature.

A gap in LED research studies exists for the comprehensive analysis of the behaviour of different phosphor configurations under both temperature and current stress. In Chapter 4, LEDs with different phosphor configurations and die-bonding architectures are compared in relation to CCT levels for insights into the role of the phosphor in the EOT characteristics.

The optical losses bring upon the implication of phosphor self-heating effect [40-43] which may exacerbate the package's thermal load and as a result, reduce the optical light output further. Huang and Yang [40] have shown that 25% to 45% of the radiant energy emitted from the LED chip is lost as heat during the process of down converting high energy blue light into relatively lower energy yellow light. The heat generated by the phosphor particles not only increase the junction temperature of the LED device, but may also cause phosphor quenching. This will inevitably lower the optical efficiency and may raise thermal issues that could cause materials degradation.

Lago et al. [41] reported significant temperature rise on remote phosphor plates under blue light irradiation. Simulations on the optical-thermal interactions in the phosphor particles were also conducted to understand the phosphor self-heating effect [42, 43]. The temperature on the phosphor layer is found to be significantly higher than the LED junction temperature and this changes the photometric and colorimetric properties of the white light emitted. Although it is recognized that the phosphor particles generate self-heating, its implications on package-level thermal performance have not been well understood. Heat generation in the phosphor layer

should be taken into consideration in the packaging design to improve the phosphor's conversion efficiency and prevent abrupt emitter failure.

As the heat generated by the LED device and the phosphor layer is transferred mainly through its package [30], poor thermal management will not only change the light output in terms of intensity and chromaticity shift but may also cause permanent deterioration in materials such as silicone yellowing, silicone carbonization and even delamination [44, 45]. As such, thermal analyses in terms of LED junction temperature T_j and thermal resistance R_{th} were conducted to understand the heat dissipation capabilities in the package [46-49]. Tao et al. [46] calculated that the R_{th} of their LED packages reduced with higher input power. However, Yang et al. [47] observed two differing R_{th} trends as a function of input power between a single- and multi-chip LED package and attributed it to the differences in the power dissipated by the internal series electrical resistances. Electrical resistance is based on a single dimensional electrical current flow path whereas R_{th} is typically three-dimensional. As such, the differing R_{th} trends can also be attributed to the packaging architecture since the amount of heat accumulation and heat transfer depends on the heat dissipation capabilities within the package [50, 51]. Under practical circumstances, the LED junction temperature and its associated R_{th} in the package are also poised to change with its operating temperature. Chapter 4 addresses this need to understand the thermal capabilities for different types of packages.

2.3 Effect of Humidity

Studies on humidity aging in LEDs are very scarce [11] with most research centred on generic reliability behaviour of LEDs. The humidity based degradation of LEDs over time may primarily be divided into LED-based failure (e.g. generation of nonradiative defects) or package-related degradation (e.g. degradation of ohmic contact, coloration of epoxy) [6]. With

chip failure, the increased defects and activated dopant caused the tunnelling components of the current to keep increasing in the subsequent ageing process [52]. The high density of line defects (dislocations) induced in the epilayer process were responsible for the tunnelling currents of GaN-based LEDs [53].

Hu et al. [5] showed that at chip level, the effect of the defects during aging may be represented by equation 2.2 which combines the expression for the Shockley–Read–Hall (SRH) recombination rate [54] into the continuity equation for injected electron density [55] at steady-state conditions to give:

$$L_e = B_{rad}\gamma^2 = \frac{J_D}{ed} - \frac{(N_d v_{th}\epsilon)\gamma}{2} \qquad (2.2)$$

where L_e is the photon emission rate, J_D is the electron current density, e the unit elementary charge, d the thickness of the active layer, B_{rad} the radiative recombination coefficient, γ the carrier density, N_d the defect density, v_{th} the thermal velocity and ϵ the capture cross section. Assuming the thermal velocities and the capture cross sections are equal for both carrier types, the increase in the defect density N_d results in a decrease in the total light intensity for a certain input current [5].

As shown in Fig. 2.7, the I-V characteristics of an LED at low bias regions, show the current increases after degradation. This indicates the generation of defects, which cause additional channels in the active layers. At high bias voltages, the LED shows an increase of series resistances due to the increase of the parasitic resistive components of the semiconductor and contact layers. This results in the decrease in the ability of the current and emission spreading at the device surface, and the subsequent loss in optical power.

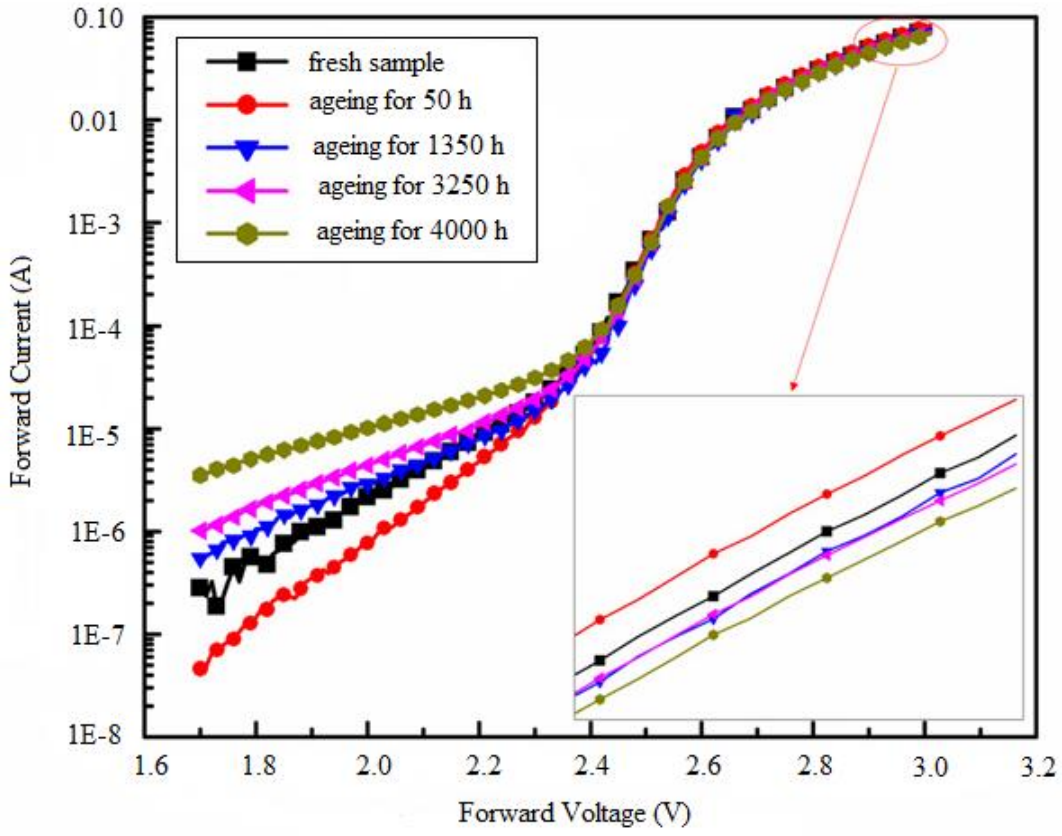

Fig. 2.7. I-V characteristics during the aging process. (Inset: Enlarged view of currents at high voltages) [5].

At the package level, Huang et al. [56] reported that some of the modes seen due to humidity include silicone carbonization, package encapsulant yellowing, blackening of silver-coating lead frames and phosphor dissolution. Under high humidity conditions, the optical output degradation is related to both these package and LED problems. Moisture diffuses into the interfaces of packaging material which causes a decrease in light output [57] while chip failure causes the blue intensity to degrade faster than the yellow intensity of the optical output [58]. Moisture inside LED packaging may also cause R_{th} to increase, due to delamination between chip and substrate in high moisture content environments [59, 60]. This exacerbates the package's thermal load, bringing about a corresponding increase in T_j and R_{th}.

There are currently no technical standards which consider LED operation under high humid conditions [61, 62], which presents an issue especially for countries with high relative

humidity. There exists a need to study the thermal characteristics of LEDs in humidity aging under different package configurations for proper thermal management. In addition, there is much potential to further the research not only on lumens output, but in particular on the colour shift and its linkage to the humidity based degradation of the LED.

2.4 LED Prognostication

Reliability studies arise from the need to understand the EOT performance of LEDs under high temperatures or humidity while over time. Armed with this knowledge, the logical progression would be to predict the future reliability by assessing the extent of deviation of the LED from its normal operating conditions [63]. Accordingly, prognostic techniques are applied to LEDs with the intention of improving future performance. Table 2.1 provides a summary of the main methods or models used in LED prognostication. Essentially, they can be divided into data-driven and physics-based methods.

Table 2.1. Summary of main LED Prognostication methods.

Statistical models	**Probabilistic models**	**Computational models**	**Physics-based Models**
Linear/non-linear regression Distance measuring Two-stage method Logistic regression Approximation method Analytical methods	Bayesian Network Kalman filter Particle filter Hidden Markov	Artificial Neural Network Support Vector Machine	General Physics of Failure (POF) Special Physics of Failure (POF) Empirical

Statistical, probabilistic and computational models generally come under the purview of data driven (DD) models because these methods utilize observed or monitored data to identify the system state and forecast future reliability without using physical models. Physics-based models on the other hand use a physical model to describe the degradation combined with measured data to predict future behaviour. DD methods are currently the most widespread methods used for LED prognostics. DD studies of LED degradation are commonly analyzed by linear or nonlinear statistical regression methods. Examples of linear regression techniques are the Euclidean Distance and Mahalanobis Distance techniques, which have been used to measure the degradation of an LED's light output based on the two variables of junction temperature and operating current [64] from which linear extrapolation is then used to predict the remaining useful life of LEDs. However, the Euclidean Distance assumes the data to be isotropically Gaussian, and does not take into account the association between the variables, whereas the Mahalanobis Distance is particularly useful for correlated variables, particularly in multivariate space. For nonlinear regression, commonly used approaches include the exponential function, the inverse power law model, and the Arrhenius model. For example, the Illuminating Engineering Society IES TM-21 standard [65] uses the exponential regression model and least-squares regression (LSR) approach to project the long-term luminous flux maintenance under different operational conditions. However, in actual practice, the IES TM-21 generates large errors caused by different types of uncertainties, such as discontinuous measurement, operating environment, and future load [66]. This methodology also does not provide statistical or detailed reliability information on its own.

There are also many variants or combinations of the regression methods such as the two-stage method, approximation methods, analytical methods, the Wiener process, the Gaussian process, and the gamma process, the use of each dependent upon specific requirements. For example, the general degradation path model by Lu and Meeker [67] describes a statistical

method in which degradation measures were used to estimate a time-to-failure distribution. Based on this general degradation path model, Fan et al. [68, 69] proposed a model combining several regression methods (approximation approach, analytical approach, and two-stage method) and statistical models (Weibull, lognormal, and normal) optimized to predict LED lifetime.

While Wiener processes are useful for many degradation modelling applications, it is appropriate when the degradation process varies bidirectionally over time with Gaussian noise. For example, Huang et al. [70] used an efficient likelihood function employing a modified Wiener process to produce results matching IES TM-21 lifetime predictions, following previous research on the Wiener diffusion process by Tsai et al. [71]. However, for one-directional processes like LED light output degradation, the gamma process is a more appropriate model where the degradation over time may be split up into sequential steps and modelled by the gamma distribution [72]. However, because this approach is inherently complicated and difficult to analyze, other algorithms (for example Markov chain Monte Carlo) are likely to be necessary to obtain the unknown parameters. Other DD methods not primarily involving statistical regression include Bayesian networks, Kalman filters and Particle filter methods. While Bayesian methods are simple to build and modify even with incomplete data, the method is only suitable for time independent data, besides needing structural historical information regarding the cause and effects of failures [73]. For example, Lall et al. use Bayesian probabilistic models [74] to analyze LED degradation with a statistical approach which establishes the failure threshold decay rate using the Arrhenius model as a basis, but omitting the effects of current or humidity. Alternatively, the Kalman Filtering method is an effective technique for state estimation for linear systems, but may not be as suitable for non-linear systems. Accordingly, variants such as the unscented Kalman Filter developed by Fan et al. [75] to predict the future LED chromaticity state alleviate this problem by using a

deterministic sampling approach. This approach is however still encumbered by the complexity of the state estimation model. On the other hand, the Particle Filtering method is better suited for highly non-linear processes. Fan et al. depict a particle filter-based approach [76] based on both Sequential Monte Carlo and Bayesian techniques to predict the lumen maintenance life. This method is reported as having a higher accuracy in predicting the long-term lumen maintenance life. However, the prediction accuracy of the Particle Filtering method is highly dependent on parametric initialization and thus limits the suitability for new LED products.

Although artificial neural network modeling is a DD method widely used in prognostics [17, 77, 78], they are almost non-existent in LED studies. ANNs provides an estimated output from a mathematical representation derived from observed data. The main advantage of ANN is that the output is not dependent upon an understanding of the physical or functional mechanism of the system it seeks to model. As such, ANN can be applied to model complex and unstable systems, although the quality of the output is determined by the integrity of the inputs which need to be well chosen.

Despite ANNs being appropriate for LED prognostic study, such methods related to LEDs are rare. LED research methodologies in companies are well established and rooted due to commercial or proprietary reasons. The benefits of new research technology introduction may not outweigh the resource or financial setbacks involved, leading to some degree of resistance to their introduction, especially given the success of existing methods [21, 22]. In addition, most of such systems are dedicated product-specific applications considered corporate secrets and are shrouded in secrecy given the intense competition within a specific industry [79, 80], explaining the lack of such models in the public domain. As such LED studies using ANNs are almost non-existent in the public domain, especially given the competitive environment and proprietary nature of LED research and developmental methodologies [23-25]. The only

such application relevant to LEDs found was a simple neural network developed by Sutharssan [81], which served as a basic preliminary prognostic tool to diagnose the state of LEDs.

The use of the highly computationally efficient ANNs has much potential for analyzing LED reliability, which can have complex, non-linear processes unsuitable for other deterministic models. The ANN model presented in Chapter 6 is a feed forward network using six key attributes or indicators of LED degradation to model the humidity based degradation model developed. Although the degradation of the LED is of great interest as this is a limiting factor to its widespread adoption, there is comparatively little research in LED reliability, particularly with humidity as a stress factor [82]. While other studies investigate lumen degradation from primarily qualitative approach [56, 83, 84], the scarcity of research taking into account the impact of relative humidity specifically and its corresponding association with colour degradation is notable. Despite LED lumen depreciation and colour shift being two critical modes of degradation of the LED which should be analyzed in tandem, most literature treat these two as independent phenomena [14, 31, 85-88]. Although the requirement for colour consistency has become more important than lumen maintenance in many applications, prediction models involving colour shift are limited [89]. The spectral power distribution (SPD) is the quantitative inference of an LED's colour shift process and both the lumen depreciation and colour shift are related to the SPD since photometric and colorimetric parameters such as luminous flux, Correlated Colour Temperature (CCT), and yellow-to-blue spectral ratio (YBR) can be computed from the SPD. Based on the SPD analysis, Qian et al. [89] predicted both lumen depreciation and colour shift by using the prediction of the evolutionary degradation process of the SPD to predict the lumen and associated colour drift curves based on the CIE (International Commission on Illumination) 1976 chromaticity coordinate system. The YBR is another indicator of colour shift which has the advantage of also being a way to indicate the LED failure mechanism. Greater degradation of the blue

intensity over yellow is likely related to chip failure while the reverse is suggested to be due to phosphor degradation [6, 58]. Under high stress conditions which incur higher degradation rates and colour change, a method to predict YBR colour shift would be particularly practical as an indication of the likely failure mechanism due to more pronounced symptoms. In Chapter 6, such a prognostication model based on the LED degradation behaviour is proposed not only to quantitatively gauge the long-term moisture incursion, but also to predict the colour shift due to the humidity.

To provide the capability to filter anomalies, the study is taken further to propose a novel trivariate Distance Measure approach. This approach is more accurate than univariate analysis and other Distance Measure techniques as it takes into account the actual correlations and covariance of the selected features, and does not require any assumptions about the data distribution. The degradation rate, the colour shift and R_{th} change are the interdependent features specifically extracted for this method as they are critical indicators of the physical state of the LED. Used together, these two methods provide powerful prognostic tools in LED health management.

Chapter 3

Effect of Temperature Control

3.1 Introduction

Currently, LEDs generate significant amount of heat fluxes with only about 40-50% of the electrical input power being converted into visible light [18]. The high heat generation affects not only the optical light output, but also the reliability of the LED package. T_j and R_{th} are typical parameters used to compare the thermal performance and heat dissipation capabilities of LEDs. System designers rely on these parameters to ensure the LED specifications are within safe operational limits [46]. T_j affects the LED optical performance and luminous efficacy [90] while the R_{th} is an indicator of the heat dissipation capabilities of the LED. Thermal resistance models can also show changes in the heat transfer path which cause irregular escalation of T_j leading to possible premature failure or accelerated degradation [50]. R_{th} may also be used as a gauge of any modifications of the thermal interface material or the GaN which occur with the increase in heat due to the changes in conductivity as a function of either drive current or operating temperature [91]. Moreover, the measured series resistance is linked to the thermal effects [28, 92] of LEDs in that an elevated series resistance is observed to be consistent with thermal degradation as the current is varied. The series resistance is also a key component in the LED conversion efficiency as the temperature increases [93]. Furthermore, the series resistance indicates the maximum chip size and power density limits within which the LED can perform effectively [92]. In consideration of the significance of the parameters discussed, it is imperative that the methodology or measurement techniques used to derive these quantities are sufficiently thorough so as to produce reliable and accurate data.

Larger LED chip sizes and higher LED packing densities such as Chip-on-Board (COB) packaging architectures are now more pervasive as the industry demand for higher power density applications increases. These high power density applications provide serious thermal challenges as the input power to the LED is controlled by the maximum temperature rating of the materials in the LED package and the intended application environment of the luminaire. With the growing pace of technological advancements in high power device fabrication and processes recently, it is important for LED characterization and measurement techniques to also keep up so that the resulting data is both dependable and reflective of the true status of the LED performance. Lighting system designers and LED integrators rely on specifications from the manufacturer to provide system solutions for their customers while the final consumers themselves use these datasheets for product comparisons. In case of data inaccuracies, the released data will be of limited functional use as the overall validity of the final performance and reliability estimations computed cannot be depended upon. This concern is highlighted by Poppe and Lasance [94, 95] who recommended a higher level of sophistication in LED thermal characterization and standardization of LEDs and LED-based products. This research highlights the possibility of ambiguity faced in optical, electrical and thermal characterization of high-power LEDs due to the temperature control set-up mode and the need for measures to ensure accurate measurement results.

3.2 Experimental Setup and Procedures

3.2.1 Instrumentation Setup

Fig. 3.1 shows the components of the measurement station set-up to study the optical-electrical-thermal properties of the LED under different temperature feedback controls. This LED measurement station comprises a Labsphere 20” integrating hemi-sphere system, a Peltier-based temperature controller (TEC), a Keithley 2602A Source Meter and a Mentor Graphics

T3ster Transient Thermal Analyzer. To establish traceable optical measurement, a reference lamp calibration and absorption correction were conducted before measurements. The LED is secured onto a temperature-controlled surface with an accuracy of up to 0.1 °C or using the T3ster thermostat module to ensure the same thermal conditions during both optical and thermal analyses. The photometric and colorimetric properties of the emitted light output are measured using a spectro-radiometer.

Thermal measurement, which includes LED T_j and transient thermal response, are approximated by means of the electrical forward voltage V_F of the LED. [96]. The time-dependent behaviour of the heat flow path in the LED packages are analyzed using the structure function-based evaluation of the thermal transient measurements. R_{th} is usually calculated from the change of temperature rise ΔT_{rise} in a package under a fixed applied heat input power P_H. Since optical light radiation is emitted out of the LED, the remaining heat dissipated power is thus determined by the difference between the supplied electrical input power and the optical radiant output. The total radiant flux emitted from the LED is factored into consideration for the calculation of the real thermal resistance, $R_{th\text{-}real}$. Electrical I-V measurement is conducted prior to and after the optical-thermal measurements to ensure that device does not degrade significantly during testing. This instrumentation setup is utilized for all electrical, optical and thermal measurements done in this and subsequent chapters.

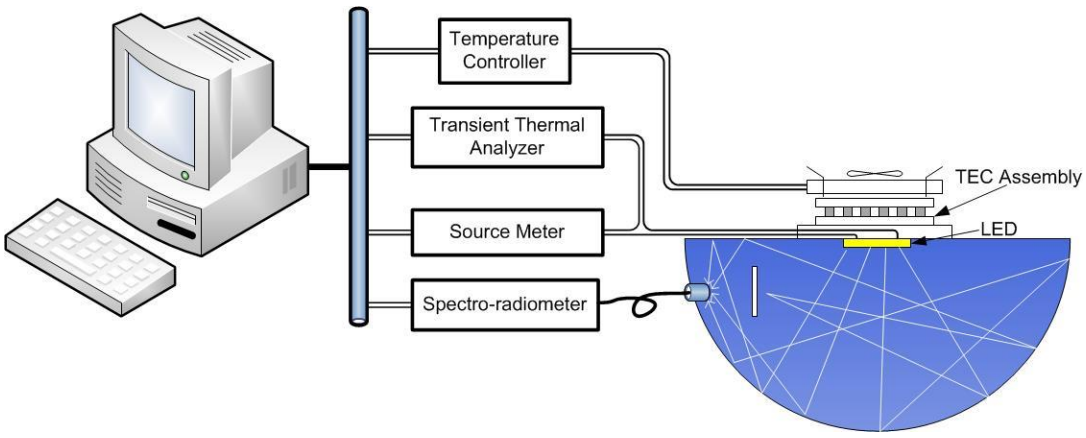

Fig. 3.1. Schematic layout of LED measurement set-up.

3.2.2 Experimental Procedures

The LED package used in this experiment was the Cree CXA1304 COB LED package which has a maximum rating of 1 A. The LED array in this COB LED package is arranged in 4 parallel paths, each with 3 LEDs connected in series. A thermistor was attached onto the T_j test point of the package to provide temperature feedback for the controller as it regulates the temperature. In view of the nature of testing, the IES LM80-08 [97] test standard was adopted with a sample size of 20 chosen to undergo electrical, optical and thermal measurements using the setup described. In Fig. 3.2 and Fig. 3.3, each data point represents the mean value of 20 samples while the rest of the figures in the chapter show the results based on the data for one LED which represents the behaviour of all the samples. In this and subsequent chapters, the figures which show individual LED results mentioned in the captions represent all tested samples include electrical sweep (I-V) measurements, spectral power distributions (SPD) and thermal responses, i.e. structure functions, where illustration of multiple results in the diagrams is impractical and where the intended focus is to demonstrate a qualitative effect or response. In all other diagrams, the data points represent the mean value of the data collected.

The controller uses two forms of temperature feedback control – open-loop (pulsed) and close-loop (adaptive) – to regulate the requisite temperature. In the open-loop mode, the temperature controller gives a constant-pulse input power under a fixed duty cycle in order to obtain the required temperature. In the close-loop mode, the thermistor supplies constant temperature feedback at 10 Hz to the controller. For all measurements, a data acquisition (DAQ) unit was used not only to monitor the input power to the TEC module and LED, but also the surface temperatures of the LED, the TEC cold plate, and its environment.

3.3 Results and Discussion

3.3.1 Optical Measurements

The optical characteristics and the relation to the heat load are initially studied. To assess the optical performance of the LED package, measurements were made at different temperature and input current settings. As the temperature increases at a fixed current input of 5W, the radiant flux and luminous efficacy show a decreasing trend (Fig. 3.2(a)). However, the heat flux from the LED $Q_{LED\text{-}heat}$, which was calculated by subtracting the total radiant flux from the electrical input power, shows a reciprocal response to the radiant flux with respect to temperature. This demonstrates that a higher heat load is brought about with increased operating temperatures. This higher heat load was caused by an increase in non-radiative recombination processes and increased leakage currents in the quantum wells of the LED at higher operating temperatures [43, 98]. On the other hand however, an elevation in power raises the quantum efficiency resulting in greater radiant flux output while producing much higher heat (Fig. 3.2(b)) at a constant operating temperature of 45 °C, which is opposite to the observed effect of increasing temperature. This considerably larger heat in turn causes a greater decrease in luminous efficacy with input power [99]. As the drive current rises, the LED self-heating effect causes a larger quantity of non-radiative recombination processes, resulting in the light output lessening with power. This decrease of luminous efficacy with rising power has been associated to mechanisms like current leakage [100, 101], which is further related to increased series resistances at elevated current levels. It has also been suggested that the Auger recombination process takes place at higher current densities [102]. From the radiant flux measured at different input power, the $Q_{LED\text{-}heat}$ trends can be derived for increasing operating temperatures as shown in Fig. 3.3. The effect of power increase on the heat load is observed to be more substantial than that of operating temperature. The large amount of heat produced

by the LED at increased temperatures and input power lead to a higher LED T_j and may correspondingly change the temperature conditions during measurement hence inadvertently altering the parameters obtained from the procedure. This issue and its consequences will be discussed in detail in the following sections.

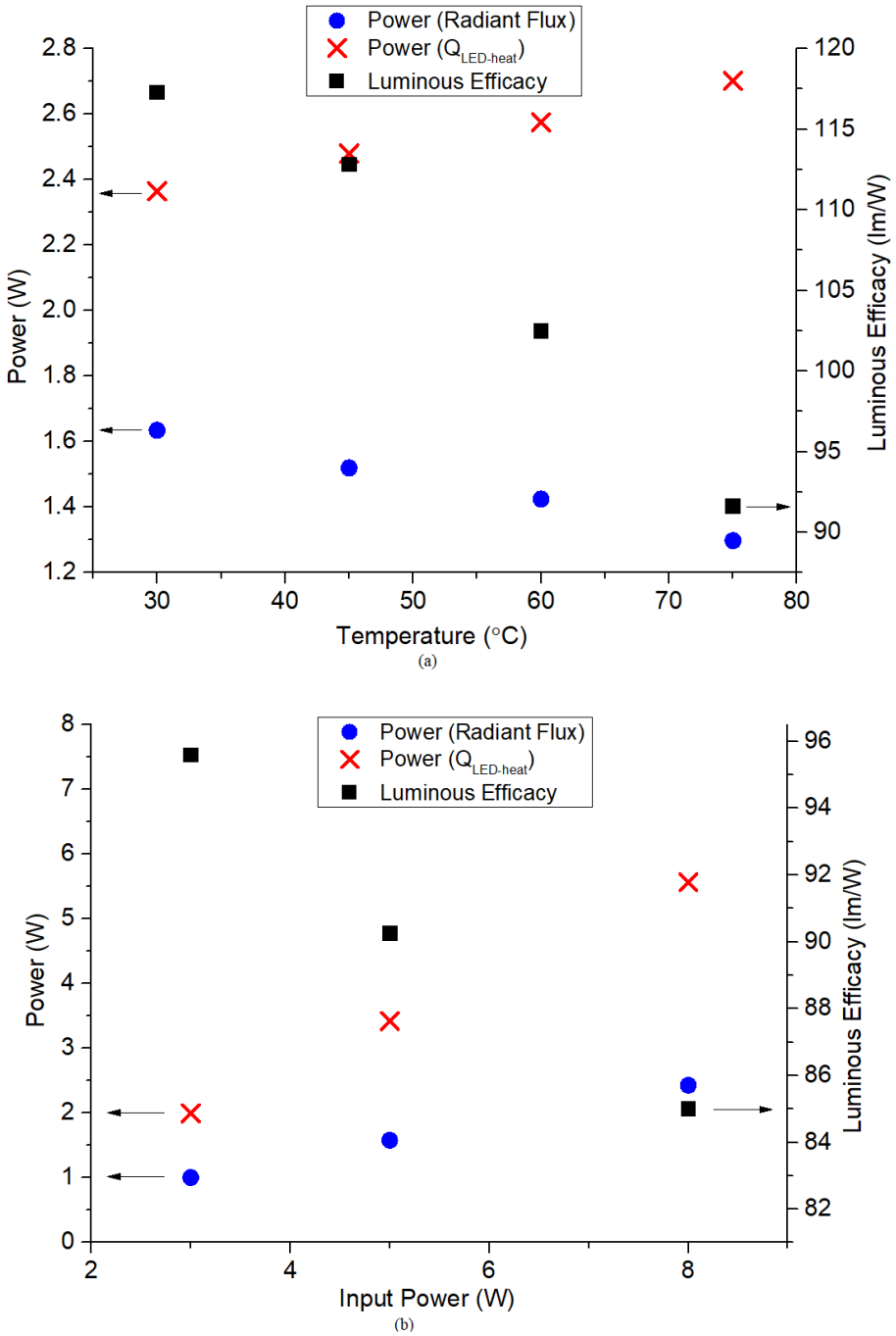

Fig. 3.2. Radiant flux, heat flux and luminous efficacy of the LED under (a) varying temperature at constant 5W input power (b) varying input power at constant 45 °C temperature.

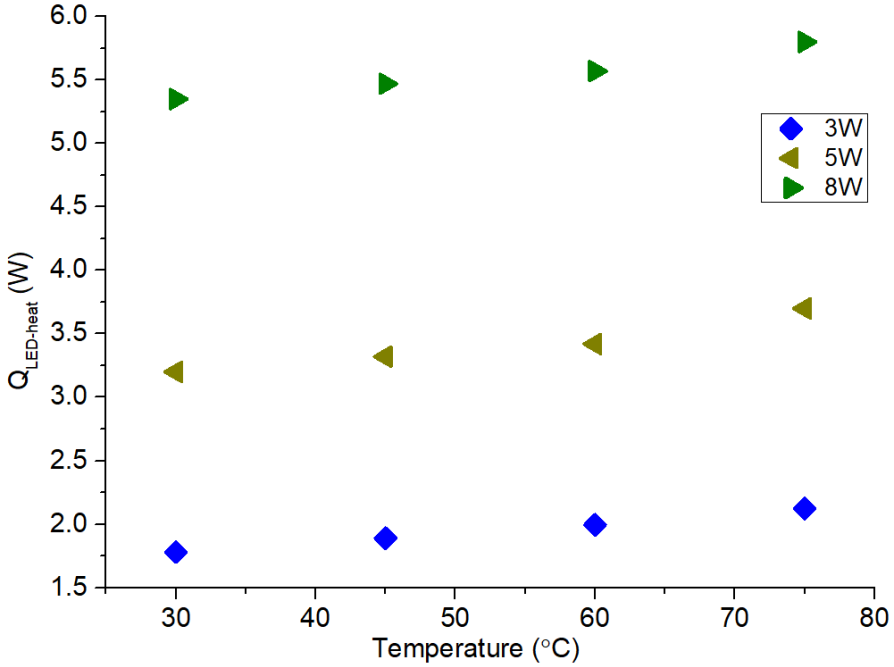

Fig. 3.3. Heat flux $Q_{LED-heat}$ rise with increasing operating temperatures for different input powers.

3.3.2 Electrical Measurements

To investigate the electrical characteristics of the LED device, current-voltage (I-V) measurements were conducted. To make sure that the device is kept at a constant temperature throughout measurement, the LED is seated onto a Peltier-controlled plate. In the closed-loop approach, a voltage sweep is applied during which a high amount of heat can be generated by the high-power LEDs. The measurements for this experiment are conducted separately at 4 different operating temperatures (30 °C , 45 °C, 60 °C and 75 °C). The surface temperature of the LED rises accordingly within this measurement period as demonstrated in Fig. 3.4(a). This temperature increase begins at 7 s, attaining a peak of 8 °C at about 12 s (Fig. 3.4(a)). After reaching the peak, temperature regulation provided by the TEC causes the temperature to gradually reduce. The heat produced by the LED activates the TEC to compensate for the increased heat load so as to control the required temperature setting and adjust it back to the

original operating temperature. However, as shown in Fig. 3.4(b), the TEC has a delayed response to the heat produced by the LED and does not compensate sufficiently fast enough to adjust the temperature back to its original setting during the measurement period. This lack of an instantaneous response from the TEC means that the LED has not been truly maintained at a fixed temperature during the entire voltage sweep. The TEC overcompensates eventually resulting in the negative temperature rise seen. The higher the operating temperature, the quicker the temperature rise reduces to a negative value. At 75 °C operating temperature, the temperature rise reduces to a negative value at 25 s while at 30 °C operating temperature, this negative decrease happens at 33 s. As the operating temperature increases, the increased heat flux brings about a more aggressive response from the TEC as it attempts to reinstate the initial temperature.

An elevated voltage indicates that the TEC attempts to decrease the temperature while a reduction in the voltage output shows that the TEC attempts to raise the temperature. The TEC voltage dip at about 17 s causes the rate of temperature decrease to slow down until the temperature rise eventually bottoms out at about 55 s. The amount of TEC outputs differs because of the greater amount of heat flux generated by the LED as the operating temperature increases. The temperature rise reaches its lowest value of -3.5 °C for 75 °C operating temperature compared to -1 °C for 30 °C operating temperature because of the larger TEC output as the heat flux increases with correspondingly higher temperatures. The TEC voltage subsequently alternates between increasing and decreasing trends in its effort of steadily facilitating the LED temperature back to its initial operating temperature at the beginning of the experiment.

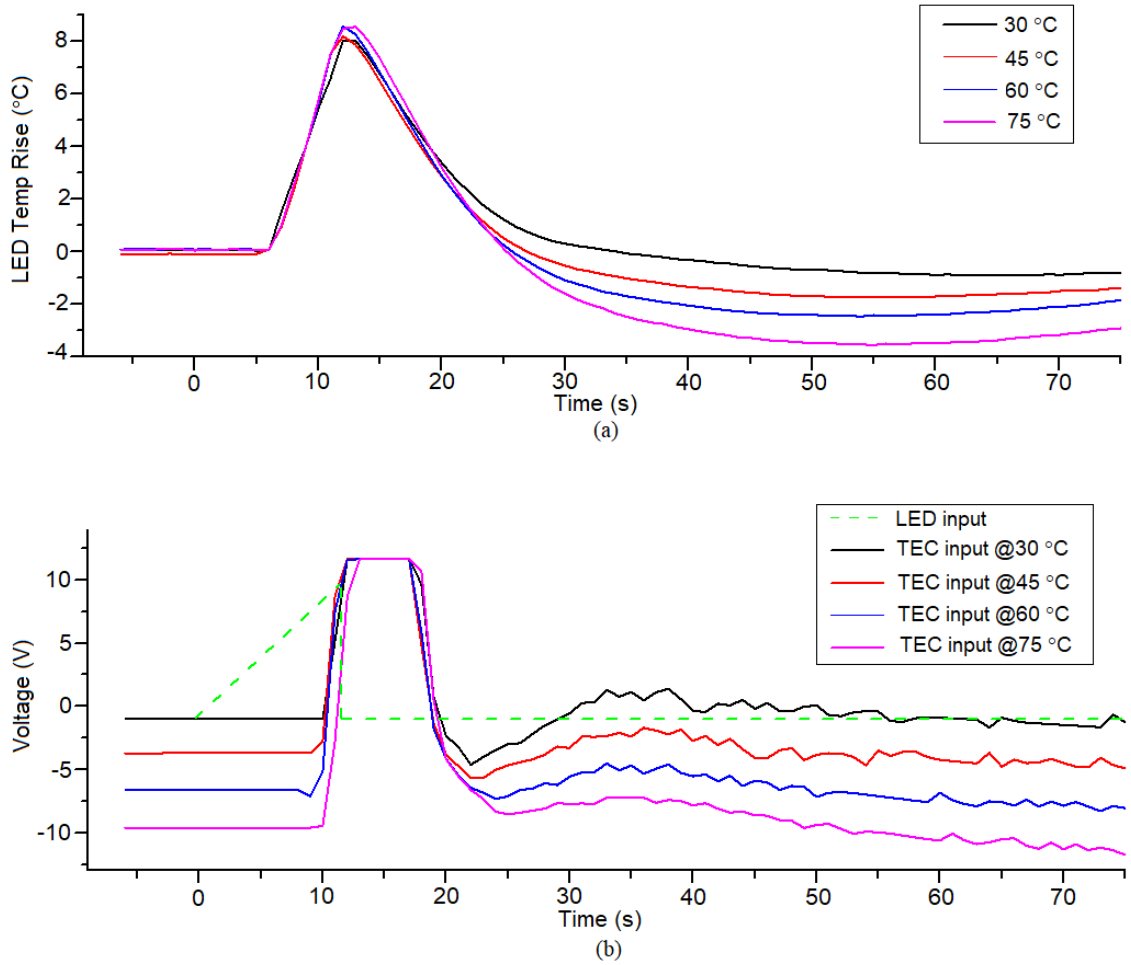

Fig. 3.4. (a) The surface temperature rise of the LED and (b) the corresponding TEC response during the voltage sweep of LED with input current 1 A. This figure shows the results based on the data for one LED and is representative of all the samples.

In order to investigate in detail the self-heating effect during electrical measurement, the I-V testing was also conducted manually. This procedure involves physically measuring the current individually at each voltage level instead of using the I-V sweep function. The manual procedure allows for the LED's self-heating to be compensated so that it reaches the final steady state condition. This tedious approach nevertheless yields fixed temperature conditions for the LED. As Fig. 3.5 shows, both the closed-loop and manual approaches produced similar I-V measurement results at the diode region of the I-V curves. At the higher voltage region however, the manual approach produced a lower voltage drop across all the operating

temperatures in comparison to the closed-loop sweep approach. As the input power was less than 0.8 W in the diode region of the I-V curve, the amount of heat produced by the LED was small.

In the high voltage region however, the input power was more than 3W, implying a considerably higher amount of the self-heating. Due to this larger self-heating effect, a greater voltage drop is needed under each current driving condition. From these results, the temperature dependent series resistance of the LED can be derived from the high voltage region of the I-V characteristics. It can be seen from Table 3.1 that for both measurement methods, there is a reduction in series resistance as the operating temperature increases. This decrease in the series resistance is because of the higher acceptor activation that occurs at higher temperatures which cause the higher conductivity of the p-type GaN layer [103]. A comparison of the series resistance for each temperature setting for both the manual and closed-loop approaches reveals that R_s for the closed-loop approach is about 1 Ω lower than that for the manual approach. The higher heat load produced by the LED in the closed-loop approach and the correspondingly higher temperature leads to the lower series resistance seen. Due to the fact that the electrical analysis of the LED is considerably affected by temperature, the instrumentation set-up requiring responsive temperature regulation is necessary to instantaneously compensate for the self-heating effect so as to provide proper diagnoses of the LED.

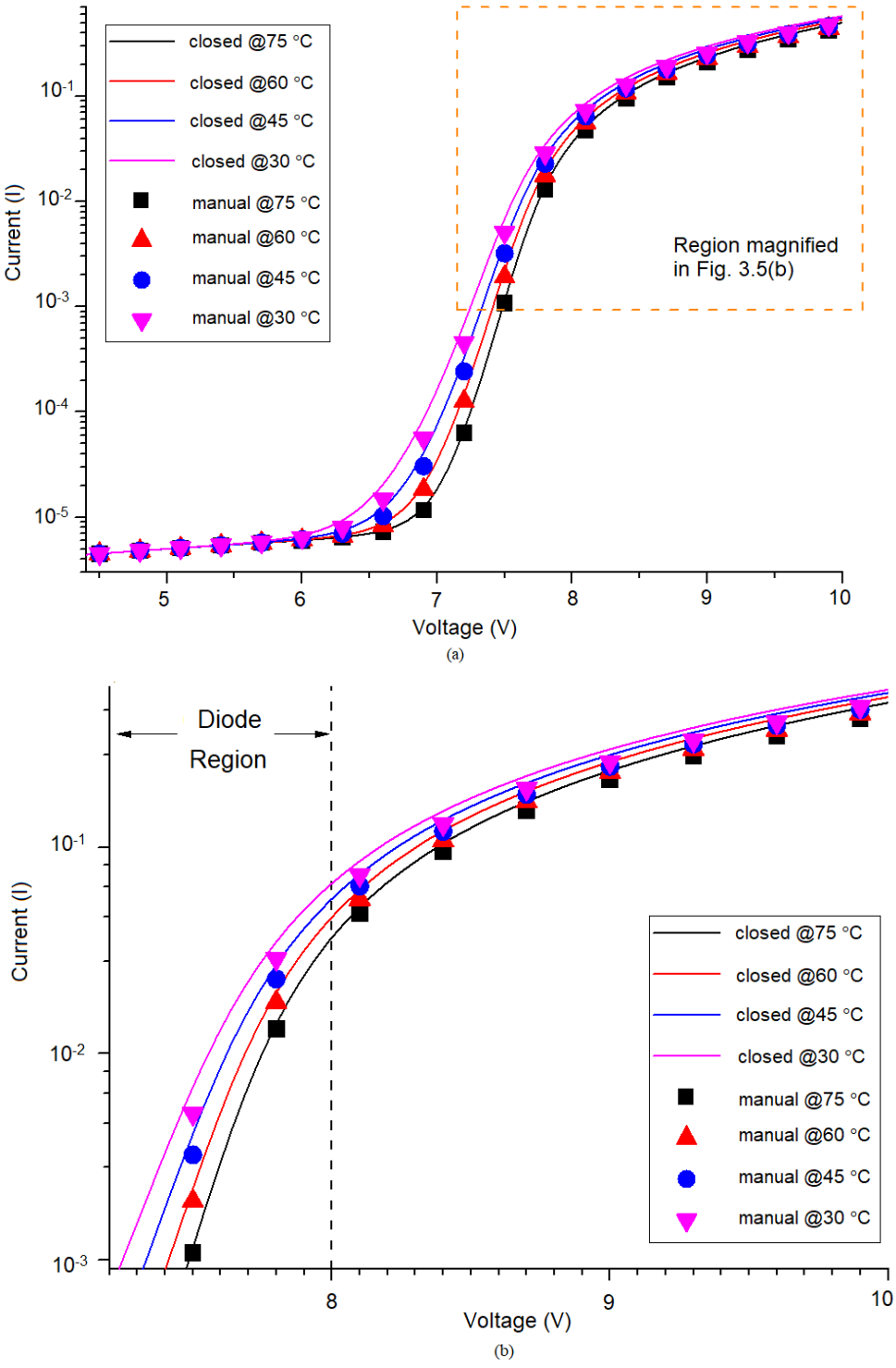

Fig. 3.5. (a) I-V characteristics of the LED under both closed-loop and manual approaches at different operating temperatures. (b) Magnification of high voltage region of I-V curves under both closed-loop and manual approaches. This figure shows the results based on the data for one LED and is representative of all the samples.

Table 3.1. Average (mean) Series Resistances R_s for both closed-loop and manual approaches at different temperature settings for all samples.

Operating Temperature	**R_s (Manual Approach)**	**R_s (Closed-loop Approach)**
30 °C	5.0 Ω	4.0 Ω
45 °C	4.7 Ω	3.7 Ω
60 °C	4.5 Ω	3.5 Ω
75 °C	4.4 Ω	3.4 Ω

3.3.3 Thermal Measurements

To understand the thermal behaviour of the LED package, transient thermal measurements are conducted in accordance to the guidelines provided by JEDEC [104]. The cooling measurement mode is used with the radiant flux (derived in Section (3.3.1)) taken into consideration in the thermal analysis. In this method, the LED is turned on for a prescribed period until such time T_j becomes constant. Once steady-state condition is achieved, the input current to the LED is reduced to only 1 mA, thereby allowing the transient change in T_j to be computed via the electrical test methodology described by the Joint Electron Device Engineering Council (JEDEC). This sequence is portrayed in Fig. 3.6. For the whole duration of the measurement window, it is imperative that the thermal conditions i.e. Q_{TEC} from the TEC be kept constant so as to ensure that the LED temperature rise is not forcibly controlled. Typically, the thermal time constant for the temperature of the LED package to drop to its ambient temperature is between 150 to 200 s. In closed-loop measurement, the TEC reacts to the abrupt change in heat flux from the LED at t = 0 s, causing Q_{TEC} to fluctuate, thereby artificially altering the actual T_j reading and corresponding R_{th} of the LED (Fig. 3.6).

The TEC response under different LED input power levels is shown in Fig. 3.7. As the LED is switched to 1 mA at t = 0 s under closed-loop control, the TEC input voltage drops immediately to negative value and the ensuing voltage changes indicate that the TEC is adjusting for the rapid loss of heat from the LED package. The greater the LED input power, the higher the heat flux produced with correspondingly higher T_j. A higher TEC input voltage is therefore needed to regulate for the higher heat load that comes with the higher input power of the LED.

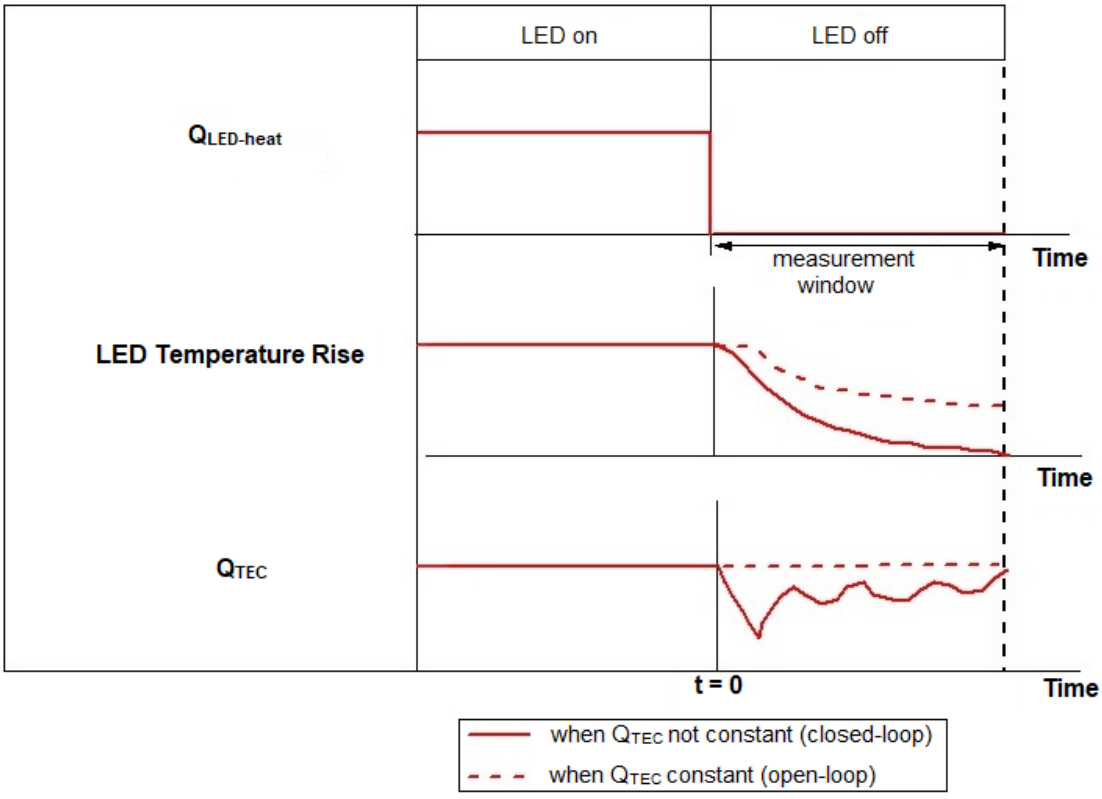

Fig. 3.6. $Q_{LED\text{-}heat}$, Q_{TEC} and LED temperature rise during measurement. Q_{TEC} stays constant throughout measurement cycle during open-loop approach as TEC does not compensate for change in $Q_{LED\text{-}heat}$ and LED temperature. In closed-loop approach however, Q_{TEC} does not stay constant throughout the measurement cycle as the TEC compensates for change in $Q_{LED\text{-}heat}$ and LED temperature.

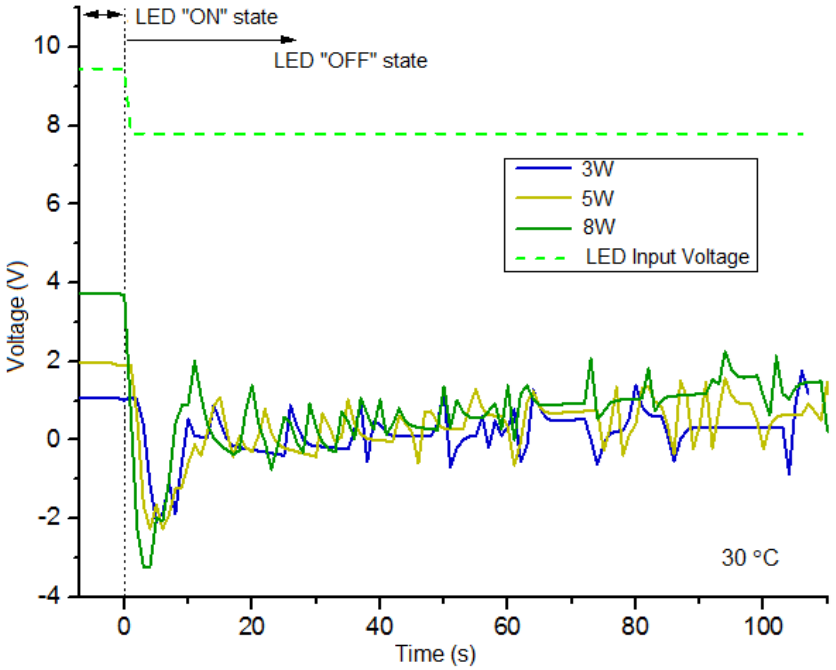

Fig. 3.7. TEC voltage response during closed-loop thermal measurement at different input power levels. The TEC reacts to the sudden change of heat load from the LED in order to reach thermal equilibrium in the system. This figure shows the results based on the data for one LED at each input power level.

As shown in Fig. 3.8, in closed-loop feedback control, the overall effect of the TEC involvement is to regulate the temperature back to its original state at t = 0 s. The sudden change of the LED's thermal load accounted for the TEC response in compensating $Q_{LED\text{-}heat}$. The initial drop in the temperature is due to the TEC overcompensation which then triggers the TEC to raise the temperature in response. During this measurement period as the TEC readjusts the temperature back to the initial state, the temperature is observed to alternate between rise and fall. Since temperature rise is related to R_{th}, this repression of the temperature could result in inaccurate computation of the R_{th}, as will be discussed later in this chapter. In contrast to the closed-loop measurement where the TEC continuously controls the temperature by utilizing a fixed duty-cycle, in the open-loop measurement mode, the TEC does not regulate the temperature change, permitting a steady Q_{TEC} flow. The TEC is non-adaptive to the temperature shifts all through the duration of the measurement window. As observed in Fig.

3.8, the LED temperature as a consequence is left completely uncontrolled and reduces steadily during the whole measurement window. This implies an unconstrained thermal analysis of the LED, allowing for accurate thermal results.

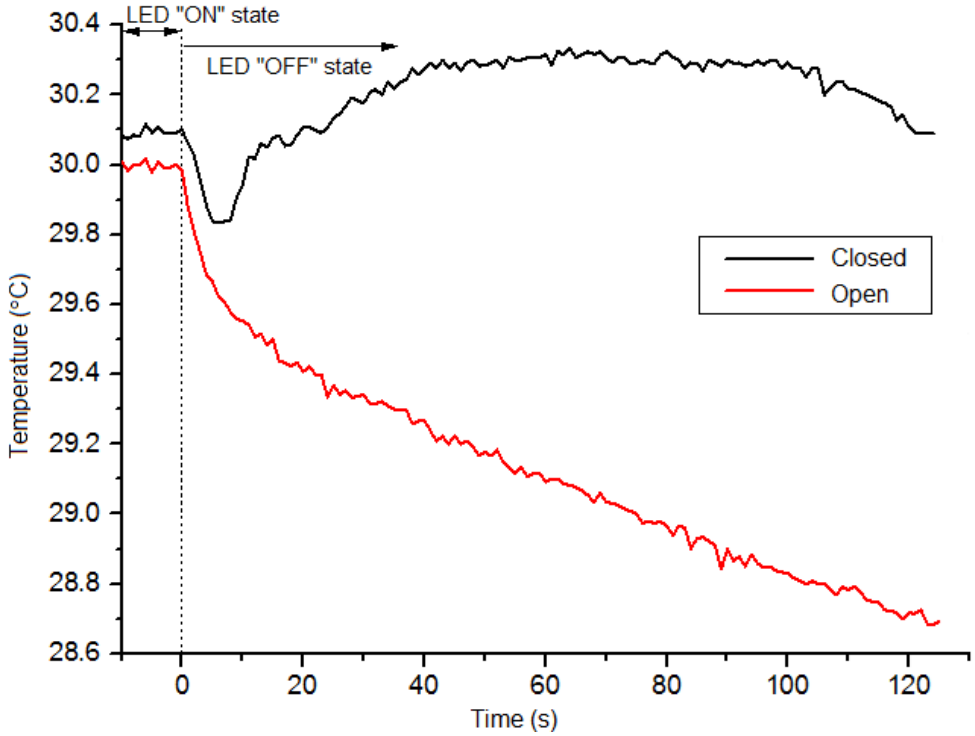

Fig. 3.8. Comparison of LED surface temperature response in both closed and open-loop thermal measurements of one LED.

Fig. 3.9 shows the LED cooling curve response for closed-loop, open-loop and thermostat based measurement approaches, while Fig. 10 shows the impact on the structure function. At 30 °C temperature setting, a temperature rise of about 4.8 °C is seen for both closed-loop and the thermostat approach while a temperature rise of 5.8 °C is observed for the open-loop approach. At 45 °C temperature setting, the temperature rise is 5.8 °C and 6.2 °C for the closed-loop and thermostat approaches respectively versus 7.8 °C for the open-loop approach. As shown in Table 3.2, these observations translate to a pronounced difference between the T_j obtained by open-loop and closed-loop measurements, with this discrepancy increasing with

higher operating temperature. As expected, the results obtained for the thermostat measurements are comparable to that obtained for the closed-loop approach

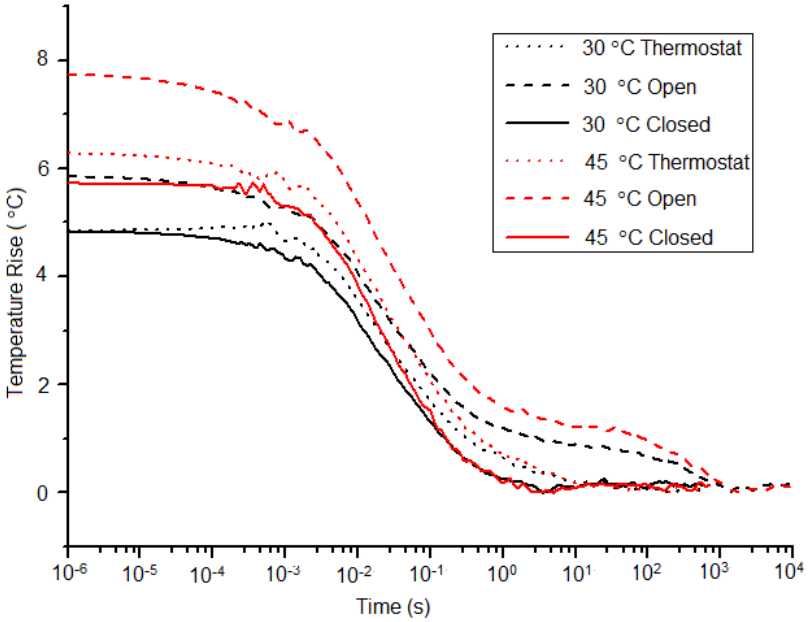

Fig. 3.9. Cooling response of LED under different temperature controls at different operating temperature settings. This figure shows the results based on the data for the same LED under the different testing conditions.

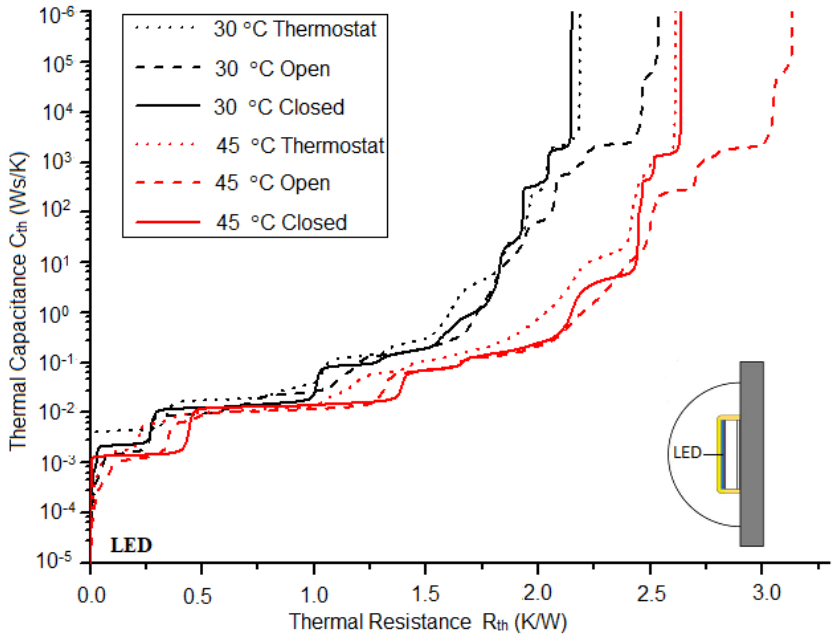

Fig. 3.10. Cumulative structure function of LED under different temperature controls at different operating temperature settings. This figure shows the results based on the data for the same LED under the different testing conditions.

as the thermostat also adopts a similar adaptive feedback control to regulate the temperature. As the operating temperature increases, the greater rise in T_j for open-loop compared to closed-loop is because of the increased heat flux produced resulting in the greater rise in temperature. Furthermore, in Fig. 3.9 it can be seen that in the open-loop method, Q_{TEC} allows the temperature to be uncontrolled during the whole measurement period while in the closed-loop and thermostat method, the temperature is regulated to the specified setting in just a few seconds. As explained above, this adaptive control of $Q_{LED\text{-}heat}$ leads to inaccuracy in the results.

The effect of open and closed-loop temperature control can be further studied via the structure function of the LED (Fig. 3.10). It was observed that the closed-loop temperature feedback control exhibits similar structure function characteristics and R_{th} values with the thermostat. The open-loop temperature control also exhibits similar structure function attributes but with higher R_{th} values at both operating temperatures. The structure functions show significant divergence towards the conclusion of the heat flow and this is repeatable at higher operating temperatures. Table 3.2 shows R_{th} of about 2.1 K/W for closed-loop/thermostat approaches and 2.5 K/W for open-loop at 30 °C operating temperature. The R_{th} at 45 °C operating temperature are respectively 2.6 K/W in closed-loop/thermostat and 3.1 K/W in open-loop. Considerable temperature shift occurs in the open-loop method due to Q_{TEC} being kept constant for the duration of the measurement period. On the other hand, in the closed-loop and thermostat methods, the temperature adapter responds to any variation in heat load to readjust the temperature back to the initial value, thereby minimizing the final change in temperature. Since R_{th} is directly proportional to temperature change, it follows that R_{th} for the open-loop approach is also larger than that for the closed-loop/thermostat approaches. Temperature rise and thermal resistance are therefore incorrectly repressed during closed-loop measurement, resulting in wrong data specifications.

Table 3.2. Average (mean) Thermal Resistance (R_{th}) and Junction Temperature (T_j) for open-loop, closed-loop and thermostat approaches at different operating temperature settings for all the samples.

Operating Temperature	**TEC Open**		**TEC Closed**		**Thermostat**	
	T_j (°C)	R_{th} (K/W)	T_j (°C)	R_{th} (K/W)	T_j (°C)	R_{th} (K/W)
30 °C	35.8	2.5	34.8	2.1	34.8	2.2
45 °C	52.8	3.1	50.8	2.6	51.1	2.6

3.4 Summary

The heat flux generated by high-power devices and assemblies must be taken into account as discrepancies during measurement can occur depending on the adaptive feedback set-up. The findings in this chapter present new perspectives on the implications of incorrect temperature control. In the case of electrical measurements, it has been shown that the temperature adapter has a delayed response to the LED heat load, meaning that the LED had not been preserved at a consistent temperature during the entire measurement cycle. This resulted in different series resistance values in comparison to when measurement were done manually. Accordingly, use of manual temperature control is suggested to compensate for the LED self-heating so as to provide proper analysis of the LED's electrical attributes. On the other hand, when conducting transient thermal measurement, a consistent heat flow from the TEC is required so that the LED is not kept at a fixed temperature throughout the whole thermal measurement period. It is therefore suggested that an open-loop temperature feedback system which is non-adaptive be used during thermal measurement to maintain such conditions. In contrast to the closed-loop system, open-loop control will allow for correct derivation of the R_{th} and T_j. It should also be noted that although these experiments were conducted using LEDs, these measures are also applicable for other similar high-power devices and assemblies.

Chapter 4

Effect of Current and Temperature

4.1 Introduction

Yttrium Aluminum Garnet: Cerium (YAG:Ce) phosphor is the most widely used phosphor in pcLEDs based on InGaN LED chips. Due to the excitation of blue light (electroluminescence) from the InGaN LED chip (with typical peak wavelength of 450 nm), the phosphor host emits yellow light (photoluminescence) (with typical peak wavelength range between 550 to 650 nm) and the mixing of the blue and yellow light produces white light.

As described in the literature review, the thickness and concentration of the phosphor layer as well as the phosphor particle size strongly influence the luminous efficacy and the colour chromaticity of the light emitted. The temperature on the phosphor layer is significantly higher than the LED T_j in many situations [27, 43, 105] and this changes the photometric and colorimetric properties of the white light emitted. While it is recognized that the phosphor particles generate self-heating [32, 42], the implications on package-level thermal performance are not well understood. Heat generation in the phosphor layer should be taken into consideration in the packaging design to improve the phosphor's conversion efficiency and prevent abrupt emitter failure.

In this chapter, two types of experiments are conducted. In the first set of experiments, the optical performance and thermal response of the LED package will be evaluated under various phosphor layer variations as well as die-bonding configurations. Through understanding the implications of light extraction losses in the phosphor layer on the thermal performance of a package, the performance and reliability of high power phosphor coated (pcLED) packages can be improved.

In the second set of experiments, the effect of the phosphor layer and die-bonding configuration on the photometric, colorimetric and thermal properties of pcLED packages under different operating conditions are investigated. The heat dissipation capabilities of the different LED die-bonding configurations are studied, from which the relationship between the optical and thermal properties in pcLED packages is established.

4.2 Experimental Setup and Procedures

4.2.1 Instrumentation Setup

For all the electrical, optical and thermal measurements done for the two experiments described in Section (4.3), the LED packages are measured using the integrated LED measurement system represented in Fig. 3.1 (Chapter 3) consisting of a Labsphere 20" integrating hemi-sphere system, a Keithley 2602A Source Meter, a Mentor Graphics T3ster, and a Peltier-based temperature controller (TEC). To ensure traceable optical measurement, reference lamp calibration and absorption correction were conducted prior to each measurement. In addition, electrical I-V measurement was conducted prior to and after the optical-thermal measurements to ensure that device did not degrade significantly during testing.

4.2.2 Experimental Procedures

For the first set of experiments, commercial 1mm^2 GaN LEDs, with a blue peak wavelength of ~450 nm, bonded onto Aluminum Nitride (AlN) substrate either conventionally (Seoul Semiconductor S1W) or in a flip-chip approach (Philips P1W) are used. In the conventional die-bonding approach, the GaN LED is grown on a 100 μm sapphire substrate and is subsequently bonded onto AlN substrate. In the flip-chip bonding configuration, the GaN LED is bonded directly onto an AlN substrate via Au bumps. For both bonding configurations, a layer of phosphor is subsequently coated over the LED chip to emit white light. The thickness

of the phosphor layer in conventional bonded LED and the concentration of phosphor particles in flip-chip bonded LED are varied to obtain different CCT values. Table 4.1 shows the phosphor thickness variation for different LED die bonding configurations. To achieve 2700 K CCT, Lutetium-based phosphor particles are used while the others use YAG-based garnet phosphor particles. Lutetium-based phosphor has better CRI properties whereas YAG-based phosphor exhibit higher efficiency [106, 107]. The elemental composition of the Lutetium-based phosphor particles is Lu (61-62 wt.%), Al (14-16 wt.%) and O (22-24 wt.%) while the YAG-based phosphor particles have average compositions of Y (42-49 wt.%), Al (15-21 wt.%) and O (30-35 wt.%).

Table 4.1. Phosphor Thickness Variation for Different CCT Values and Die-Bonding Configurations.

Die-Bonding Configuration	**CCT (K)**			
	2700	4000	5000	7000
Conventional (C)	95 µm	85 µm	48 µm	32 µm
Flip-chip (FC)	60 µm			-

To understand the implications of the phosphor layer in the package, absolute optical and thermal properties of each of the LED packages is evaluated. In view of the nature of the testing, the data collection methodology in the IES LM-80-08 test standard is adopted with 20 samples of each type of LED (FC and C) for each CCT level selected for experimentation. An input drive current of 350 mA is used for the LEDs, which are 1 W rated LEDs.

For the second experiment, three different sets of pcLED packages – 1 W (Philips P1W and Seoul Semiconductor S1W) and 0.3 W (Seoul Semiconductor S03W) rating – are used. Stratified sampling was performed using both their photometric and colorimetric properties to achieve tight radiant tolerance with zero CCT shift tolerance. Each pcLED packages has a fixed CCT value of 4000 K with a radiant flux variation of ± 3.5 mW at 25 °C. For the S1W

and S03W LED packages, GaN LED is grown onto sapphire and subsequently bonded onto a heat spreading substrate. The P1W LEDs adopt a flip-chip die-bonding approach whereby the GaN LED device is directly bonded onto a heat spreading substrate via Au bumps, while the S1W and S03W LEDs adopt conventional die-bonding approach. In terms of phosphor deposition, the S03W LEDs applied dispersed phosphor coating method whilst the P1W and S1W LEDs adopt conformal phosphor coating approach. The details of these LED packages are summarized in Table 4.2. To evaluate the effect of phosphor coating and light scattering losses caused by the packaging architectures, LED packages with and without their phosphor layers are compared. Throughout this thesis, the blue emitting LED and pcLED packages are labelled as blue and white LEDs, respectively. 20 samples of blue and white LEDs for P1W, S1W and S03W were selected for experimentation. Except for the experiment for current density variation (Fig. 4.7(a)), an input drive current of 350 mA is used for P1W and S1W, while 100 mA is used for S03W.

Table 4.2. Physical Characteristics of the LED packages.

LED	**LED Chip Size**	**Die-Bonding Configuration**	**Phosphor Material**	**Phosphor Coating**
P1W	10.45 X 10^{-3} cm^2	Flip-chip	YAG:Ce	Conformal
S1W	4.78 X 10^{-3} cm^2	Conventional		Conformal
S03W	6.01 X 10^{-3} cm^2	Conventional		Dispersed

4.3 Results and Discussion

4.3.1 Impact of Phosphor Coating

In the first experiment to analyze the impact of the phosphor coating, the spectral power distribution (SPD) characteristics of the blue and pcLEDs are first measured as shown in Fig. 4.1. Both sets of LEDs exhibit a blue peak emission of ~450 nm at 20 °C. After phosphor is

deposited over the LED, the blue peak intensity reduces significantly, and a broad yellow-orange spectrum is produced.

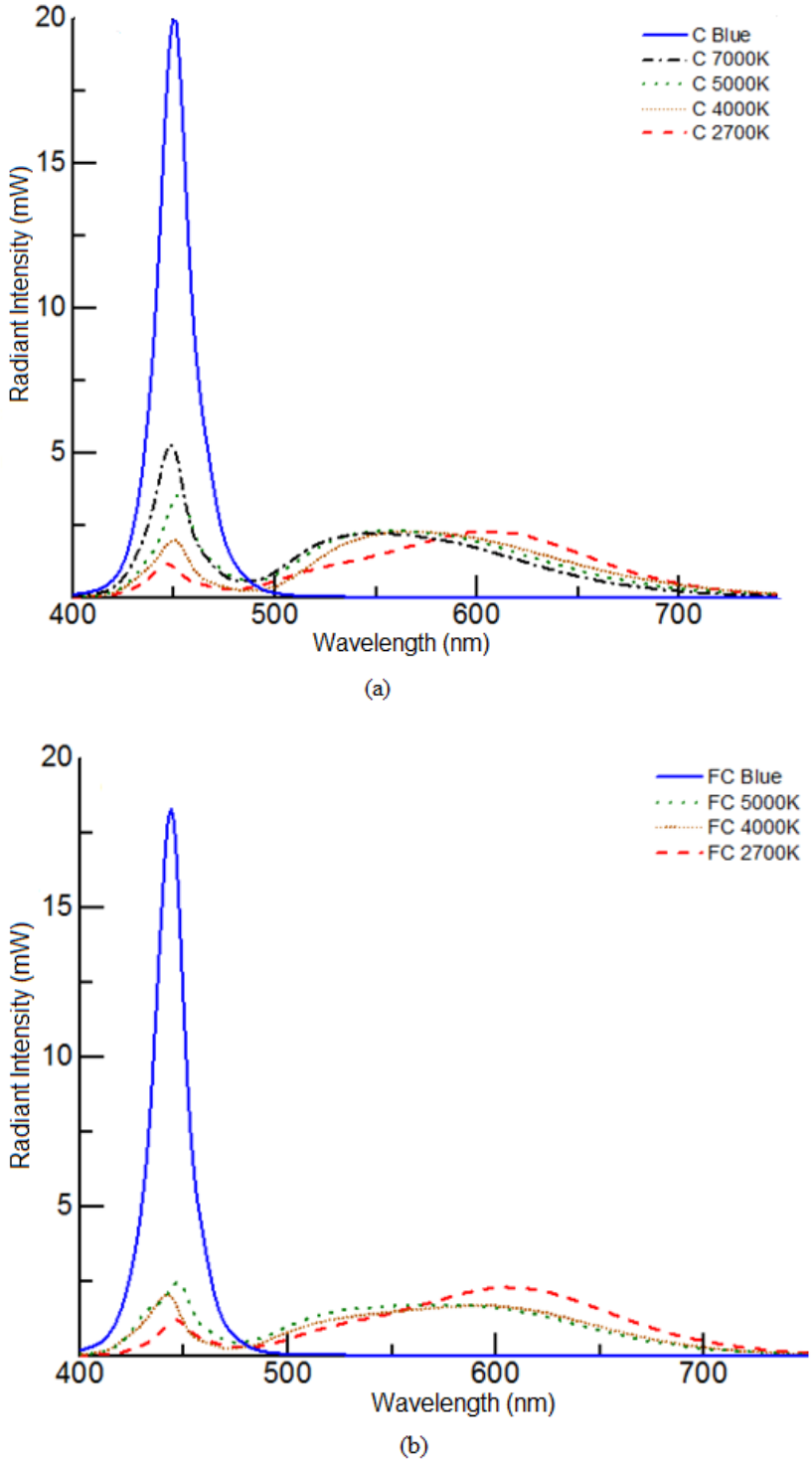

Fig. 4.1. Typical spectral power distribution of (a) conventional (S1W) and (b) flip-chip (P1W) bonded LEDs at different CCT rating. This figure shows the results based on the data for one LED at each CCT level and is representative of all the samples.

Depending on the CCT rating, different proportion of blue and yellow light is acquired. As the CCT value decreases, the blue peak intensity will reduce while the yellow-orange spectrum broadens and shifts to longer wavelength accordingly. This shows that a higher proportion of down-conversion processes occurring in the phosphor particles increase the yellow-orange spectral intensity. From the SPD characteristics, the efficiency of the blue and pcLEDs are subsequently evaluated at various operating temperatures in Fig. 4.2. The conventional bonded LEDs exhibit a high external quantum efficiency of ~43% at 20 °C and reduce steadily with higher operating temperature. On the other hand, flip-chip bonded LEDs have a lower efficiency of ~39% at 20 °C but demonstrate improved optical stability at elevated temperatures. The efficiency for the pcLEDs also exhibits a similar trend compared to their respective blue LEDs but with a difference in magnitude. This efficiency drop might be attributed to a number of factors; (i) increased non-radiative recombination processes and increased leakage currents in the quantum wells of the LEDs, (ii) phosphor quenching and (iii) increase of transmission loss in the silicone [43, 108, 109]. After blue light is emitted out of the LED, two types of losses could occur within the package: Stokes energy loss and package-related losses. Stokes loss is determined by the amount of down-conversion processes in the phosphor particles while package-related loss is due to light scattering and absorption losses. Light scattering may occur within the phosphor particles or in the packaging material. On the other hand, the emitted light from the LED and phosphor particles can be (re-)absorbed by the surfaces of the LED device, phosphor particles, and its packaging materials. These aggregations of losses are termed as light extraction losses. The light extraction losses for both die-bonding configurations were found to increase with lower CCT value.

In Fig. 4.2 to Fig. 4.5, each data point represents the mean value of 20 samples while the error bars represent the standard deviation of the mean. As shown in Fig. 4.2, the radiant efficiency for the conventional bonded and flip-chip bonded LEDs dropped to ~32% and ~23%

respectively at CCT value of 2700 K. Since the packaging material and physical construction of the package are similar for the particular LEDs under test, the efficiency difference between the various CCT ratings is assumed to be attributed mainly to the phosphor layer.

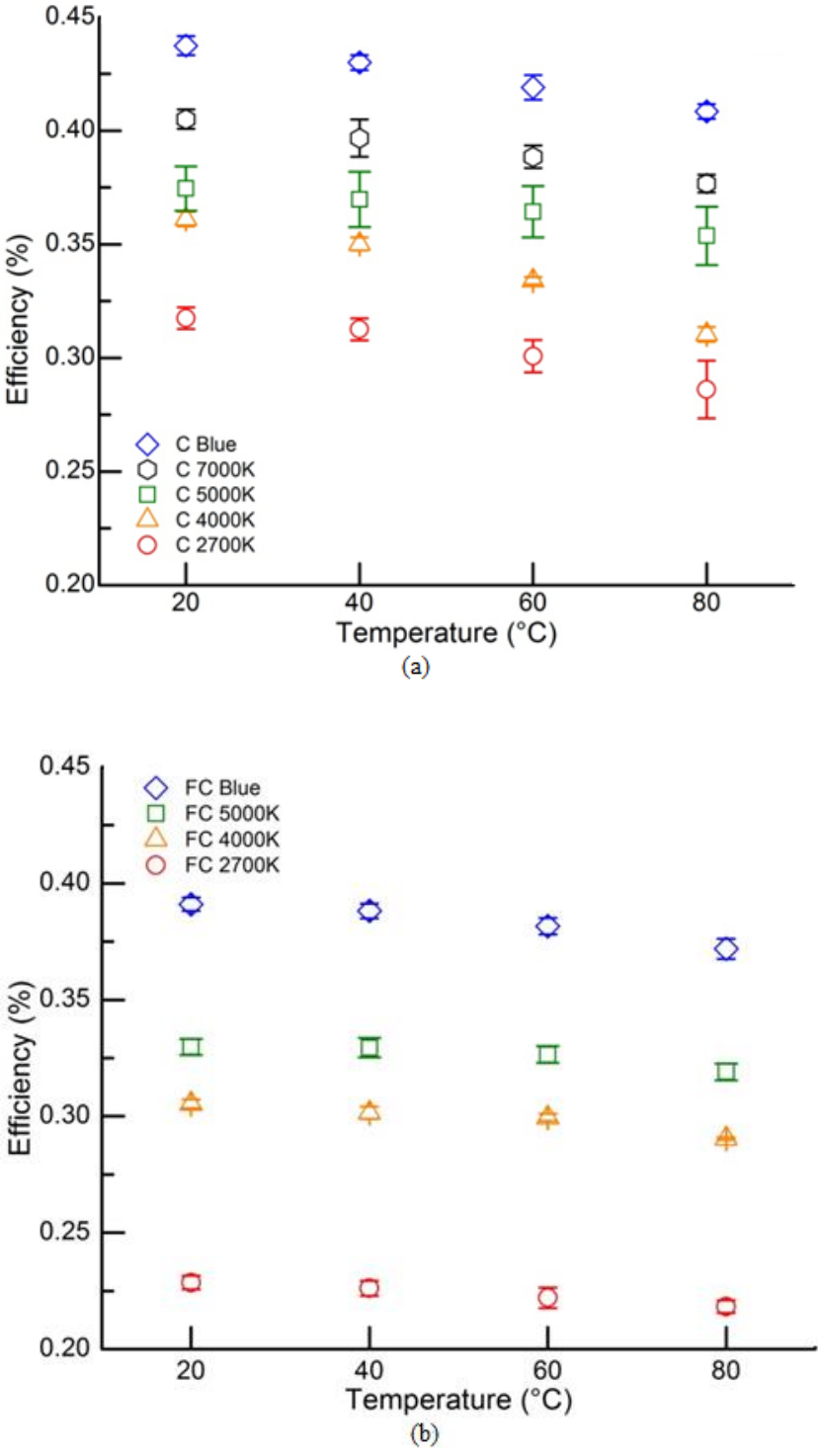

Fig. 4.2. Radiant efficiency of (a) conventional and (b) flip-chip bonded LEDs. Radiant efficiency reduces with respect to higher operating temperatures for all the CCT values.

In a pcLED package, the light emitted from the package is determined by both the LED device and the phosphor layer. To study the light extraction losses contributed by the phosphor layer, the yellow (phosphor) and blue (LED) light outputs are computed separately as yellow-blue ratio (YBR). The YBR is computed by evaluating the spectral power distribution for the respective LEDs based on the two decomposed peaks, one for the phosphor converted yellow light and the other for the blue light emitted from the LED.

Typically, a low CCT value would yield a high YBR due to a higher proportion of yellow light emission and vice versa. Generally, the YBR was observed to reduce with temperature for all the CCT values as shown in Fig. 4.3. The reduction of YBR at elevated temperature is assumed to be caused by the phosphor conversion efficiency, which decreases as the temperature increases. However, the YBR decay rate increases with higher CCT values for both the conventional and flip-chip bonded LEDs, with the implication that a thicker phosphor layer or a higher phosphor concentration increases the amount of light extraction losses. It is also possible that the different phosphor species used in the 2700 K CCT of both the C and FC LEDs may cause the change of YBR due to their different temperature-dependent and optical properties. The lower phosphor conversion efficiency and higher light extraction losses as the operating temperature increases may generate significant self-heating in the phosphor layer and cause the LED T_j to increase.

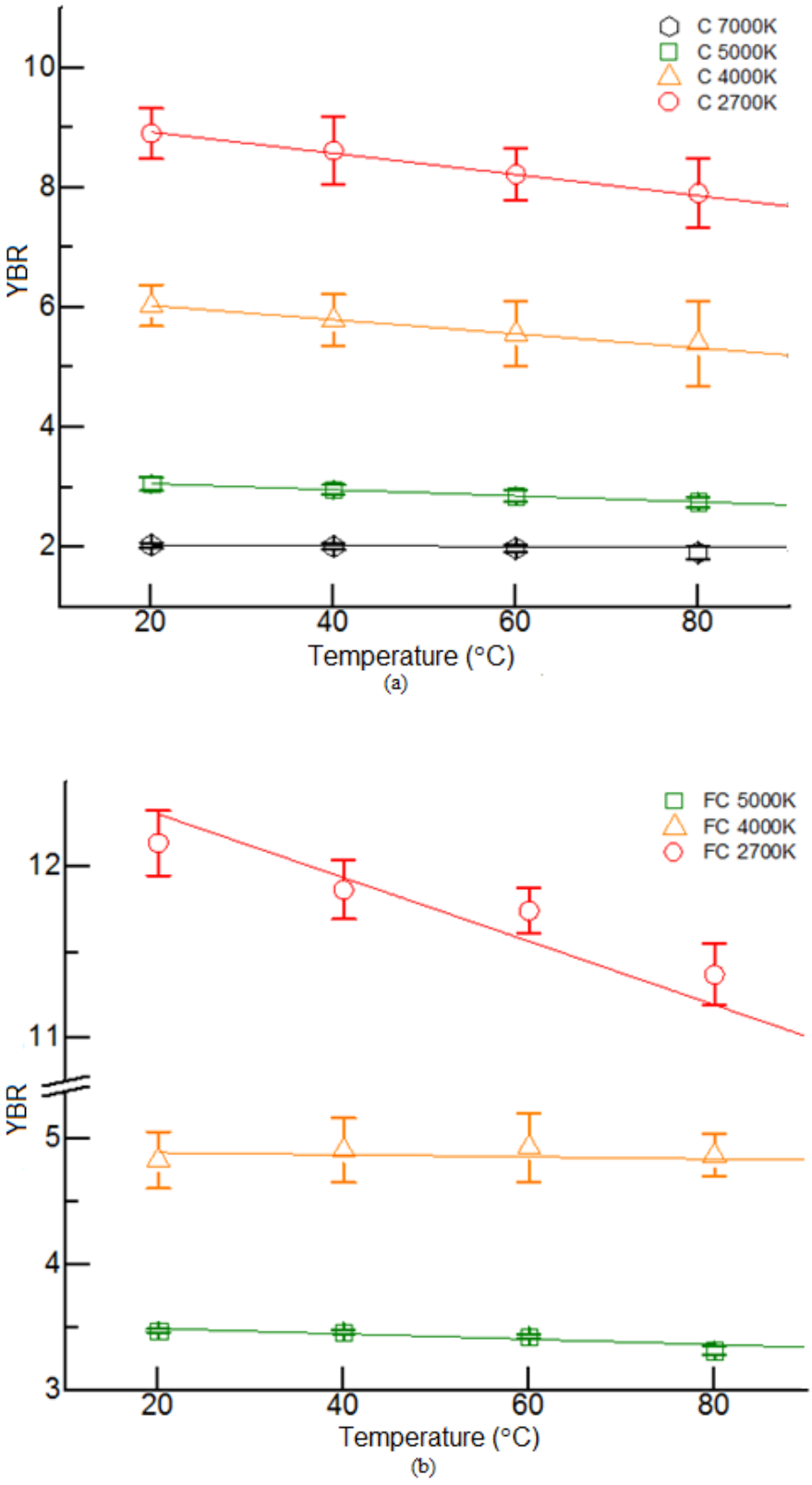

Fig. 4.3. Yellow-Blue ratio of (a) conventional and (b) flip-chip bonded LEDs. Significant YBR shift was observed for the 2700 K CCT as compared to the remaining CCT values.

To understand the implication of light extraction losses on the thermal response of the LED package, the T_j of the LED has been approximated using the electrical forward voltage method. The T_{rise} is the temperature difference between the LED's T_j with respect to the operating temperature. Both conventional and flip-chip bonded pcLEDs exhibit the same characteristics of a higher temperature rise with decreasing CCT as shown in Fig. 4.4. This phenomenon is attributed to 2 main factors; (i) low phosphor quantum efficiency, which induces phosphor self-heating, (ii) light absorption losses in the phosphor layer.

As presented in the literature review in Chapter 2, the thickness and concentration of the phosphor layer as well as the phosphor particle size are found to strongly influence the luminous efficacy. However, as the thickness or concentration in the phosphor layer increases, higher amount of light scattering and absorption losses is likely to occur. Together, these factors will exacerbate the heat load in the package, leading to significant temperature increase. This is clearly demonstrated for both sets of LEDs where the temperature rise increases by as much as ~2.6 times and ~1.4 times at 2700 K CCT for the conventional bonded and flip-chip bonded LEDs, respectively. This temperature rise has a direct impact on the R_{th} value since R_{th} is derived directly from the temperature rise. Accordingly, the R_{th} performance for both types of LEDs at the different operating temperatures is expected to exhibit similar trends to the temperature rise. A higher temperature rise will typically lead to a higher R_{th} value and this will imply greater heat accumulation and a larger temperature gradient that exists within the package.

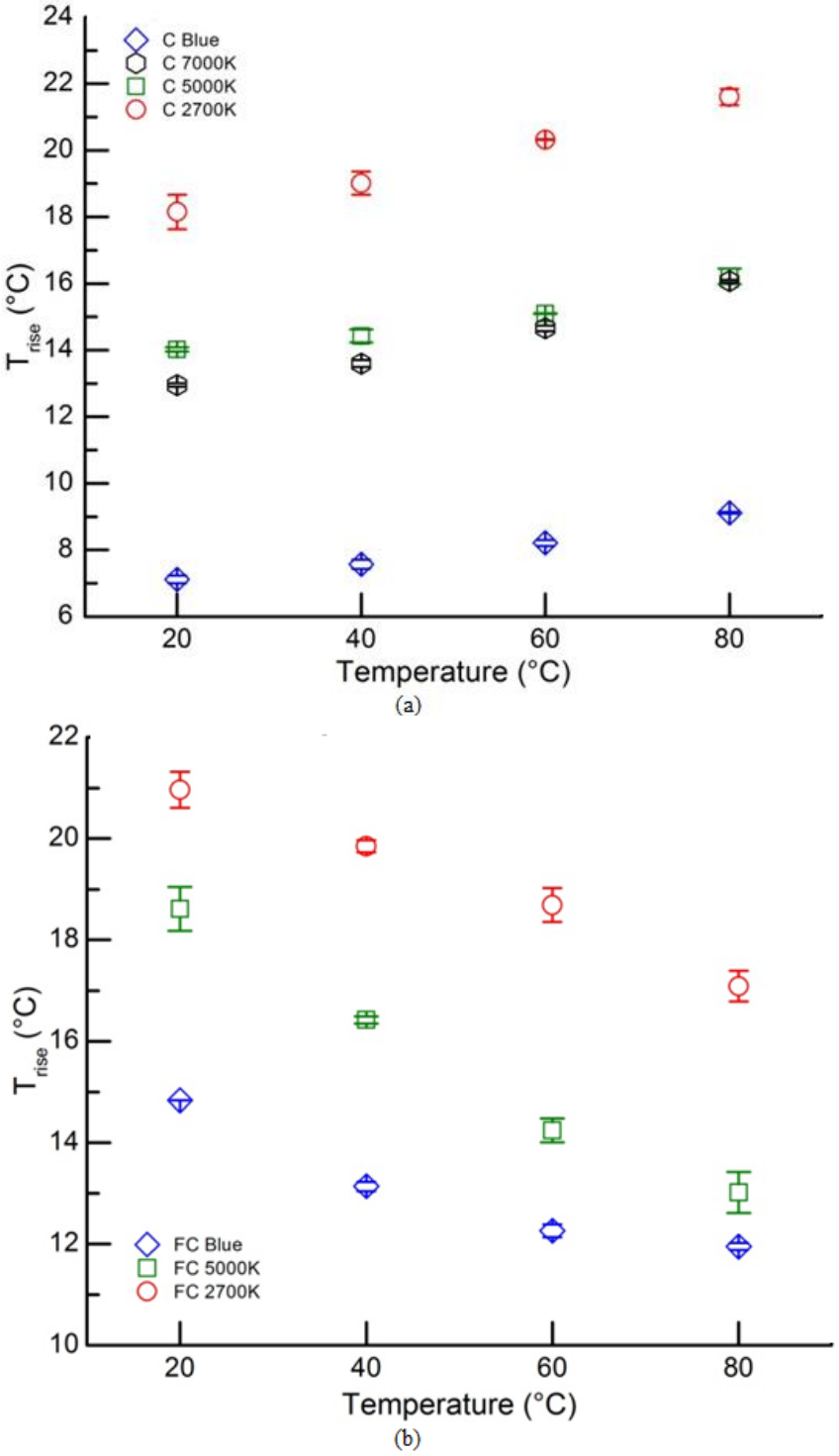

Fig. 4.4. Temperature rise of (a) conventional and (b) flip-chip bonded LEDs. Conventional bonding exhibits an upward temperature rise trend whereas flip-chip bonding can readily reduce the temperature rise due to its improved heat dissipation capabilities.

For the conventional bonded LEDs, an upward temperature rise and R_{th} trend is observed for all the CCT levels as the operating temperature increases. This means that the conventional bonded LEDs experience more heat accumulation within the package as the operating temperature increases. However, the flip-chip bonded LEDs showed an opposite downward response at all CCT levels. For the FC LEDs, the R_{th} exhibits a decreasing trend as the temperature increases. This conflicting result is observed is in spite of the fact that a higher operating temperature will increase the amount of non-radiative recombination processes, leading to even higher heat flux generation in the LED package. The differing temperature rise or R_{th} trend is attributed to its packaging architecture since the heat accumulated in the package depends not only on the heat generated by the LED device itself, but also on its heat dissipation capabilities. The results in Fig. 4.5 indicate the superior dissipation effectiveness for the flip-chip configuration.

It is worth noting that manufacturers currently report a fixed R_{th} value for all CCT values under a fixed operating temperature [7, 110]. However, the preceding investigations have shown that the R_{th} depends on the CCT values as well as operating temperature, which leads to a recommendation that reported R_{th} values in LED data sheets and test documents be stated alongside the corresponding CCT and operating temperature of the test conditions. These results are in line with studies demonstrating dependency on ambient temperature and CCT [111-113]. Inaccurate LED metrics reporting can be detrimental as overexposure to high temperature can adversely affect the lumens performance and service life span of the LED package [14].

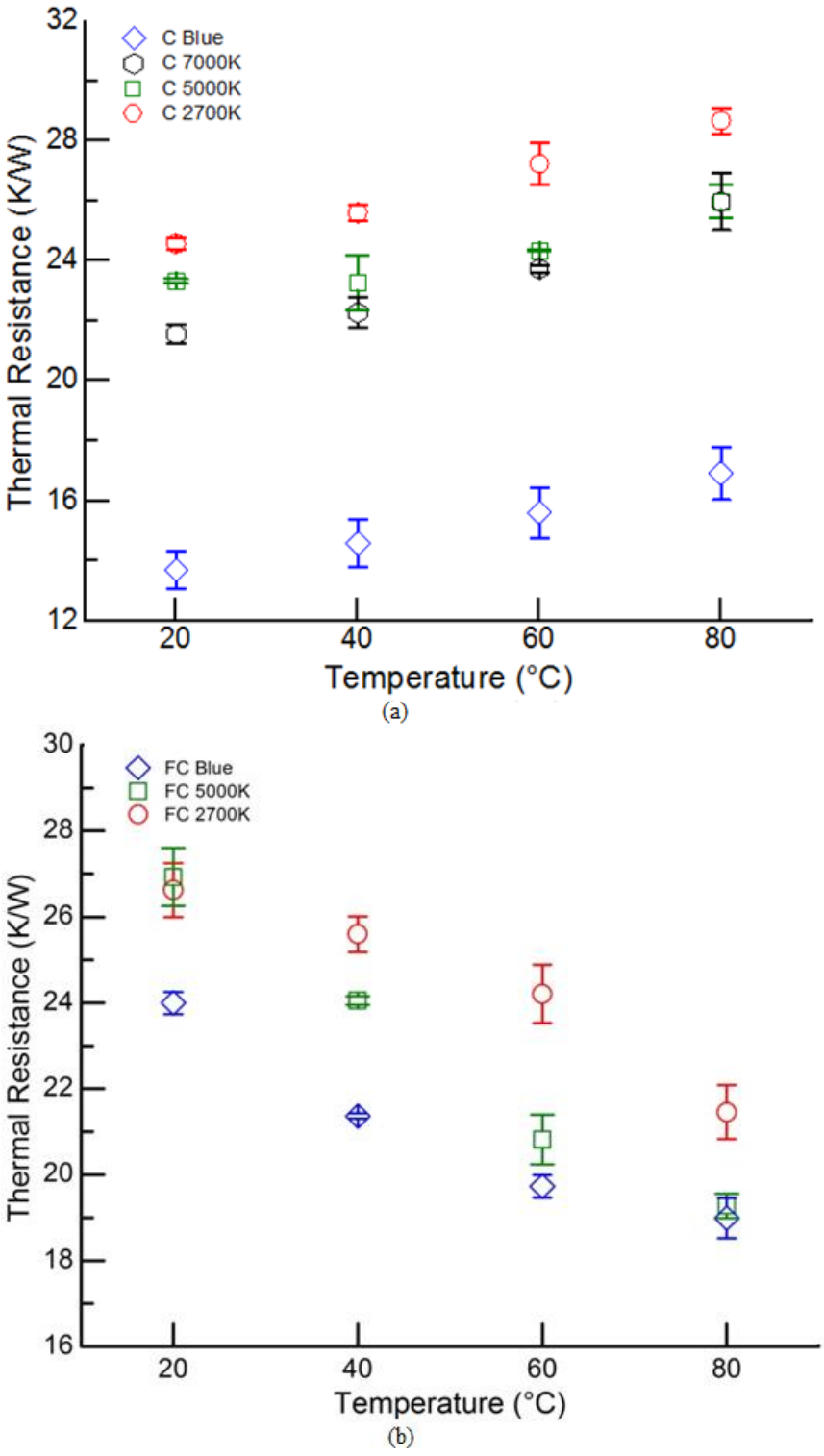

Fig. 4.5. Real thermal resistance of (a) conventional and (b) flip-chip bonded LEDs at different operating temperatures.

Although flip-chip bonding offers a more effective heat dissipating capability as compared to conventional bonded LEDs, the flip-chip bonded LEDs exhibit a slightly lower optical efficiency than the conventional bonded LEDs for all the CCT values. It is postulated that the flip-chip bonded LEDs have a higher total internal reflection (TIR) within the LED structure. For an effective comparison between the different die-bonding configurations, the total light extraction losses due to light scattering and absorption losses are computed with reference to their corresponding blue emitting LEDs and the normalized optical efficiency is depicted in Table 4.3. A higher phosphor concentration or a thicker phosphor layer increases the light trapping efficiency due to the higher probability of the blue light emitting from the LED interacting with the phosphor particles. The trapping of light lowers the light output substantially and causes higher heat generation. At 2700 K CCT, the flip-chip bonded LEDs exhibit a normalized optical efficiency of about 59% whereas conventional bonded LEDs have a higher efficiency of 74% as compared to their respective blue emitting LEDs. The higher light extraction loss for the flip-chip bonded LEDs is attributed to the higher amount of light scattering and back reflection of light from the high phosphor particle concentration in the phosphor layer. This finding substantiates Tran et al. [3]'s simulations that a thicker phosphor layer with lower concentration of phosphor particles can reduce the amount of light extraction losses. However, a lower light extraction loss does not translate to a lower temperature rise. In the case of the conventional bonded LEDs at 5000 K CCT, a low light extraction loss of about 12% can cause the LED T_j to increase by almost 2 times as compared to its blue LEDs. In comparison to the flip-chip bonded LEDs at the same CCT values, 15% light extraction losses only constitute 1.3 times increase of T_j.

Table 4.3. Optical and thermal comparison of LED Packages under different light emission properties. 7000K CCT Flip-chip LEDs are not part of product line at time of experimentation [7].

Colour	Conventional bonding/phosphor thickness variation			Flip-chip bonding/phosphor concentration variation		
	Efficiency	T_{rise} (^{o} C)	T_{rise} (relative)	Efficiency	T_{rise} (^{o} C)	T_{rise} (relative)
Blue	100%	7.1	1X	100%	14.8	1X
7000K	93%	12.9	1.8X			
5000K	88%	14.0	2.0X	85%	18.6	1.3X
2700K	74%	18.2	2.6X	59%	20.9	1.4X

When heat is generated in a material, i.e. LED device or phosphor particles, heat will accumulate in the material and the extent of temperature rise depends on the thermal properties of itself as well as the heat dissipating means within the package. Analogous to an electrical circuit, the heat flow path depends on the thermal conductivity of its materials and contact thermal resistance between adjoining materials. A thin and high thermal conductive material will transfer heat fluxes more effective than a thick and poor thermal conductor. For the blue emitting LED, the top surface of the LED device is exposed to air, which has much poorer thermal properties as compared to the packaging materials such as phosphors, silicone etc. Hence, the bulk of the heat generated in the LED device is dissipated downwards through the LED package. When phosphor is deposited over the LED, the additional heat source(s) from the phosphor layer increases the LED T_j. The physical presence of the phosphor layer and the packaging materials allow possible heat flow paths from the top of the LED package. Hence, to analyze the influence of the phosphor layer on the thermal response in the LED package, structure function evaluation of the blue LEDs and their corresponding pcLED packages were computed. Heat accumulation and the change of heat flow paths within the LED package are identified by analyzing the change of transient thermal response. In the case of the

conventional bonded LEDs (Fig. 4.6(a)), heat accumulation is observed from the merging of structure function peaks, which is the separation point between two thermally contrasting materials (Fig. 4.6(a) inset). As the phosphor thickness increases, the heat generated at the LED and phosphor layer intensifies due to the low phosphor quantum efficiency in addition to higher light extraction losses. The heat accumulation at the LED-phosphor layer region gradually converges and, at a low CCT rating of 2700 K, the heat flux generated by both the LED and phosphor layer dominate such that the thermal interfaces at the LED-phosphor layer region became indistinguishable. It was also possible that the heat generated in the phosphor layer first dissipated upwards and around the LED chip and then subsequently onto the AlN substrate.

As illustrated in Fig. 4.6(a), the heat generated by the GaN LED device is transferred to the AlN substrate through the thick sapphire material. Due to the poor intrinsic thermal conductivity of the sapphire material ($K_{Al_2O_3}$ ~46 W/m·K), there is significant heat accumulation within the GaN LED device. As such, the conventional bonded LEDs exhibit an upward temperature trend. On the other hand, flip-chip bonding allows effective heat transfer onto the AlN substrate due to the high thermal conductivity of the gold bumps (K_{Au} ~318 W/m·K). The heat generated by the LED is transferred effectively to the AlN substrate. Hence, the high optical loss in flip-chip bonded pcLEDs does not cause any significant changes to its thermal paths and merely exhibits a shift of partial R_{th} in the structure function evaluation as compared to its blue LEDs (see Fig. 4.6(b)). This shows that almost all the heat fluxes generated in the LED dissipated through the Au bumps and reinstates the fact that the packaging architecture has a significant influence on the temperature rise and thermal resistance of the package.

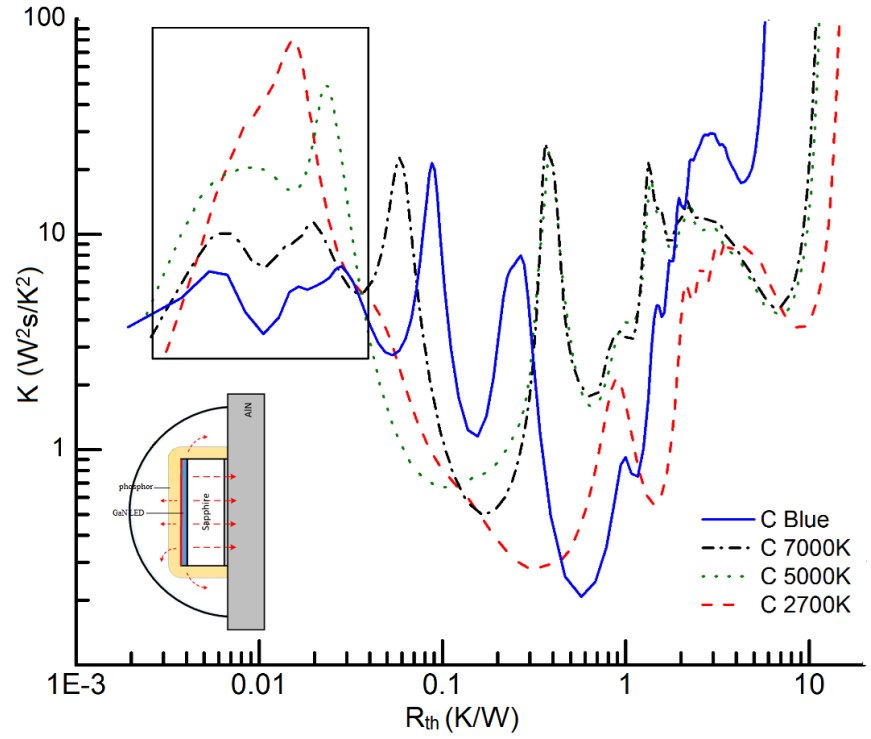

(a)

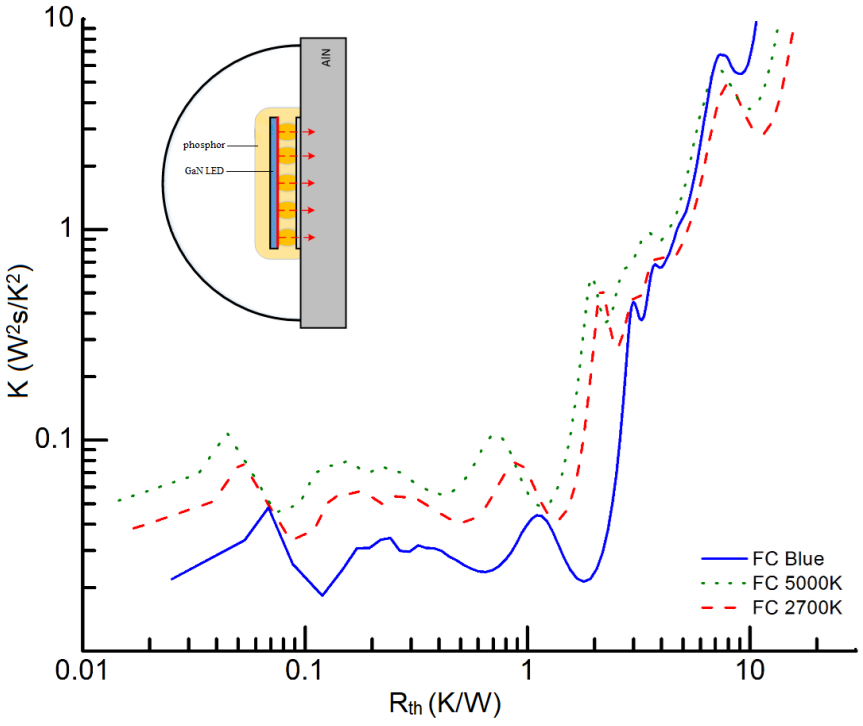

(b)

Fig. 4.6. Derivative structure function at 20 °C of (a) conventional (inset: heat accumulation at the phosphor-LED region can be observed when the phosphor layer thickens, leading to the merging of the structure function peaks), and (b) flip-chip bonded LEDs. The figures show the results for one LED at each CCT level and is representative of the findings for the samples tested.

4.3.2 Impact of Packaging Architecture

In this experiment to assess the impact of the packaging architecture, the light output of the blue and white LEDs was first measured at different operating temperature and drive current conditions. The radiant flux was found to increase both with higher current density and lower operating temperature. Since the forward voltage V_F changes with the operating condition, the light output efficiency of the LED is utilized for effective comparison. The efficiency is defined as the radiant flux emitted by the LED divided by the electrical input power supplied to the LED.

As described in Section (4.2.2), 20 samples each of blue and white LEDs for P1W, S1W and S03W were selected for experimentation. To establish the overall behaviour in Fig 4.7 and Fig. 4.9 to 4.11, the data points represent the mean value of the 20 samples used while the error bars represent the standard deviation of the mean. As shown in Fig. 4.7, the optical efficiency was observed to reduce with temperature and current density. The optical efficiency reduces more significantly with current density due to the higher amount of Joules heating [114-116] and Auger recombination processes [101, 102]. Table 4.4 shows the variation of the mean voltages with temperature demonstrating the temperature dependence of the LED forward voltage. Although the mean voltages for all the LEDs decrease with temperature, the overall efficiency still decreases due to the higher rate of nonradiative recombination leading to the corresponding radiant flux reduction, which means the radiant flux has a higher decrease compared to V_F with increasing temperature.

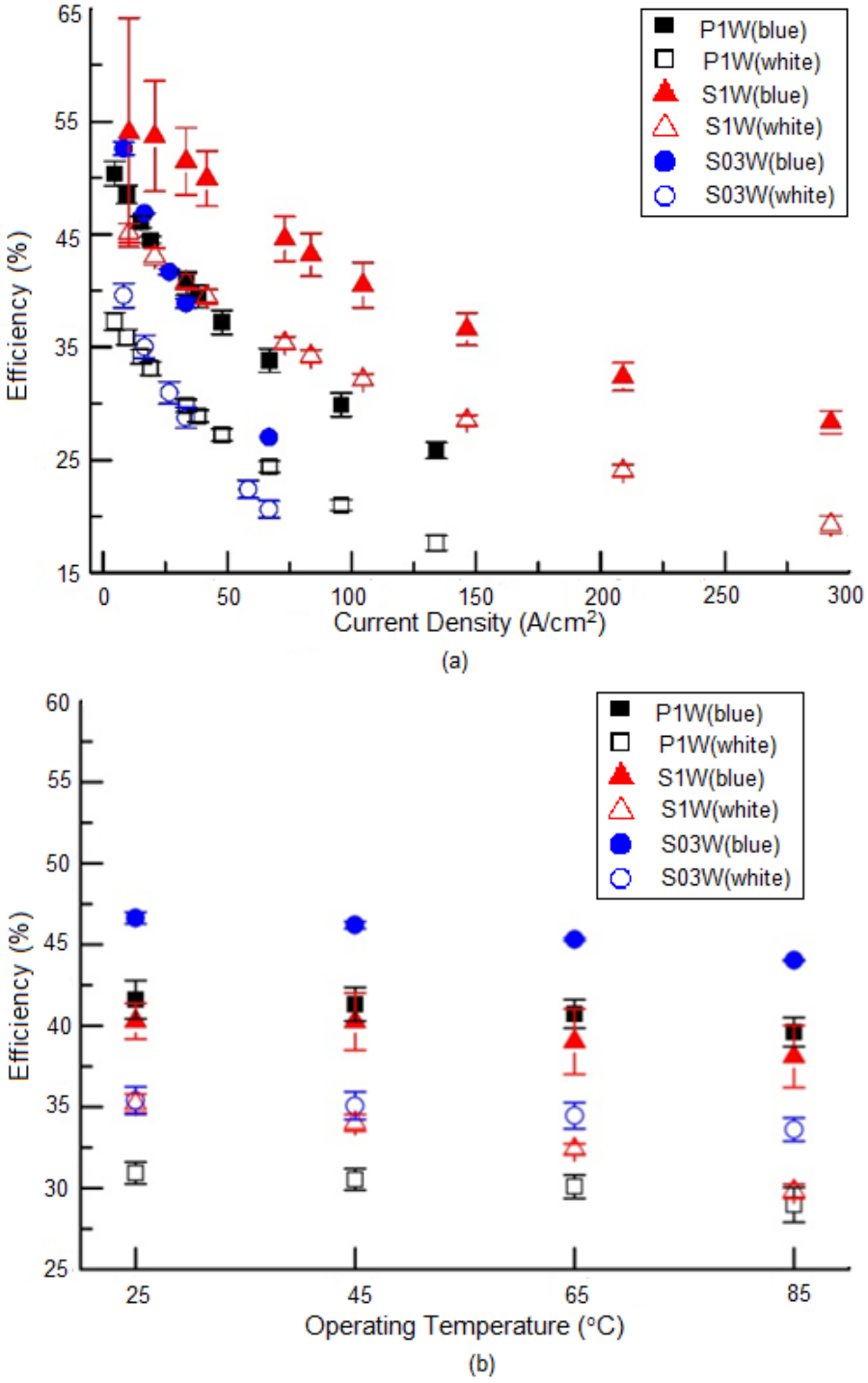

Fig. 4.7. Radiant efficiency of various LED packages at different (a) current densities at 20 °C and (b) operating temperatures.

Table 4.4. Temperature-dependent forward voltage of the LEDs decreases with temperature, with low variability from the mean indicated by the standard deviation.

	P1W		S1W		S03W	
Temperature	**Mean Voltage (V)**	**Standard Deviation (V)**	**Mean Voltage (V)**	**Standard Deviation (V)**	**Mean Voltage (V)**	**Standard Deviation (V)**
25 °C	2.971	0.021	3.071	0.084	3.047	0.022
45 °C	2.940	0.033	3.022	0.070	2.999	0.024
65 °C	2.890	0.019	2.967	0.067	2.962	0.025
85 °C	2.883	0.044	2.950	0.084	2.923	0.024

For a pcLED package, a layer of phosphor is usually deposited over the LED chip either in a dispersed or conformal approach. The light extraction efficiency depends on the phosphor down-conversion process (Stoke's energy loss) and package efficiency (light scattering and absorption losses). Due to these losses, the blue LEDs exhibit higher optical efficiency as compared to their associated white LEDs for all the operating conditions shown in Fig. 4.7. The total light extraction loss is calculated based on the difference in radiant efficiency between the blue and white LEDs. Both the P1W and S03W LEDs exhibit a higher light extraction loss of 10-11% as compared to about 5% for the S1W LEDs. Light emission studies (see inset of Fig. 4.8(b)) reveal that more direct blue light emission was observed through the phosphor layer for the S1W LEDs than the other two LED packages. As such, the amount of light scattering and absorption losses in the phosphor layer as well as the down-conversion processes are reduced. This resulted in lower light extraction losses for the S1W LEDs.

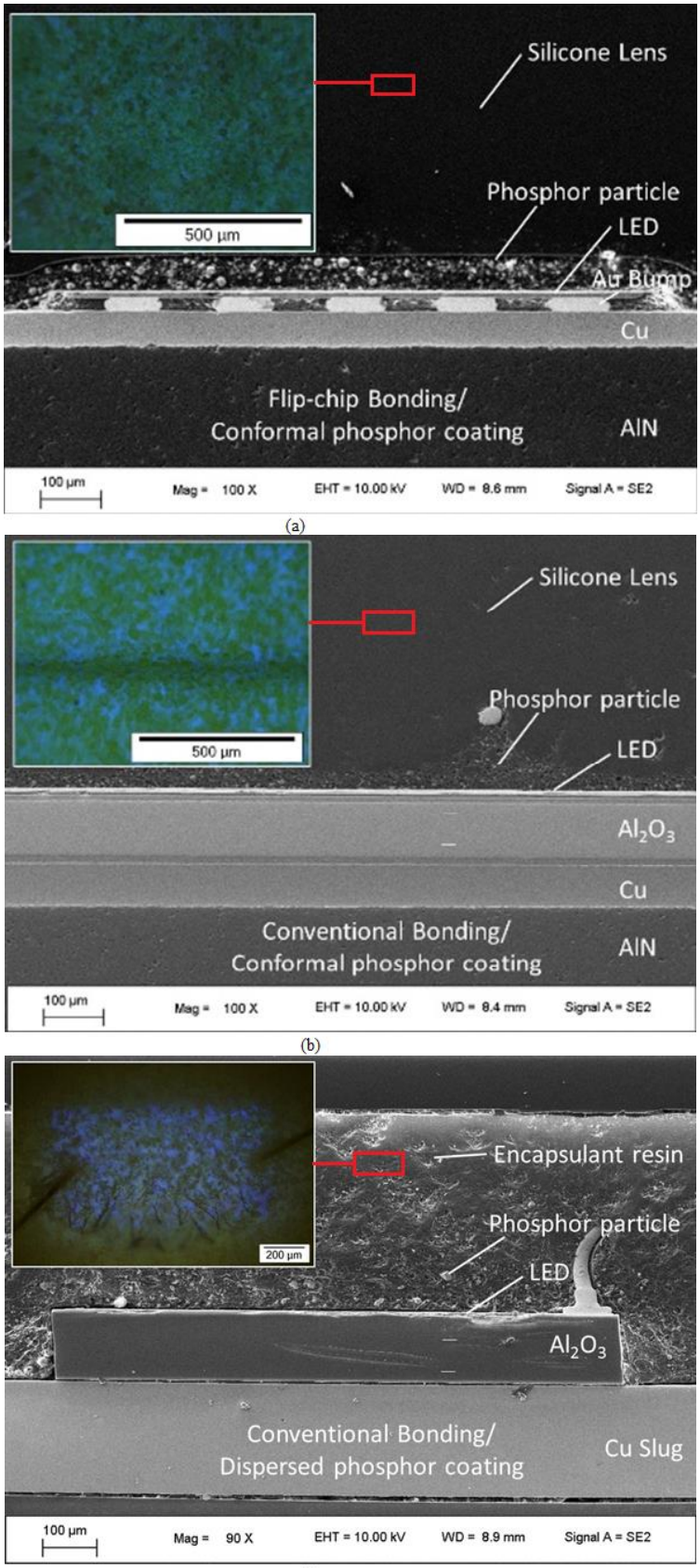

Fig. 4.8. Typical light emission (inset) and cross-sectional SEM images for one sample of each pcLED package (a) P1W, (b) S1W and (c) S03W. Direct blue light emission can be observed through the phosphor layer (yellow-orange emission).

To analyze the light emission contribution between the LED device and the phosphor material, YBR is utilized (Fig. 4.9). YBR is derived from the spectral power distribution where Y represents the yellow emission from the phosphor material and B represents the blue emission from the LED. The S1W pcLEDs exhibit the lowest YBR value as compared to the other two LED packages. As shown in the inset image of Fig. 4.8(b), this is due to the larger amount of blue light emission escaping through certain regions of the phosphor layer. As temperature increases, the disproportionate contribution of light emission between the LED device and the phosphor layer will cause the chromaticity properties i.e. CCT and YBR to change. It is observed that the P1W LEDs exhibit a fairly stable YBR with higher operating temperature whereas the YBR decays significantly for both S1W and S03W LEDs. This may be attributed to the uniform distribution of phosphor particles over the P1W LED, providing a more consistent down-conversion of yellow light emission across the phosphor layer. Hence, the S1W pcLEDs exhibit a much more significant YBR decay. It is also possible that the YBR decays with temperature due to lower phosphor conversion efficiency [117].

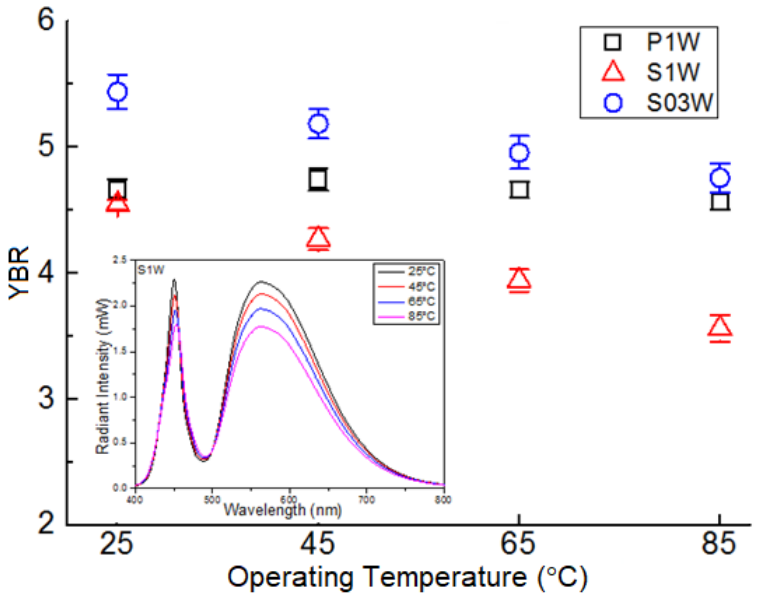

Fig. 4.9. YBR of different white pcLED packages as a function of operating temperatures. (Inset: Typical spectral power distribution of white pcLED package).

To evaluate the thermal performance of the LED package, the self-heating effect and heat dissipation capabilities are analyzed in terms of relative junction temperature rise T_{rise} and thermal resistance R_{th}. In response to the efficiency drop with operating temperature (see Fig. 4.7(b)), a higher LED T_j was expected. As shown in Fig. 4.10, it is also observed that the white LEDs exhibit a higher temperature rise as compared to their respective blue LEDs. As the white LEDs exhibit lower optical efficiency due to the light extraction losses incurred in the phosphor layer and their associated packaging materials, these light extraction losses will inevitably increase the LED T_j. Interestingly, as the operating temperature increases, the S1W and S03W LEDs both exhibit a higher junction T_{rise} whereas an opposite trend is observed for the P1W LEDs. The downward T_{rise} trend is in spite of the fact that higher operating temperature increases the amount of non-radiative recombination processes in the LED, leading to higher heat flux generation in the package. However, as temperature increases, V_F of the LED reduces and this will lower the heat generation due to the lower electrical input power. Furthermore, the LED T_j depends not only on the heat generated by the LED device, but also on its heat dissipating means. As shown in Fig. 4.8(a), the GaN LED device for the P1W is flip-chip bonded onto the AlN substrate via gold bumps. The heat generated by the LED is transferred effectively to the AlN substrate due to the high thermal conductivity of the gold bumps (k_{Au}~318 W/m·K). On the other hand, for the S1W and S03W LED packages, the GaN LED device is grown onto a sapphire substrate ($k_{Al_2O_3}$~46 W/m·K) and is then die-bonded to the AlN substrate. Due to the low thermal conductivity of the thick sapphire, the heat generated in the GaN LED device is accumulated within the material. Although the V_F of the S1W and S03W LEDs also reduces with temperature, their heat dissipating capabilities are not as efficient due to its conventional die-bonding configuration. This causes the heat to accumulate within the GaN LED device, resulting in higher LED T_j. As such, both S1W and S03W LEDs exhibit an upward temperature rise trend.

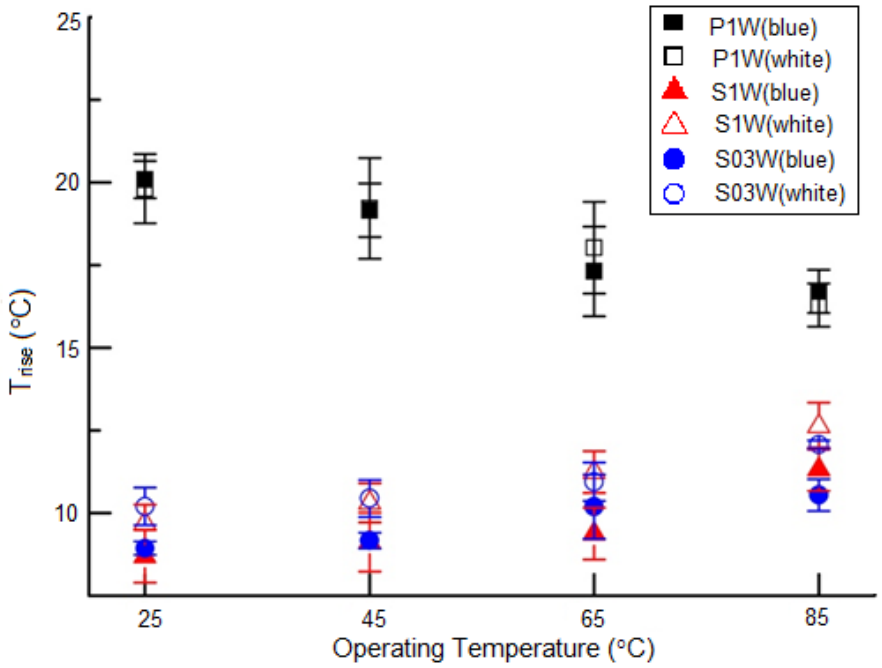

Fig. 4.10. LED junction temperature rise of blue and white LED packages at various operating temperatures.

As shown in Fig. 4.11, the R_{th} of the LED packages correlates with the trend of the junction temperature rise. An increase of R_{th} means there is a build-up of heat accumulation within the LED package. The S03W LED packages exhibit a much higher R_{th} value as compared to the other two LED packages. The significant heat accumulation in the LED package causes the light output to decrease and explains the YBR decay with higher operating temperature. The R_{th} for all the different LED packages is observed to exhibit an inverse relationship with the YBR as a function of operating temperature (see Fig. 4.9). At higher operating temperatures, an increase of Stoke's energy and light extraction losses will lower the YBR and increase the LED T_j and R_{th} accordingly. This further shows that the inter-dependency between the optical and thermal characteristics in a pcLED package. By alleviating the heat accumulation in the package, higher photometric and more stable colorimetric properties can be achieved.

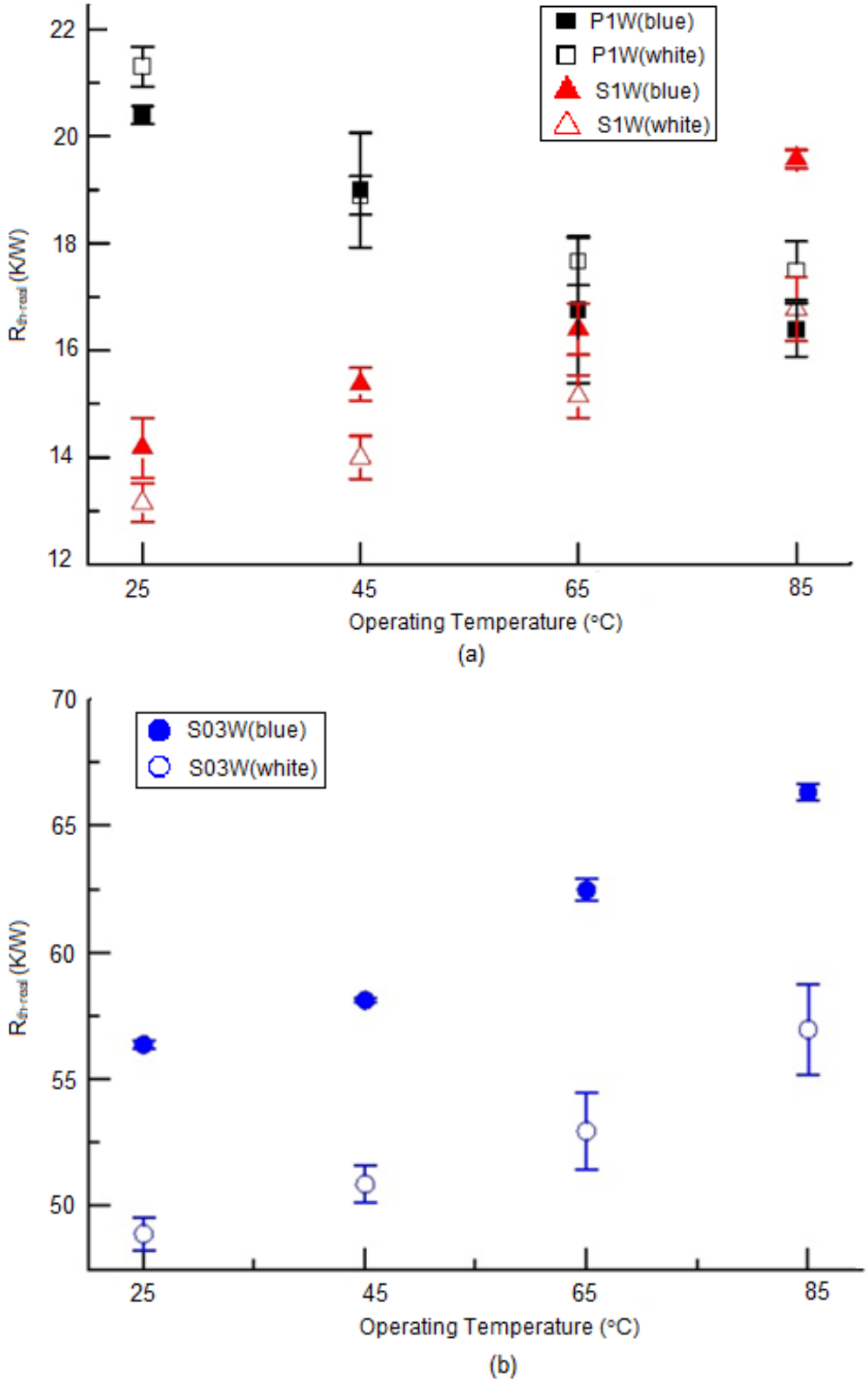

Fig. 4.11. Thermal resistance of (a) P1W & S1W and (b) S03W LED packages at different operating temperatures.

4.4 Summary

The two experiments in this chapter demonstrate the effect of the phosphor layer and the die-bonding configuration on the optical and thermal performance of the LED. The first experiment highlights the impact of phosphor concentration and thickness on both the photometric and colorimetric qualities of conformal phosphor coated LEDs and the subsequent thermal effects with different bonding configurations. It has been shown that white light emission with various colour qualities can be attained by varying the phosphor particle concentration or thickness of the phosphor layer in a pcLED package. A thicker phosphor layer and a higher phosphor particle concentration increases the amount of light trapping due to light scattering and back reflection of light. The light extraction losses in the phosphor layer induce heat accumulation at the phosphor layer and increase the temperature and R_{th} in the LED package. Hence, the R_{th} of the LED package changes with the CCT values. However, the temperature rise and R_{th} can be reduced with a flip-chip die-bonding configuration where the heat generated in the LED chip and phosphor layer is dissipated effectively onto the AlN substrate. This is verified by observing the thermal paths in the structure function evaluation of both flip-chip and conventional die-bonding configurations. As the R_{th} of the LED package is found to change with different operating temperatures, CCT values and die-bonding configurations, there is a need to provide detailed thermal information for different LED packages. Insufficient or inaccurate reporting of thermal data may change the photometric and colorimetric properties of the white light emitted from the LED package.

In the second experiment, it has been shown that the packaging method is critical in enhancing the light extraction efficiency and heat dissipation capabilities in high-power LED applications. The uniformity and concentration of the phosphor particles affects both the optical efficiency and colour quality. A non-uniform and sparse phosphor layer causes the YBR to shift significantly due to the disproportionate contribution of light emission between

the LED and phosphor layer. It was also observed that the YBR exhibits an inverse relationship with R_{th}. A higher Stoke's energy and light extraction losses will increase the LED T_j, causing higher heat accumulation within the package. The amount of heat accumulation depends on the die-bonding configuration and heat dissipation capabilities within the package. Flip-chip die-bonding can reduce the LED junction temperature rise and R_{th} under higher operating temperature due to the superior heat dissipation capabilities.

Chapter 5

Effect of Humidity

5.1 Introduction

Besides drive current and operating temperature, high humidity can also lead to internal build-up of heat and subsequent damage of the LED package. Moisture infuses into the interfaces of packaging material resulting in a number of issues which may cause a decrease in light output [57] or a change in the colour output [58]. Moisture inside LED packaging may also cause R_{th} to increase, for example due to delamination between chip and substrate causing impedance to the heat flow [59, 60]. This exacerbates the package's thermal load, bringing about a corresponding increase in T_j.

This chapter focuses on the impact of long-term humidity effects on three different types of LEDs based on their power rating (1 W or 0.3 W), die-bonding configuration (flip-chip or conventional) and phosphor coating method (conformal and dispersed). The goal of the experiments is to understand the implications of high moisture environments on the electrical, optical and thermal (EOT) performance of the different LED packages. Chapter 6 thereupon builds on this information to develop a humidity based prognostication model.

5.2 Experimental Setup and Procedures

5.2.1 Instrumentation Setup

Electrical, optical and thermal measurements conducted in this chapter were done using the same integrated LED measurement system represented in Fig. 3.1 (Chapter 3) consisting of a Labsphere 20” integrating hemi-sphere system, a Keithley 2602A Source Meter, a Mentor Graphics T3ster, and a Peltier-based temperature controller (TEC). To ensure traceable optical

measurement, reference lamp calibration and absorption correction were conducted prior to each measurement. In addition, electrical I-V measurement was conducted prior to and after the optical-thermal measurements to ensure that device did not degrade significantly during testing. Capacitance-voltage (C-V) tests for the LED heterostructure degradation were conducted using a Keysight E4990A Impedance Analyzer. In-depth failure analyses of the samples were done by means of Scanning Electron Microscopy with Energy Dispersive X-ray Spectrometry (SEM–EDX). Humidity reliability aging tests were conducted using the CTS Climatic Test System environmental cabinets.

5.2.2 Experimental Procedures

As in Chapter 4, the same three sets of pcLED packages – 1 W (Philips P1W and Seoul Semiconductor S1W) and 0.3 W (Seoul Semiconductor S03W) rating – are used. The LEDs have different configurations in terms of power rating, die-bonding and phosphor coating methods, as summarized in Table 5.1. Details of these configurations including their graphical representations have been disclosed in Chapter 4.

Table 5.1. Configurations of LEDs used in experiments.

LED	Power Rating	Die-bonding Configuration	Phosphor Coating
P1W	1 W	Flip-chip	Conformal
S1W	1 W	Conventional	Conformal
S03W	0.3 W	Conventional	Dispersed

As recommended in IES TM-21 standard [65] which stipulates the procedures for projecting long term LED lumen maintenance for at least 6000 h, a sample size of 20 was used for each LED (P1W, S1W and S03W) at each humidity level (10% and 85% relative humidity). To simulate actual environmental conditions, the selected humidity condition of 85% is within the range of daily relative humidity levels in several countries in Southeast Asia [118]. The LED packages were mounted onto heatsinks and placed into the environmental test chambers preset at 10% and 85% relative humidity (RH) at a temperature of 55 ºC, driven at a bias current of 350 mA for the 1 W LEDs (P1W and S1W) and 100 mA for the 0.3 W LED (S03W). Electrical, optical and thermal measurements were conducted using the integrated LED measurement setup at every 1000 h interval up to 8000 h.

On completion of the 8000 h humidity aging tests on all the LED packages, the integrated LED measurement system described in Section (5.2.1) was used to evaluate the electrical-optical-thermal properties of the LED packages. The same bias currents (350 mA for P1W and S1W, 100 mA for S03W) were applied for the optical and thermal measurements, while the optical and electrical measurements were conducted at 20 ºC. Capacitance-voltage measurements were conducted at 20 ºC with the LEDs biased from −7 V to 2 V.

In Fig. 5.1, 5.2, 5.3 and 5.7, each data point represents the mean value of the 20 samples tested for the specified LED while the error bars show the standard deviation from the mean. The rest of the figures depict the performance for individual LEDs but are representative of that for the entire sample tested.

5.3 Results and Discussion

5.3.1 Optical Characteristics

Depreciation of optical characteristics is related to both the chip and package degradation. At the chip level, the decrease in optical power is attributed to increased non-radiative recombination processes due to the generation of defects in the active region. This in turn leads to increased heat losses and higher T_j. At the package level, dissolution of the phosphor and discoloration of encapsulation materials [58, 119] are mechanisms that could exacerbate the optical output degradation.

The humidity based degradation of the both radiant flux and luminous flux of both types of LEDs is shown in Fig. 5.1 and Fig. 5.2. The radiant flux is the total radiant or electromagnetic energy emitted by the LED in watts while the luminous output is the perceived power of light adjusted to reflect the varying sensitivity of the human eye to different wavelengths of light measured in lumens. While both these interchangeable quantities indicate the optical performance of LEDs, they provide specifically different information on the light output. Radiant flux characterizes light physical in terms of the energy in the light waves, while luminous flux characterizes how light is perceived by humans [120]. Both these quantities are measured by means of the integrating sphere and spectro-radiometer at 1000 h intervals until 8000 h with the experimental procedures specified in Section (5.2.2). The test methodology abides by the LM80-08 [97] test procedure for photometric measurement of LEDs, which provides a standard for the consistent use of methods and physical test conditions for the LED industry.

In Fig. 5.1 and Fig. 5.2, each data point on the dotted line represents the mean value of 20 samples while the error bars represent the standard deviation of the mean. The dotted line represents the trend of the sample mean for each 1000 h interval measurement. As the least squares curve fit method is prescribed by the TM-21 [65] standard for projecting the long term light output maintenance of LED light sources for minimum 6000 h duration (or until the light output decreases to a stipulated level), only the lumen and radiant light output data over the 8000 h test period was used to produce the straight line in Fig. 5.1 and Fig 5.2 with the general equation:

$$y = mx + c \tag{5.1}$$

For a set of n experimental data points represented by (x, y), m is the slope of the graph (which is used to derive the lumens and radiant flux degradation rate in Table 5.2) and c is an intercept of the straight line graph.

$$m = \frac{n\sum xy - \sum x \sum y}{n\sum x^2 - (\sum x)^2} \tag{5.2}$$

$$c = \frac{\sum y - m\sum x}{n} \tag{5.3}$$

To normalize the data to [0, 1] in Fig. 5.1 and Fig 5.2, the following formula was applied:

$$E' = \frac{E - E_{min}}{E_{max} - E_{min}} \tag{5.4}$$

where E' is the value to be normalized, E the original raw value, E_{min} the minimum value in the data set or range, and E_{max} the maximum value in the data set or range. The use of both Microsoft Excel and OriginPro software was used in the data analysis, curve fitting computations and graph productions. This methodology is explored further in Chapter 6 in relation to the development of a humidity based degradation model (HBDM) [121] .

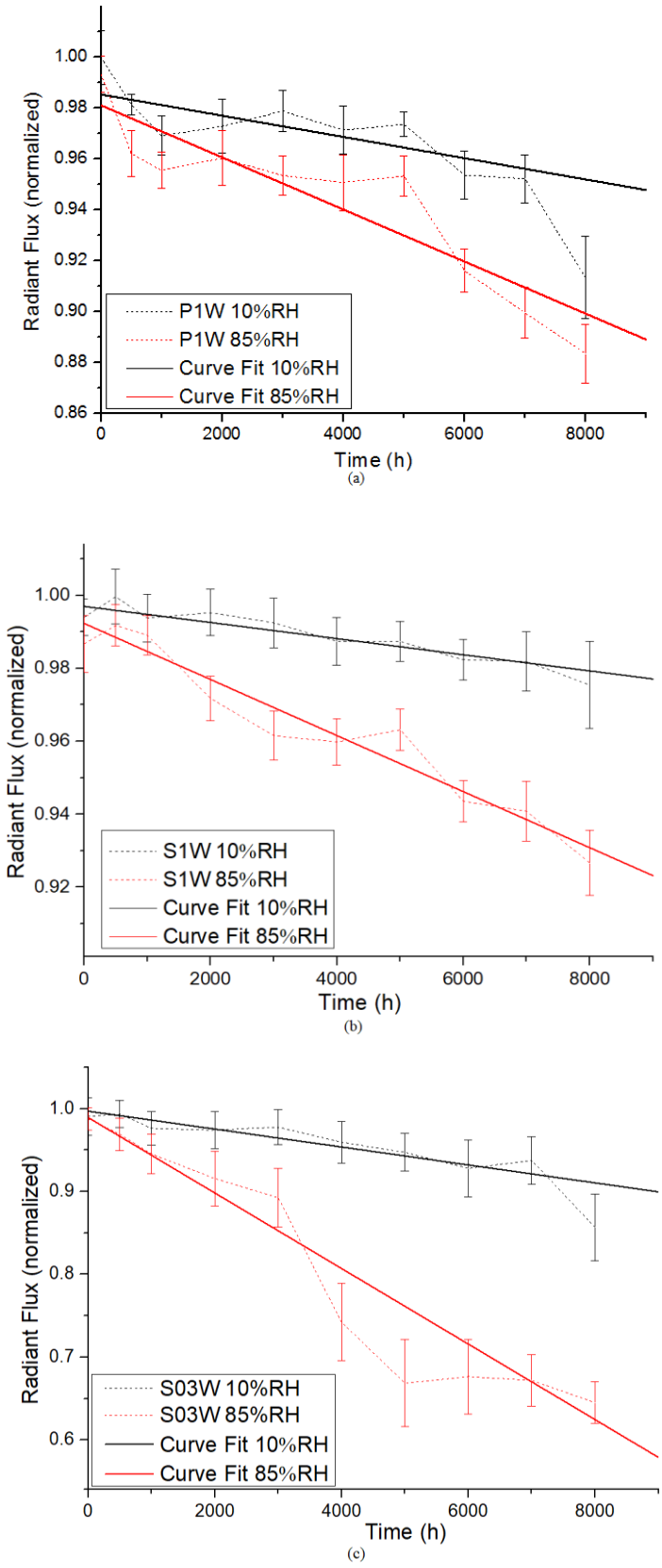

Fig. 5.1. Radiant flux degradation of (a) P1W, (b) S1W and (c) S03W at 10% RH and 85% RH. Radiant flux data is normalized into the interval [0,1]. The dotted line shows the trend of the sample mean.

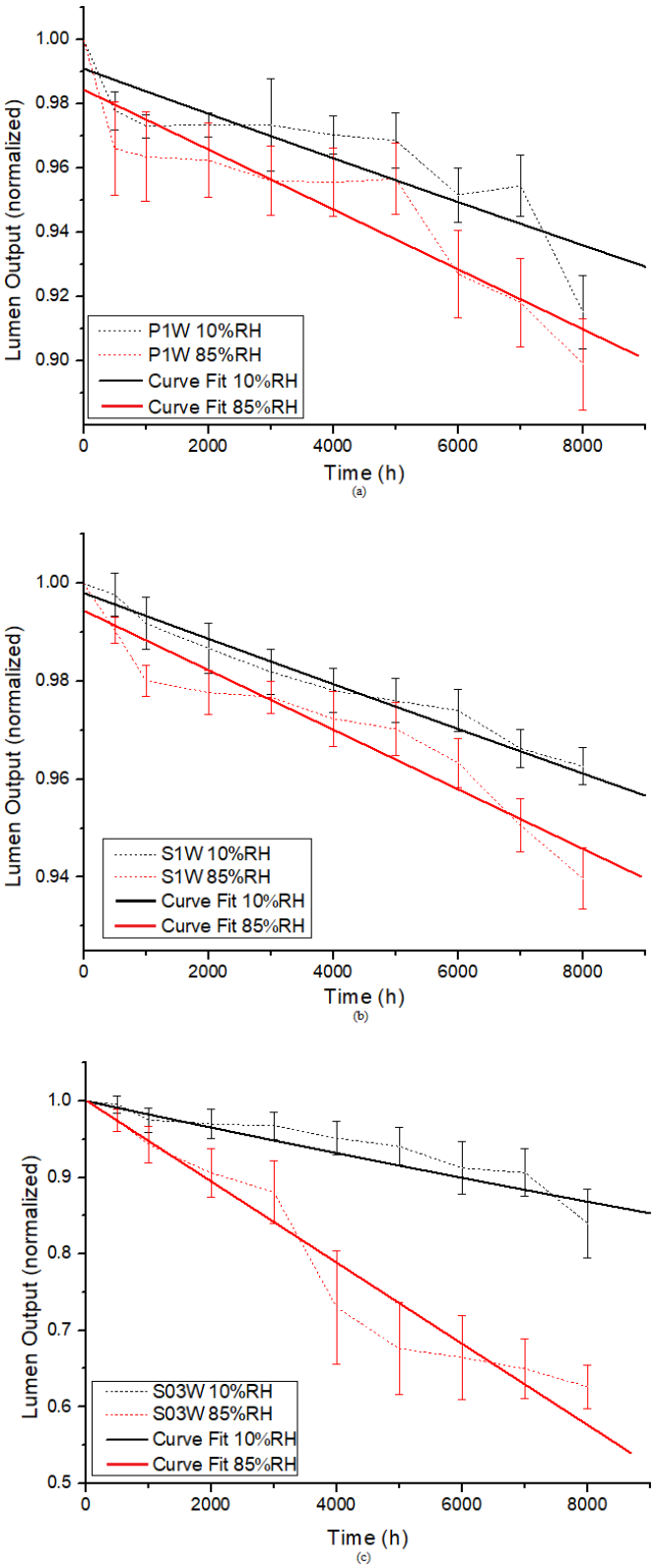

Fig. 5.2. Lumens degradation of (a) P1W, (b) S1W and (c) S03W at 10% RH and 85% RH. Lumen output data is normalized into the interval [0,1]. The dotted line shows the trend of the sample mean.

All the LEDs exhibit a high external quantum efficiency at both relative humidity (RH) levels and both radiant power and luminous flux have a higher rate of degradation with time at 85% RH. The results in Table 5.2 indicate that the higher relative humidity results in a higher amount of degradation for all LEDs. It is observed that the S03W has a much more severe degradation rate at 85% RH compared to the 1 W LEDs. This is in line with the observations of the electrical characteristics (Section (5.3.2)) in that the change in series resistance is much more pronounced for S03W indicating a different failure mechanism from the 1 W LEDs. It is postulated that the suspected package deterioration is responsible for the significantly higher optical degradation seen. Investigation by failure analysis to confirm this failure mode in S03W is reported later in this chapter.

Table 5.2. Computations of the degradation rates (in Fig. 5.1 and Fig. 5.2) for various LEDs at differing RH levels for 8000 h (using Equation 5.2).

LED	**%RH**	**Lumens Degradation Rate**	**Change in Lumens Degradation Rate**	**Radiant Degradation rate**	**Change in Radiant Degradation Rate**
P1W	10	7.145E-06	2.772E-06	1.341E-6	1.946 E-06
	85	9.917E-06		3.287E-6	
S1W	10	4.702E-06	1.495 E-06	8.218E-7	1.934 E-06
	85	6.197E-06		2.756E-6	
S03W	10	1.765E-05	4.708 E-06	1.169E-6	3.756 E-06
	85	6.473E-05		4.924E-6	

In a phosphor converted LED package, the light emitted from the package is determined by the LED device, the phosphor layer and the packaging materials [122]. To further examine optical degradation contributed by the phosphor layer and the LED, the blue (LED) and yellow (phosphor) light outputs are computed separately as yellow-blue ratio (YBR). Fig. 5.3 shows the comparison of YBR of all the LEDs at 10% RH and 85% RH. The data points represent the mean values of the 20 samples tested for each LED.

For both P1W and S1W, the samples at 85% RH stress demonstrate higher YBR than 10% RH, indicating a higher yellow emission than blue emission at higher humidity. This suggests that LED degradation may be more pronounced than phosphor degradation at the higher humidity level. Table 5.3 tabulates the change in YBR over 8000 hours of the S1W and P1W are about 3.4 and 2.4 times at 85% RH compared to 10% RH respectively. As shown by Tan et al. [58, 123], the reduction of blue light output may indicate LED chip degradation as a possible predominant failure mechanism in the two 1 W LEDs. On the other hand, for the S03W, the YBR trend is reversed, i.e. the YBR decreases for both 10% and 85% RH. This change in YBR is more significant at about 4.6 times higher for 85% RH over 10% RH. In contrast to the 1 W LEDs, the decrease in yellow emission may indicate deterioration of the phosphor layer or packaging materials [124], which is consistent with the inference from the electrical results. Under high humidity conditions, it is postulated that moisture content affects the functioning or efficiency of the phosphor layer [125-128].

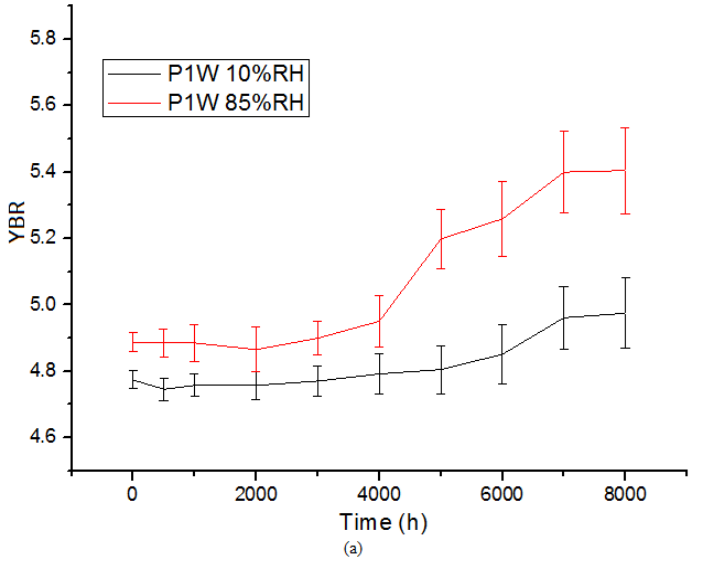

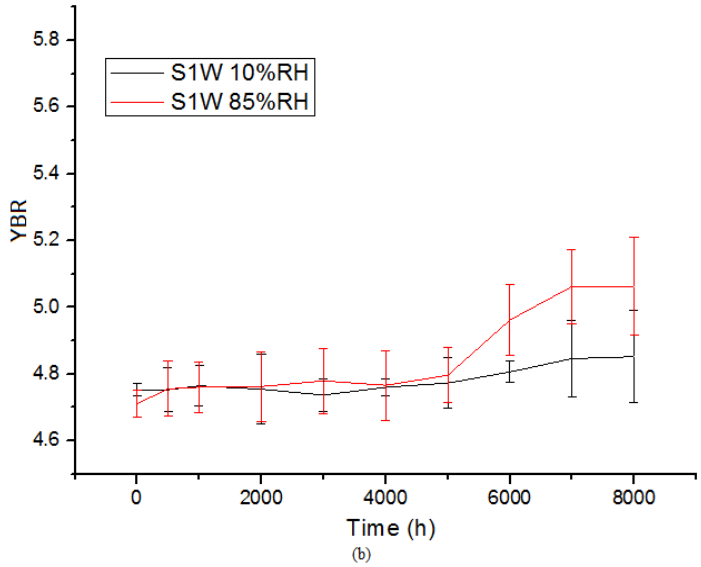

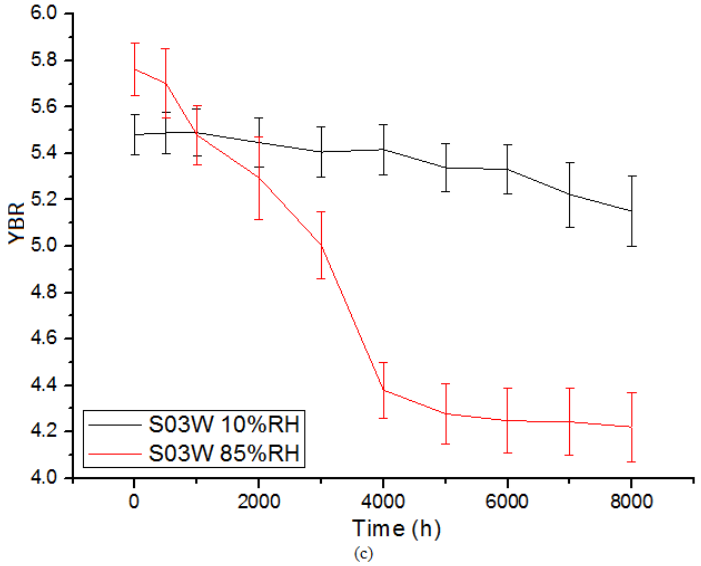

Fig. 5.3. YBR of (a) P1W, (b) S1W and (c) S03W at 10% RH and 85% RH.

Table 5.3. Change in YBR over time and RH levels computed from the data points (mean values of YBR) used in Fig. 5.3.

LED	YBR change over 8 Kh @10% RH (a)	YBR change over 8 Kh @85% RH (b)	Ratio of YBR change between RH [(b)/(a)]
P1W	0.204	0.502	2.460
S1W	0.102	0.351	3.441
S03W	-0.331	-1.547	-4.673

To provide further insight into the YBR trends, the normalized spectral power distribution (SPD) characteristics of the LEDs at both RH levels are derived as shown in Fig. 5.4. All three sets of LEDs exhibit a blue peak emission of ~450 nm and yellow peak emission of ~600 nm. The S1W LED maintains both higher blue and yellow intensity throughout the test period compared to the P1W LED even as the humidity level increases. In contrast to the 1 W LEDs, the yellow intensity of the S03W LED is seen to degrade much more severely, in particular at 85% RH. The absolute change in the YBR or ΔYBR appears to have a positive correlation with the lumen degradation rate and is explored in detail in Chapter 6.

While the decrease of both blue and yellow emission in the LEDs are related to both chip failure and phosphor degradation, the more pronounced reduction in blue over yellow intensity for the 1 W LEDs at 85% RH may indicate chip failure as a primary failure mechanism while severe reduction in the yellow emission of the S03W suggests a failure mechanism involving the packaging/phosphor layer. In addition, the more pronounced increase in series resistance R_S at 85% RH compared to 10% RH for S03W (discussed in the next section) possibly indicates degradation of the electrical properties of the devices due to increased resistivity of the contact and to the degradation of the properties of the ohmic contacts [129]. Failure analysis is subsequently performed (described in Section (5.3.4)) to investigate the cause of failure.

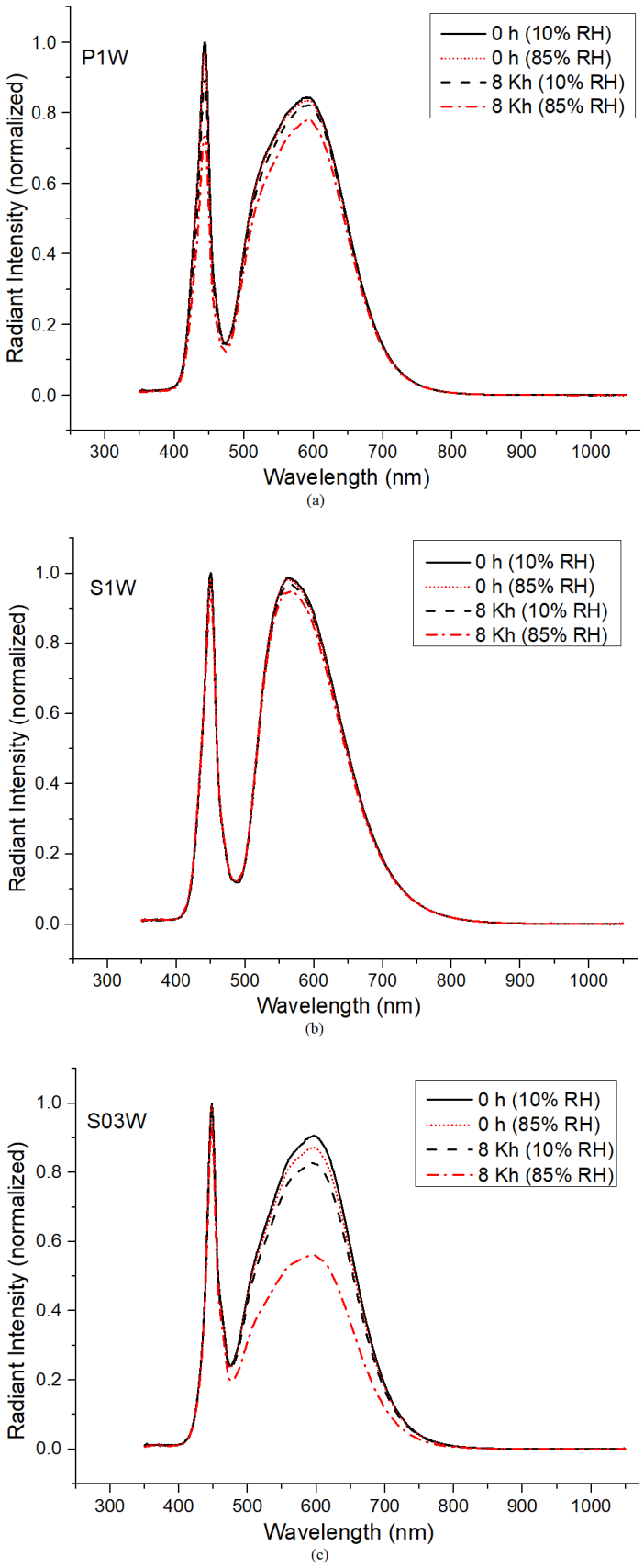

Fig. 5.4. Spectral power distribution of (a) P1W, (b) S1W and (c) S03W at 10% RH and 85% RH. The figures show the results for individual LED at each RH level and is representative of the findings for the samples tested.

5.3.2 Electrical Characteristics

Current–voltage (I–V) characteristics of the 3 LEDs at 10% and 85% RH are shown in Fig. 5.5. The three characteristic regions of diode operation can be seen from the curves [130]. In the low bias region (less than 1.5 V), the I–V characteristic is dominated by non-radiative recombination of carriers in the space charge region. At both humidity levels, P1W and S1W both exhibit significant current increase in this low forward bias voltage region in comparison to S03W due to humidity aging. As the bias voltage becomes larger than about 1.5 V the radiative processes become dominant. Beyond the bias voltage of about 3 V the I–V characteristic becomes ohmic due to the device series resistance. S03W exhibits significant change in this region due to humidity aging in comparison to P1W and S1W.

Below 2.5 V, the effect of the humidity aging is to shift the I–V curve to higher currents at the same forward bias voltage at the same time increasing the ideality factor. This effect is not seen beyond 2.5 V approaching the ohmic region as the radiative recombination dominates over the nonradiative. This shifting of the I–V curve is believed to be due to defect generation in the LED chip which increases the non-radiative recombination rates in the LED chip. Electromigration of the metal atoms in the electrical contact to the surface of the LED die, and instability in Mg diffusion in p-GaN layer and dislocation generation and movement at chip level had been reported [131-133]. Significant current increase (and hence defect density increase) due to aging is seen only in the low and mid bias region (0.5 V - 2.5 V). This low-injection characteristics are dominated by carrier tunneling to the active region because of the highly doped junction and high-density defects in the space-charge region [134, 135]. It is postulated that the higher moisture incursion at the higher humidity level causes increased defects in the LED chip for P1W and S1W. On the other hand, the I-V profile of S03W indicates that the failure mechanism in S03W due to higher humidity may be related to the series resistance instead.

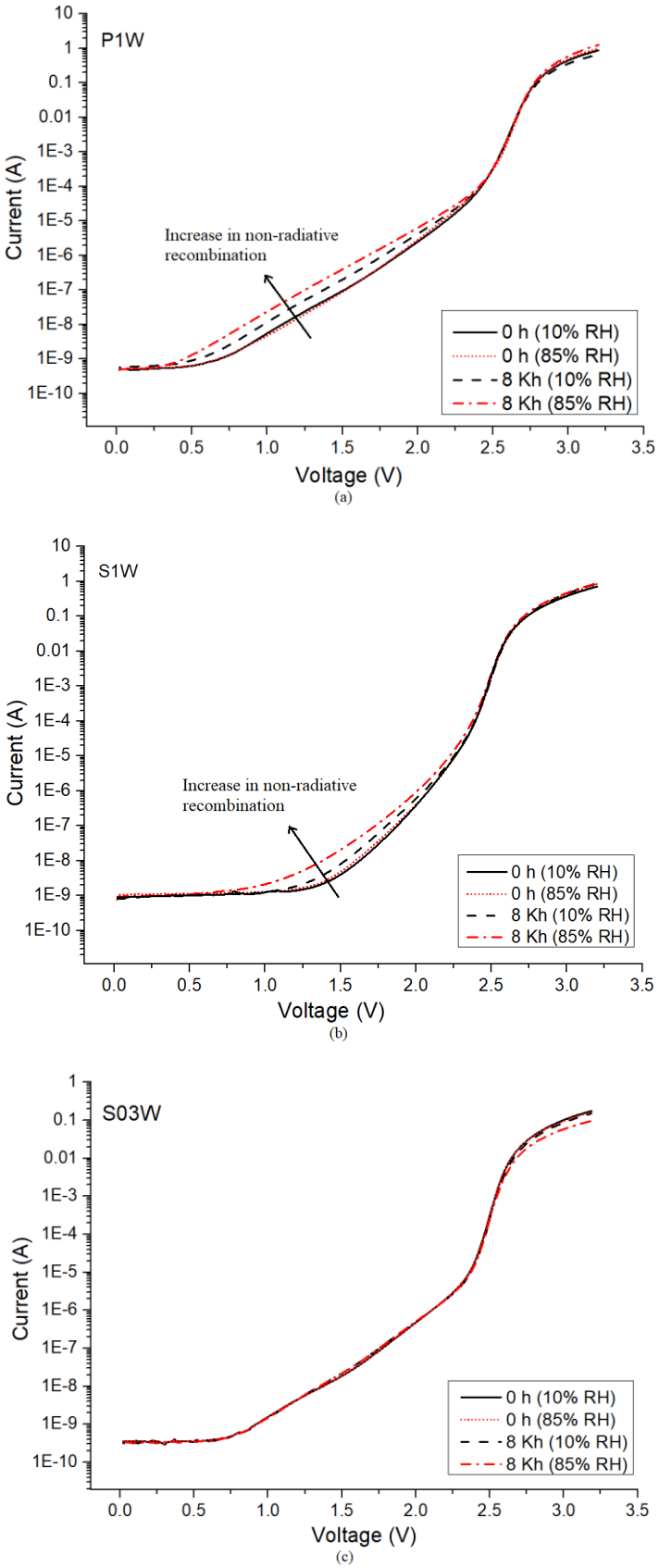

Fig. 5.5. I-V characteristics of (a) P1W, (b) S1W and (c) S03W at 10% RH and 85% RH. The figures show the results for individual LED at each RH level and is representative of the findings for the samples tested.

From the current-voltage electrical measurements done on the LEDs, the series resistance R_S is computed in Table 5.4. Compared to S03W, the series resistance of both P1W and S1W showed less change over the test period of 8000 hours and between the two RH levels. This implies less deterioration of the ohmic contacts of the LED, suggesting that the failure mechanism for P1W and S1W is not related to the packaging materials. The significantly larger increase of the series resistance for S03W would indicate greater reduction of the emission efficiency of the chip, explaining the higher lumen degradation (as shown in the subsequent optical discussion). This increase in series resistance could possibly be due to metal–metal and metal–semiconductor inter-diffusion [128, 129, 136]. The larger shift in the S03W series resistance could possibly be due to the interaction between hydrogen and magnesium, which causes a reduction of the active acceptor concentration. This leads to the deterioration of the properties of the anode contact, thereby changing the resistivity and p-layer injection properties [137].

Table 5.4. Change in Series Resistance R_S over time and RH levels.

LED	**R_S change over 8 Kh @10% RH (a) (ohms)**	**R_S change over 8 Kh @85% RH (b) (ohms)**	**Ratio of R_S change between RH [(b)/(a)]**
P1W	0.325	0.589	1.812
S1W	0.261	0.362	1.387
S03W	0.485	1.091	2.249

For further validation of the LED reliability characteristics based on electrical analyses, investigation of the physical mechanisms due to the degradation of LEDs is conducted using capacitance-voltage (C-V) tests (Fig. 5.6). C-V measurements provide a tool to detect any modification of the heterostructure of GaN based LEDs. The technique uses the LED p–n junction to create a depletion region which may contain electrically active defects or traps, whose width varies according to the voltage applied. The dependence of the depletion width upon the applied voltage provides information on the semiconductor's internal properties, such as its doping profile and defect densities [138]. An increase in capacitance may indicate an increase in the charge concentration in the active region of the LEDs due to either a rise in the concentration of defects or a redistribution of the charge in the space-charge region, because of a doping or impurity diffusion process [136, 139].

In Fig. 5.6, it is observed that the capacitance-voltage curves change for both P1W and S1W. At the P1W reverse bias region between -1 and -3 V, there is a distinct step-like change in capacitance at 85% RH which suggests a doping increase attributable to an increase in charge concentration within the quantum well. The decreasing slope at this region implies that the net fixed charge concentration in the depletion region is not uniform and that the small increase of capacitance with voltage increase implies a high net fixed charge concentration as a greater amount of bias voltage increase is required to achieve the same increment of depletion layer width [140, 141].

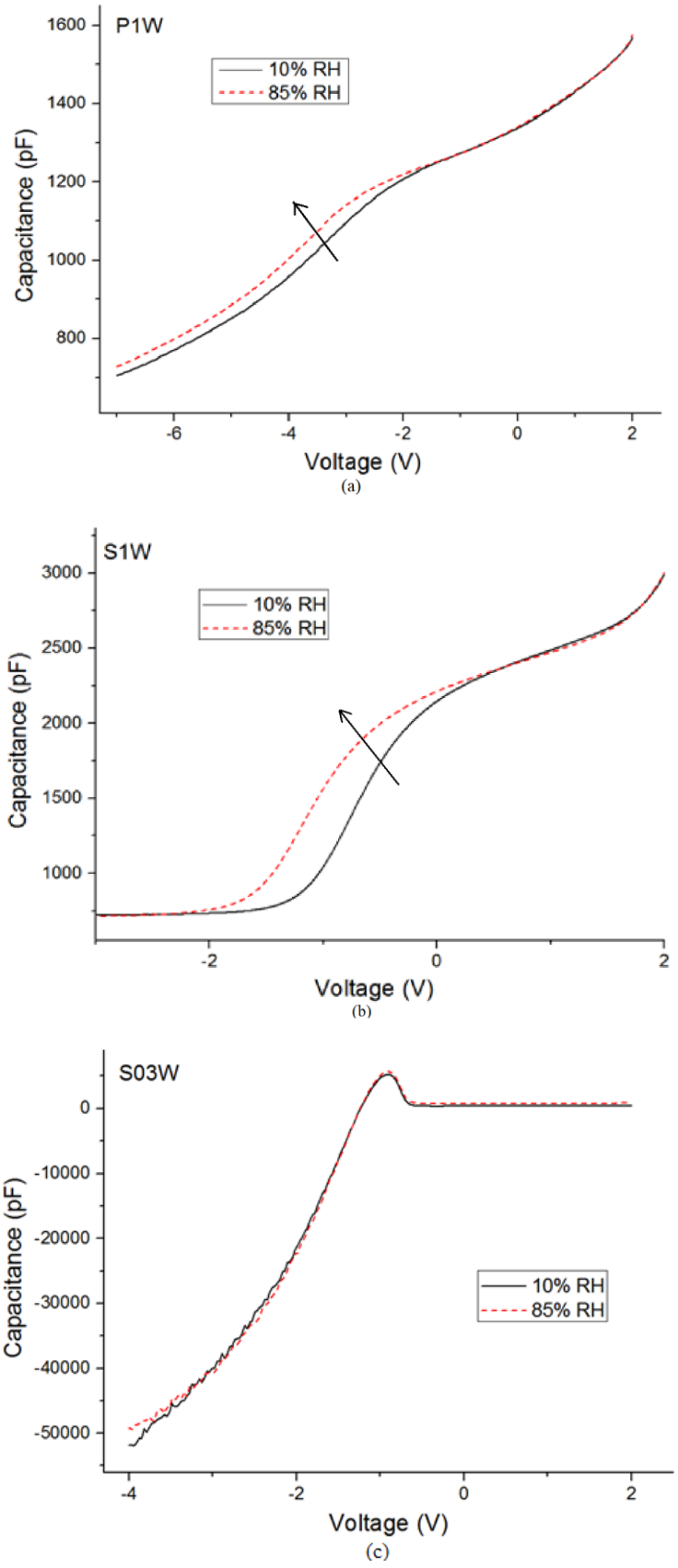

Fig. 5.6. Capacitance-Voltage (C-V) measurements for (a) P1W, (b) S1W and (c) S03W at 10% RH and 85% RH. The figures show the results for individual LED at each RH level and is representative of the findings for the samples tested.

For S1W, the increased capacitance at the S1W reverse bias region at 85% RH demonstrates 2 distinct gradient changes. From 0 to -0.5 V, similar to P1W, a gentler slope is seen at 85% RH while between -1.5 to -2 V, a steeper slope is observed for 85% RH. As with P1W, the gentler gradient indicates a highly charged area. However, the steeper gradient between -1.5 to -2 V implies a lowly charged region. The resulting carrier concentrations have been attributed to the accumulation of carriers within the quantum wells resulting in the movement of charged defects towards the active layer of the LEDs. The rate of non-radiative recombination is directly correlated to the density of defects located within the active region and an increase in charged defect density can lead to a decrease in the optical efficiency of the LED [127]. This corresponds to the non-radiative region of the I-V curves of P1W and S1W.

On the other hand, the C-V measurements for S03W do not display any discernible changes in the C-V profile from 10% to 85% RH, which preliminarily may indicate little modifications to the LED itself. These C-V results are in line with the I-V measurements in Fig. 5.5 which indicate defect generation in the active layers of both the 1 W LEDs, but no such visible deterioration for S03W. Accordingly, a different physical degradation mechanism for S03W compared to the two 1 W LEDs is proposed to account for the more pronounced optical degradation in S03W compared to P1W and S1W. Although the S03W has a greater lumen and radiant degradation rate together with a marked YBR change, the C-V measurements support the inference that LED chip deterioration is more likely not to be the cause for S03W compared to P1W and S1W.

5.3.3 Thermal Characteristics

The previous electrical and optical discussions suggest that the defect generation in the active layer may be the predominant degradation mechanism in both the 1 W LEDs. Comparing the two 1 W LEDs, the ratio of the change in series resistance between RH for P1W was computed as 1.8 versus 1.3 for the S1W (Table 5.4). In addition, P1W shows higher degradation rate changes for both lumen and radiant flux over the test period over S1W (Table 5.2). Accordingly, this comparatively greater optical deterioration should lead to a higher increase on the thermal load for P1W leading to greater heat accumulation and subsequent expected increase in R_{th} for P1W over S1W. However, this is not reflected in the graphs shown in Fig. 5.7, with both S1W and S03W demonstrating higher changes in R_{th} over 8000 hours compared to P1W.

Table 5.5 summarizes the change in R_{th} over the test period for each humidity level. Compared to the other LEDs, P1W exhibits the lowest increase in R_{th} over 8000 hours from 10% RH to 85% RH, with a change ratio of 2.7 versus 4.5 for S1W and 6.4 for S03W. The difference in this R_{th} increase between 10% and 85% RH is only about 60% of that of S1W and 40% of that of S03W. It is postulated that the relatively lower R_{th} in the P1W could be due to the impact of the P1W flip-chip die bonding configuration, which could reduce the heat accumulation significantly. A flip-chip bonded LED dissipates the heat generated in the GaN LED effectively, and results in a decrease in temperature rise compared to the other LEDs.

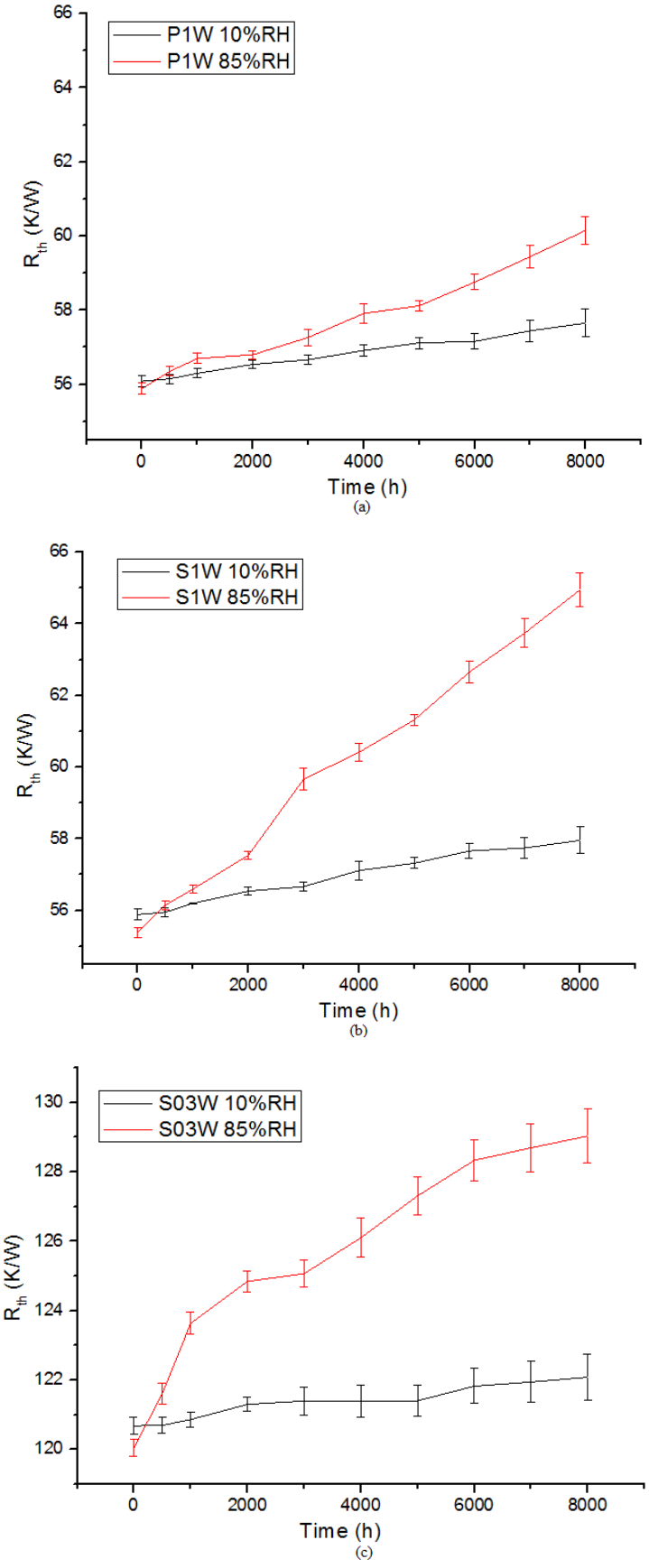

Fig. 5.7. R_{th} of (a) P1W, (b) S1W and (c) S03W at 10% RH and 85% RH.

Table 5.5. Change in R_{th} over time and RH levels computed from the data points (mean values of R_{th}) used in Fig. 5.7.

LED	R_{th} change over 8 Kh @10% RH (a) (K/W)	R_{th} change over 8 Kh @85% RH (b) (K/W)	Ratio of R_{th} change between RH [(b)/(a)]
P1W	1.57	4.27	2.719
S1W	2.07	9.37	4.527
S03W	1.40	8.99	6.418

Most of the heat generated in the LED device is dissipated through the LED package, thereby creating variable heat flow paths. To provide a visualization of the heat flow from the phosphor layer to the ambient, the schematic in Fig. 5.8 illustrates the layers through which the heat dissipates. To derive the layer configuration of the LED, a three-pronged approach using SEM/EDX, thermal capacitance computation and the cumulative structure function is utilized [142, 143]. By using information obtained from the SEM/EDX analysis, the various materials constituting the layers of the LED can be confirmed by comparing the calculated thermal capacitances with that obtained in the cumulative structure functions. Fig. 5.8 also provides an orientation of the differential structure functions with respect to the heat flow paths (Fig. 5.9) and SEM/EDX micrograph analysis (Fig. 5.11) presented later.

Structure function evaluation of all the LEDs were computed for both RH levels (Fig 5.9) to analyze the thermal response of the LEDs. The recorded cooling curves in the transient thermal measurements from the T3ster were evaluated to extract the thermal characteristics and derive the differential structure functions.

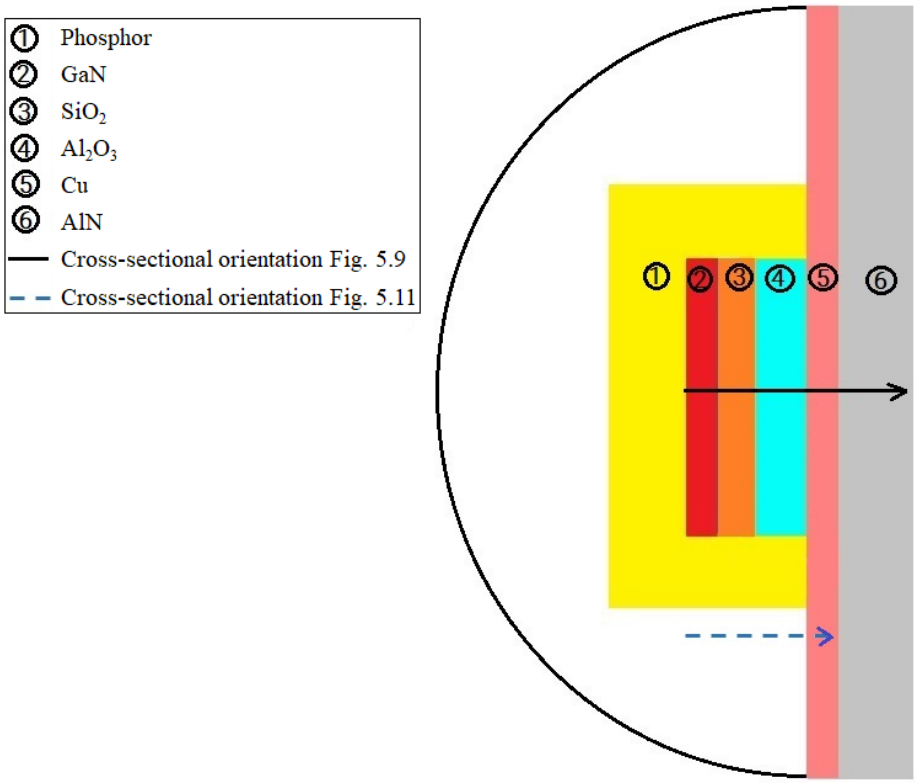

Fig. 5.8. LED schematic with cross-sectional orientation in Fig. 5.9 and Fig. 5.11.

At 85% RH, the S03W and S1W show greater increase in R_{th} compared to the P1W over the test period. The smaller R_{th} change seen in P1W could be attributed to the flip-chip die-bonding which allows for effective heat transfer onto the AlN substrate. Consequently, the P1W has a lower measured R_{th} compared to the two other LEDs where heat generated is directly transferred to the AlN substrate through the thick sapphire material. The low thermal conductivity of the sapphire material ($K_{Al_2O_3}$ ~46 W/m·K) implies inferior heat dissipation allowing for greater heat accumulation within the device compared to flip-chip devices. Conversely, flip-chip bonding allows effective heat transfer onto the AlN substrate due to the higher thermal conductivity of the gold bumps (K_{Au} ~318 W/m·K). The heat fluxes generated in P1W through the Au bumps allows for lower temperature rise and R_{th} of the package, in spite of the degeneration of the electrical and optical properties, which might suggest otherwise.

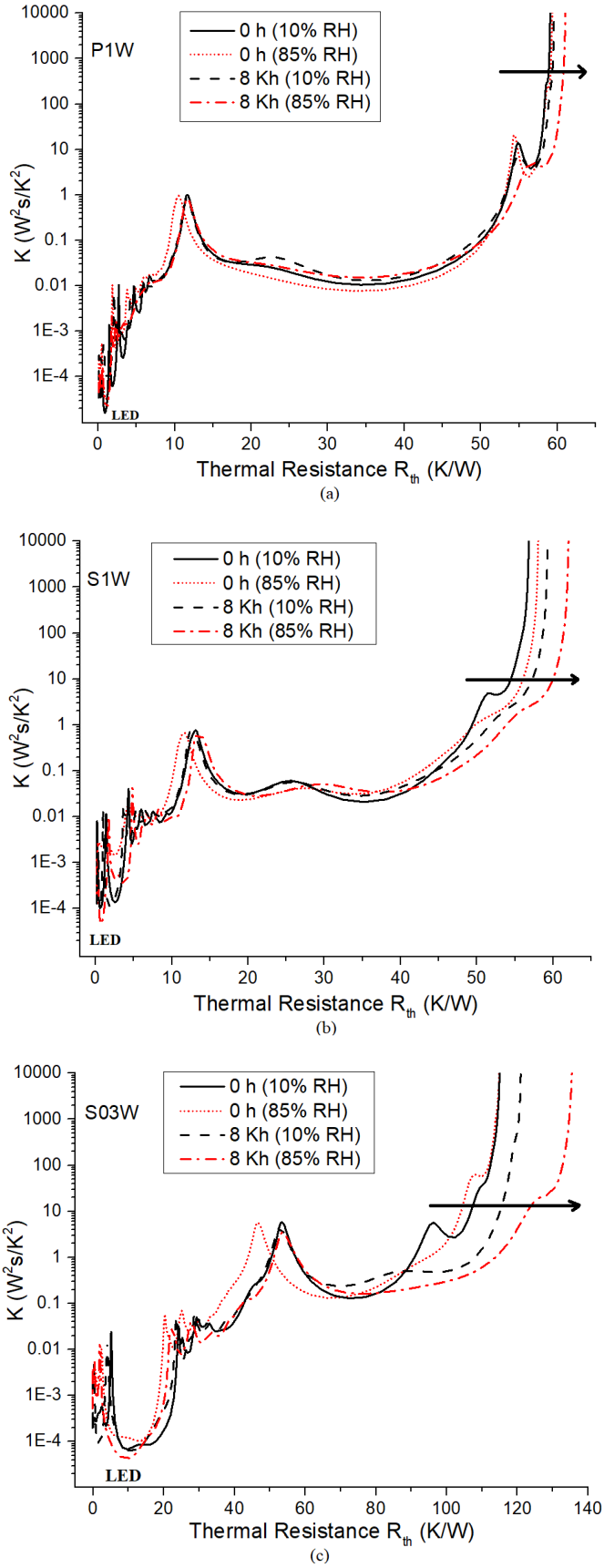

Fig. 5.9. Derivative structure function of (a) P1W, (b) S1W and (c) S03W at 10% RH and 85% RH.

5.3.4 Failure Analysis

The implication of the EOT analysis is that the S03W underwent package based degradation in contrast to the 1 W LEDs where defect mechanisms is suggested to cause the LED to degrade. The S03W exhibited significant changes due to the increase in humidity in particular the series resistance, lumen degradation and YBR change. These changes consequently had the effect of a pronounced change in the R_{th} of the package. On the other hand however, S03W exhibited little change in the low forward bias voltage region during the I-V tests and displayed little variation for the C-V tests due to the increased RH levels. These observations lead to added justification of degradation to the package instead of to the LED chip due to the effect of humidity on S03W.

To validate these results and observations, further investigation by SEM-EDX was conducted to discover the failure mechanism on dissected S03W samples. A close examination of the degraded S03W (Fig. 5.10) reveals that there was delamination at the Cu/AL_2O_3 interface of the LED at 85% RH, whereas there appeared to be no visible damage at 10% RH. This delamination is depicted by the encircled area in Fig. 5.10(b). A possible reason is cited as von Mises stress at the interface due to hygroscopic stress caused by moisture ingression over time [144]. It is postulated that higher relative humidity levels cause further moisture inception leading to greater degrees of delamination which has been shown to be a mechanism for white LED light degradation [145].

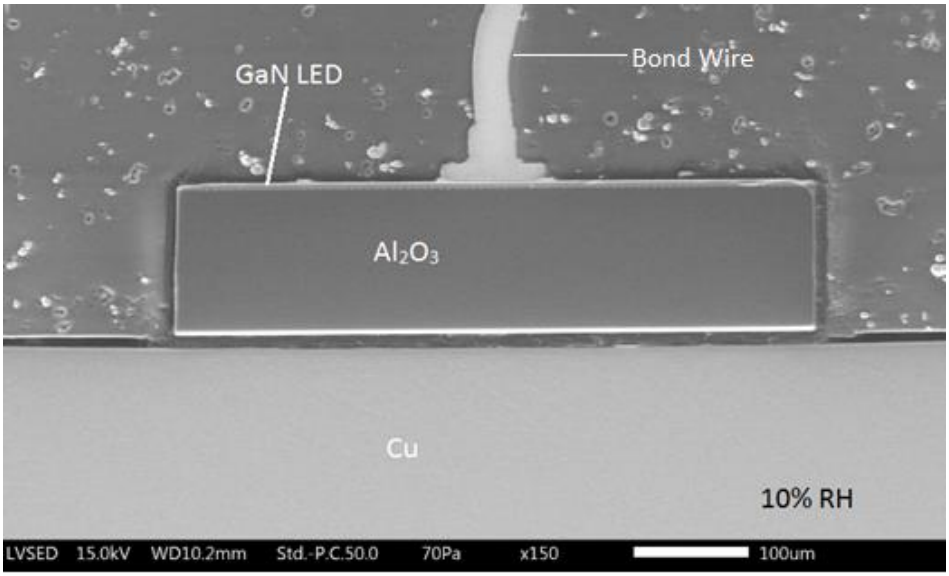

..

(a)

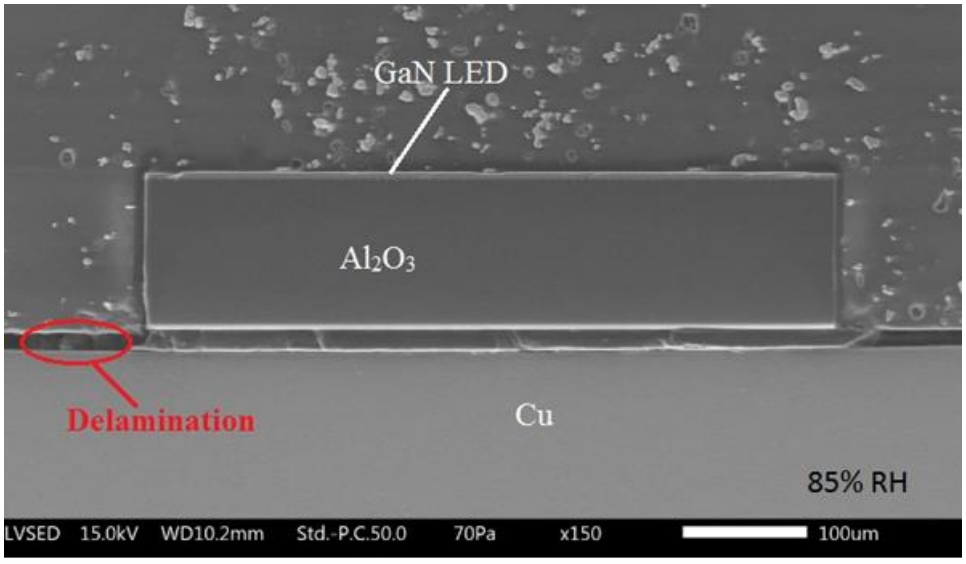

(b)

Fig. 5.10. Micrographs of S03W at (a) 10% RH and (b) 85% RH.

In addition, SEM–EDX analysis of the LED (Fig. 5.11) indicates an increase of elemental oxygen at 85% RH compared to 10% RH at the interface of the chip and the lead frame, which is coated with silver to enhance light reflectivity. As shown in Table 5.6, there is a significant increase in the weight percentage of oxygen and this observation is consistent for all the S03W samples subjected to failure analysis. It had been reported by Chen et al. [146] that in the presence of humidity, atomic oxygen will react with the absorbed water to form a hydroxyl

(OH) radical, which reacts with Ag to form Ag_2O which is the cause of silver corrosion on the surface of the lead frame. This oxidation leads to a change of the reflective properties of the silver layer [147-149] which impairs its light reflectivity and affects the colour output of the LED. This result aligns with the shift in YBR reported earlier in the chapter.

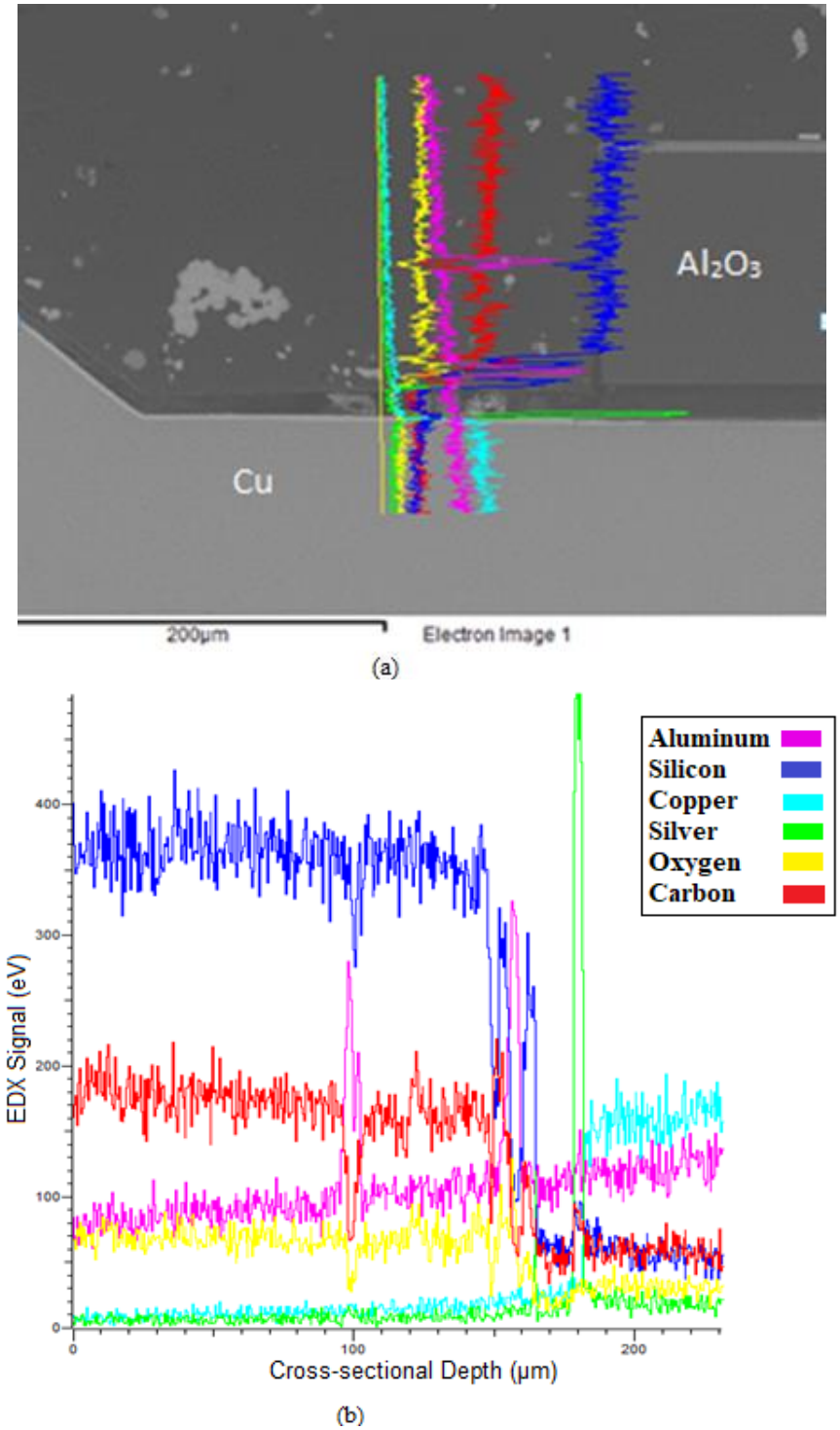

Fig. 5.11. (a) SEM micrograph and (b) EDX analysis of die after 85% RH aging.

Table 5.6. S03W Elemental weight by percentage at 10% RH and 85% RH.

Element	Element weight percentage @10% RH	Element weight percentage @85% RH
Carbon C	2.41	2.25
Oxygen O	7.76	13.04
Magnesium Mg	0.4	0.58
Silicon Si	0.51	0.76
Titanium Ti	0.86	0.78
Zinc Zn	1.38	1.42
Silver Ag	86.68	84.38

In addition, it is theorized that at higher humidity levels, the water vapour reaches the die, causing phosphor degradation. Light scattering due to the water layer and internal reflection of the light from the die occurs due to the change in the refractive index of the water layer, leading to a reduction in the phosphor conversion efficiency [61, 150-152], which corresponds to the YBR reduction.

5.4 Summary

Three different LEDs of varying power, die-bonding configurations and phosphor coating methods were analyzed for their EOT performance under the conditions of two relative humidity levels, 10% RH and 85% RH. The I-V and C-V profiles and R_S changes suggest package or phosphor deterioration in S03W, and defect generation in the active layer of the 1 W LEDs. This postulation is supported by the pronounced reduction in yellow intensity for S03W versus the increase in YBR for P1W and S1W. The package deterioration for S03W is confirmed by SEM-EDX analysis which show delamination and silver corrosion on the lead frame. These results form the basis of the prognostication model developed in Chapter 6.

For the 1 W LEDs, in spite of the expected high thermal load and heat accumulation, P1W exhibits significantly better thermal performance compared to S1W. The R_{th} is only 60% of that of S1W and this is due to the superior heat dissipating capabilities by the flip-chip die-bonding configuration.

Chapter 6

Prognosticating the Effect of Humidity

6.1 Introduction

Based on an understanding of the effects of the humidity stressor on the EOT performance of the LED covered in Chapter 5, the challenge is to quantitatively associate these changes observed with the impact of humidity. Such a model would provide not only an indicative assessment of the current state of the LED but also provide prognostication into the likely development of future problems. In spite of the need for greater LED reliability research to ensure its universal adoption, there are comparatively few studies in this area [82], in particular regarding lumen depreciation and colour shift, two critical indicators of LED reliability. Although these two factors should be analyzed in relation to each other, most existing literature treat these two as independent phenomena [14]. Prediction models involving colour shift are also limited [89] despite the requirement for colour consistency being more important than lumen maintenance in many applications. In spite of the need for information on LED chromaticity shift, there are still no official standards providing acceptability guidelines of colour shift [18]. Even more scarce is the availability of studies investigating the colour degradation in high humidity conditions. As conditions of high humidity can incur significant lumens degradation and colour change, a method to predict colour shift has both academic and industrial significance as an indication of the impending nature and amount of this change. Based on degradation data of different types of LEDs under humidity stress, this study in this chapter proposes a data driven humidity based degradation model (HBDM) using the lumen depreciation data to predict the time-dependent effect of humidity on the LED. The humidity index, derived using Hallberg-Peck's model and the IES TM-21 approach is developed to provide a practical indication of the impact of moisture incursion according to the lumen decay

under varying humidity levels. Subsequently, the yellow-blue ratio (YBR) shift is analyzed from experimental data and the association of this humidity index with the magnitude of the change in YBR is investigated and analyzed.

To further build on the HBDM, an artificial neural network (ANN) model is then developed as an efficient tool to predict the YBR changes based on the humidity degradation data, taking advantage of its high computational efficiency. The use of ANNs for LED prognostication is extremely rare, with only one such application currently uncovered, despite their suitability for LED prognostic study [81]. The model presented is a feed forward network using six key attributes or indicators of LED degradation to model the HBDM.

There is also a need to be able to identify potential failures under such conditions of high humidity by sensing the current condition of the LED [63]. The degree of deviation from the expected normal operating condition provides warning of impending failures and also improves LED reliability qualification, helping to design future products. As such, a novel Trivariate Distance Measure Approach (TDMA) for LEDs based on the Mahalanobis method [153] to identify outliers based on the combined characteristics of R_{th} change, colour shift and the degradation rate of the LEDs is developed. The advantage of this approach is that it does not make any assumptions regarding the underlying distribution of data. This method draws its strength from the data and its inherent features, without requiring specific knowledge of the LEDs under test, and is ideal for the suspected or presumed correlation between the parameters used. The results demonstrate that this approach is a more effective gauge of anomalies than using the usual screen test of one or two variables.

6.2 Experimental Setup and Procedures

6.2.1 Instrumentation Setup

The work in this chapter comprises primarily data and results obtained from previous chapters, which were collected using the same integrated LED measurement system represented in Fig. 3.1 (Chapter 3). Humidity reliability aging tests (Chapter 5) were conducted using the CTS Climatic Test System environmental cabinets. The failure analyses of the samples described in Section (6.3.2) were done by means of Scanning Electron Microscopy with Energy Dispersive X-ray Spectrometry (SEM–EDX).

6.2.2 Experimental Procedures

For the derivation of the HBDM and TDMA, results from the same LEDs used in humidity experiments described in Section (5.3) were used. The test procedures and conditions as recommended in IES TM-21 [65] described in Section (5.2.2) were used. A sample size of 20 was used for each LED (P1W, S1W and S03W) at each humidity level (10% and 85% relative humidity). The results and discussion that follow in this chapter are based on this LED set.

The figures used in this chapter vary in presentation based on purpose and the type of data or results available. As Fig. 6.1, 6.3 and 6.12 are statistically based diagrams and display the distributions of the entire sample of LEDs used, the data points in these figures are computed from all the LED samples. However, in Fig. 6.2, for the purpose of quantifying the humidity index's correlation to the average change in YBR, the mean data extracted from the 20 samples of each LED type is used (Section (5.3.1)). Similarly, in Fig. 6.4 to Fig. 6.8, the figures are based on data provided from external sources using mean values for computation of the data points similarly to demonstrate the validity of the HBDM. The procedure to derive the slope showing the lumens degradation in Fig. 6.4 and Fig. 6.6 are as described in Section (5.3.1).

6.3 Results and Discussion

6.3.1 The Humidity Based Degradation Model (HBDM)

6.3.1.1 Derivation of the HBDM

As the degradation of the lumen performance follows an exponential trend [154], from IES TM-21 [65], the following degradation equation can be used to fit the averaged degradation data:

$$\Phi(t) = Bexp(-\alpha t) \tag{6.1}$$

where t is the operating time and $\Phi(t)$ the averaged normalized luminous flux output at time t. The projected initial constant $B = exp(c)$ and the decay rate $\alpha = (-m)$ where both c and m are parameters obtained from the least squares curve-fit described in Section (5.3.1). To incorporate the effect of both temperature and humidity on LED life, the Hallberg-Peck model [155] is typically used and the acceleration factor due to this model can be described as follows:

$$A_H = (\frac{R_{use}}{R_{stress}})^{\theta} exp(K\left[\Delta\left(\frac{1}{T}\right)\right]) \tag{6.2}$$

where A_H is a humidity acceleration factor, R_{stress} and R_{use} the testing and reference relative humidity respectively, K and θ are predetermined humidity specific constants and T the operating temperature in kelvin. For the purpose of providing information on the sole effects of humidity stress, equation (6.2) is treated as having one independent variable (relative humidity) with stress conditions at constant temperature, leading to the factoring out of the exponential term. Under such conditions then, A_H reduces to $\left[\frac{R_{use}}{R_{stress}}\right]^{\theta}$ and the time t_{stress} to reach a specified lumen level in terms of the reference t_{use} is described as:

$$t_{stress} = \left[\frac{R_{use}}{R_{stress}}\right]^{\theta} t_{use} \tag{6.3}$$

For the same specified lumen output level Φ reached at use and stress conditions, the expression in (6.1) under the reference and stress conditions can then be equated giving:

$$\alpha_{stress} t_{stress} = \alpha_{use} t_{use} \tag{6.4}$$

where α_{use} is the lumens degradation rate under stated initial humidity conditions and α_{stress} the degradation rate under the stress humidity conditions. On assumption that during the stress tests, the failures induced by temperature and humidity are independent, a functional form describing the light degradation can be developed to account for the exponential loss in luminous flux under conditions of increasing relative humidity. From equations (6.3) and (6.4), a degradation model developed as a function of some base degradation rate α_{use} that caters to both these factors would fundamentally be described as:

$$\alpha_{stress} = H\alpha_{use} \tag{6.5}$$

where H is a humidity expression. From both experimental observation and parameter fitting, this humidity expression derived from the Hallberg-Peck's model may be described as:

$$H = \left[\frac{R_{stress}}{R_{use}}\right]^{\psi_H} \tag{6.6}$$

where ψ_H is described as a humidity constant which represents the level of moisture related degradation in the LED. The expression is incorporated into the original exponential curve-fit equation (6.1) to give the following combined model:

$$\Phi(t) = Bexp(-\left[\frac{R_{stress}}{R_{use}}\right]^{\psi_H} \alpha_{use} t) \tag{6.7}$$

The combined expression (6.7) can be described as a humidity-based degradation model (HBDM) which can be fitted to LED lumen maintenance data. Using degradation data, the HBDM describes the effect of assumed moisture ingress in an LED at an operational RH level compared to a specified base RH level.

Using the procedure prescribed in IES TM-21 for 20 units of each of the 3 types of LED used for experimentation, the nonlinear least squares method was utilized for the degradation curve-fit. The extracted parameters are used to extrapolate the lumen maintenance value to where the luminous flux output decreases to L70 (70% of initial luminous flux). The lumens exponential curve-fit based on equation (6.1) for the 3 types of LEDs used at both 10% RH and 85% RH was presented in Fig. 5.2 in Chapter 5. Using 10% RH as the baseline for all tests, ψ_H is assigned an initial value of 0 at α_{use} at this humidity level. Accordingly, rearranging equations (6.5) and (6.6) above, ψ_H can be derived as:

$$\psi_H = \frac{log\left(\alpha_{stress}/\alpha_{use}\right)}{log\left(R_{stress}/R_{use}\right)} \tag{6.8}$$

For the validity of ψ_H, the baseline values α_{use} and R_{use} are set below that of α_{stress} and R_{stress} respectively. The results for ψ_H for the experimental data is as shown in Table 6.1. As RH increases with corresponding increase of the degradation rate α, ψ_H increases in proportion

to the degradation rate. This indicates the relative level of moisture incursion in the LED associated to the lumen decay. At 85% RH, it is observed that ψ_H = 0.607 for the lower powered S03W compared to ψ_H = 0.129 and 0.153 for the higher powered S1W and P1W respectively corresponding to a higher ψ_H at higher degradation rates α.

Table 6.1. Computations of ψ_H for various LEDs at differing RH levels.

LED power rating	**LED**	**%RH**	**Degradation rate α**	ψ_H
1 W	P1W	10	7.145E-06	0
		85	9.917E-06	0.153
1 W	S1W	10	4.702E-06	0
		85	6.197E-06	0.129
0.3 W	S03W	10	1.765E-05	0
		85	6.473E-05	0.607

Assuming the normalised expression for lifetime L_P based on TM-21 where:

$$L_p = \frac{ln(100\frac{1}{p})}{\alpha_{stress}} \tag{6.9}$$

where L_p is the lumen maintenance life and p is the percentage of the initial lumen output that is maintained. By substituting in equation (6.9), ψ_H may then be used to predict the lifetime at a particular RH level. The lumen degradation mechanisms of the experimental data were explored using statistical methodology. The lifetime data of each individual sample at 10% RH and 85% RH was collected for probability distribution analysis and plotted in Fig. 6.1. Lognormal distribution is commonly used for demonstrating fatigue-stress failure modes. The

degradation mechanisms for both humidity stress conditions for P1W are similar as the shape parameters of the lognormal distributions are close to each other as shown in Table 6.2. Similarly, the degradation mechanisms for S1W at both 10% and 85% RH are noted to be similar. However, because of the comparatively larger difference in the scale factor and shape parameter for S03W between 2 RH levels, the degradation mechanism is expected to be different [6, 56].

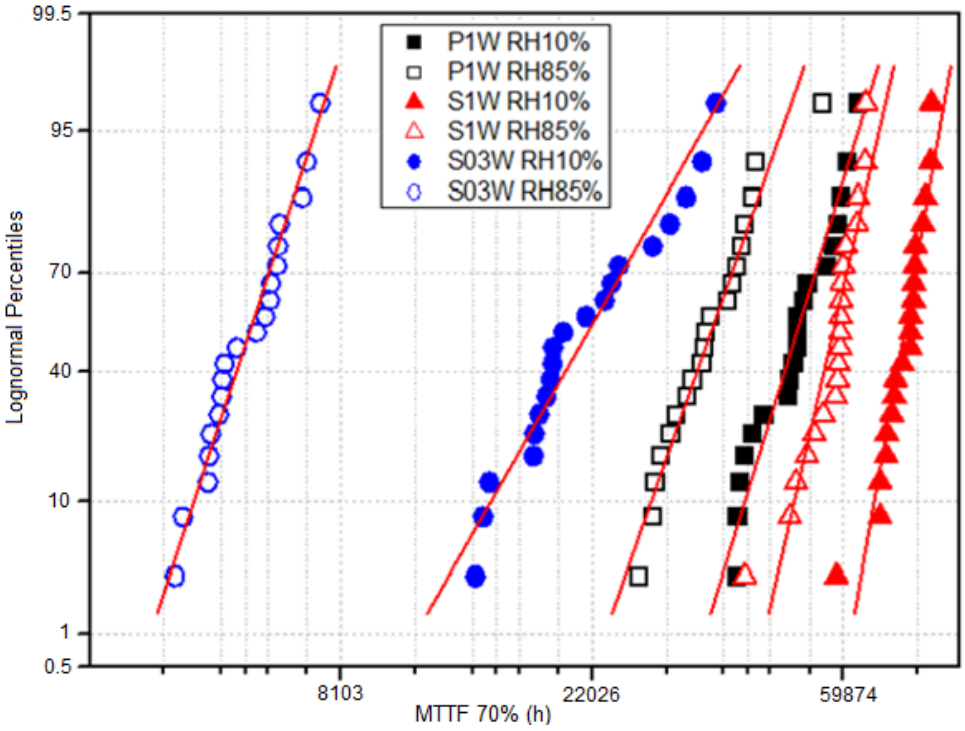

Fig. 6.1. Lognormal Distribution of P1W, S1W and S03W at 10% RH and 85% RH. MTTF 70% is the Mean Time to Failure for L70. Data points are computed from all the LED samples to demonstrate the distribution.

Table 6.2. Lognormal Distribution shape and scale parameters. The shape parameter indicates the standard deviation while the scale parameter indicates the median of the distribution.

	P1W		**S1W**		**S03W**	
Lognormal Distribution Parameters	**10% RH**	**85% RH**	**10% RH**	**85% RH**	**10% RH**	**85% RH**
Shape	10.804	10.461	11.234	10.951	9.965	8.626
Scale	0.154	0.177	0.089	0.115	0.287	0.165

6.3.1.2 Prediction of Colour Change by the HBDM

Colour output is evaluated from the LED spectral power distribution (SPD). Based on the two decomposed peaks, the ratio of the phosphor converted yellow light (SPD^P) to blue light (SPD^B) emitted from the LED or yellow-to-blue ratio (YBR) could be calculated from [156]:

$$\text{YBR} = \frac{\int SPD^P(\lambda)d\lambda}{\int SPD^B(\lambda)d\lambda} \tag{6.10}$$

where the SPD^P and SPD^B are derived from the radiant flux as a function of the wavelength λ. The SPDs for all 3 LEDs at the different RH levels were presented in Fig. 5.4 in Chapter 5. Computed over the entire test period of 8000 hours, the trend of YBR change was demonstrated for all 3 LEDs for 10% (base) and 85% (stress) RH in Fig. 5.3 and Table 5.3. Based on these results, the difference between $\Delta(\text{YBR})_{\text{RH}}$ at stress and use RH are computed in Table 6.3 along with the corresponding ψ_H using equation (6.8). It is observed that the experimental $\Delta(\text{YBR})_{\text{RH}}$ computations correspond closely to twice the value of ψ_H. This correlation is explored further in detail later and tested in different experiments to validate the relationship. Fig. 6.2 illustrates the comparison between the measured YBR shift and the HBDM predicted shift computed in Table 6.3 over the entire test period. The dashed lines demonstrate the overall HBDM predicted $\Delta(\text{YBR})_{\text{RH}}$ based on the same R_{use} for each LED type.

Table 6.3. Measured versus HBDM predicted YBR shift over RH levels.

LED	YBR Change over test period @base condition		YBR Change over test period @stress condition		YBR Difference between RH = (b) - (a)	ψ_H	HBDM predicted Δ(YBR)
	R_{use}	Δ(YBR)$_{RH}$ (a)	R_{stress}	Δ(YBR)$_{RH}$ (b)			
P1W	10% RH	0.204	85% RH	0.502	0.298	0.153	0.306
S1W	10% RH	0.102	85% RH	0.351	0.249	0.129	0.258
S03W	10% RH	-0.331	85% RH	-1.547	-1.219	0.607	-1.214

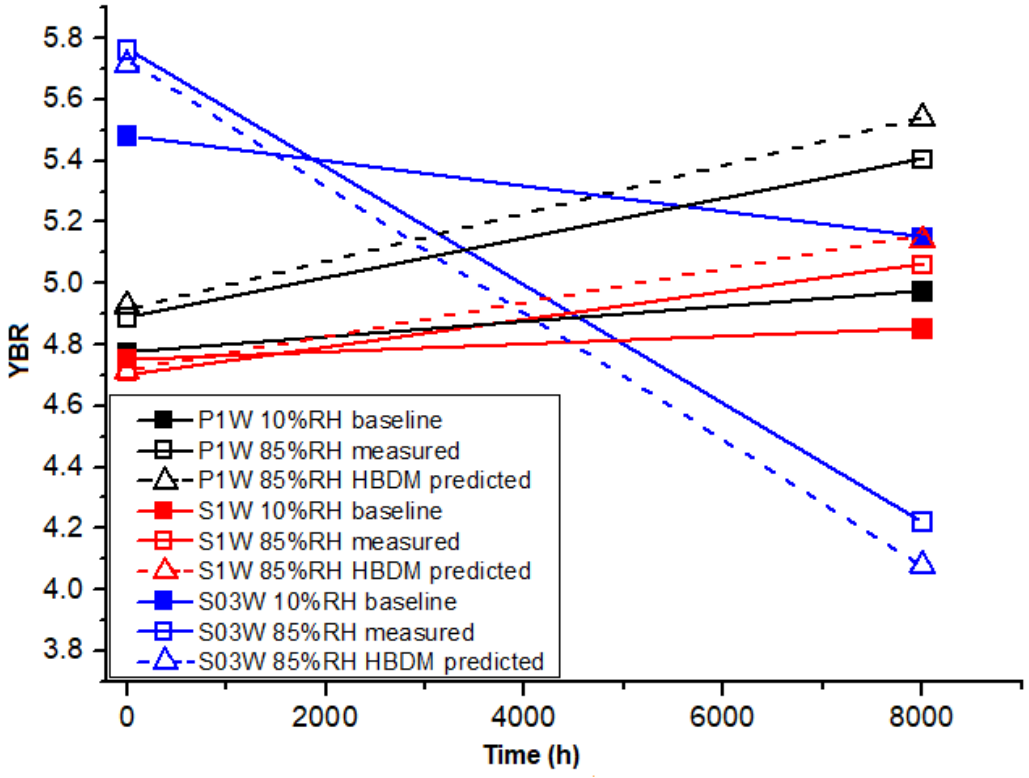

Fig. 6.2. Measured and HBDM predicted YBR shift at different RH levels. The solid lines display the shift of the mean value of the 20 samples for each LED after 8000 h.

It is observed from Fig. 6.2 that at all RH levels, the P1W and S1W both exhibit increasing trends while the S03W conversely has a decreasing yellow-blue light output ratio. Table 6.3 summarizes this YBR change over the test period for each RH level as well as the difference in YBR change $\Delta(\text{YBR})_{RH}$ between the stress condition R_{stress} and the base condition R_{use}. S03W has a significantly larger YBR change over the test period at both RH levels and between the RH levels, the negative sign for S03W denoting the decreasing YBR. The results correlate with the larger difference in scale parameter computed for S03W (Table 6.2) in relation to the other LEDs, indicating a different degradation mechanism for this LED. It is observed for all the LEDs that ψ_H is positively associated to the absolute value of $\Delta(\text{YBR})_{RH}$ in that an increase in $|\Delta(\text{YBR})_{RH}|$ is reflected by a corresponding increase in ψ_H. The correlation of colour shift to lumen depreciation has been corroborated in several studies [6, 58, 89] and since ψ_H is based on the degradation curves of lumen depreciation, it is proposed that ψ_H serves as an degradation based index to estimate the colour shift in the LED related to the relative humidity. As a means of statistically measuring the strength of the relationship between ψ_H and $\Delta(\text{YBR})_{RH}$, the Pearson correlation coefficient value r [157, 158] is computed based on:

$$r = \frac{N\sum q_1 q_2 - (\sum q_1)(\sum q_2)}{\sqrt{[N\sum {q_1}^2 - (\sum q_1)^2][N\sum {q_2}^2 - (\sum q_2)^2]}} \tag{6.11}$$

where q_1 and q_2 represent the ψ_H and $\Delta(\text{YBR})_{RH}$ variables respectively, and N is the number of pairings of the two respective variables. The correlation coefficient r is computed to be greater than 0.99 indicating a high positive association in that as ψ_H increases, the value of $\Delta(\text{YBR})_{RH}$ increases correspondingly. Applying the t-test [158] for the data where:

$$t = \left| r\sqrt{\frac{N-2}{1-r^2}} \right| \tag{6.12}$$

gives t = 170, which at P-value < 0.001 implies that the correlation coefficient may be regarded as significant. Fig. 6.3 shows the correlation scatter matrix which shows good association between the two variables, with all the data points falling within close proximity in the confidence ellipse. The proposed HBDM thus serves to provide an indication of the impact of humidity correlating the value of ψ_H with the absolute value of the change of YBR caused by this moisture incursion.

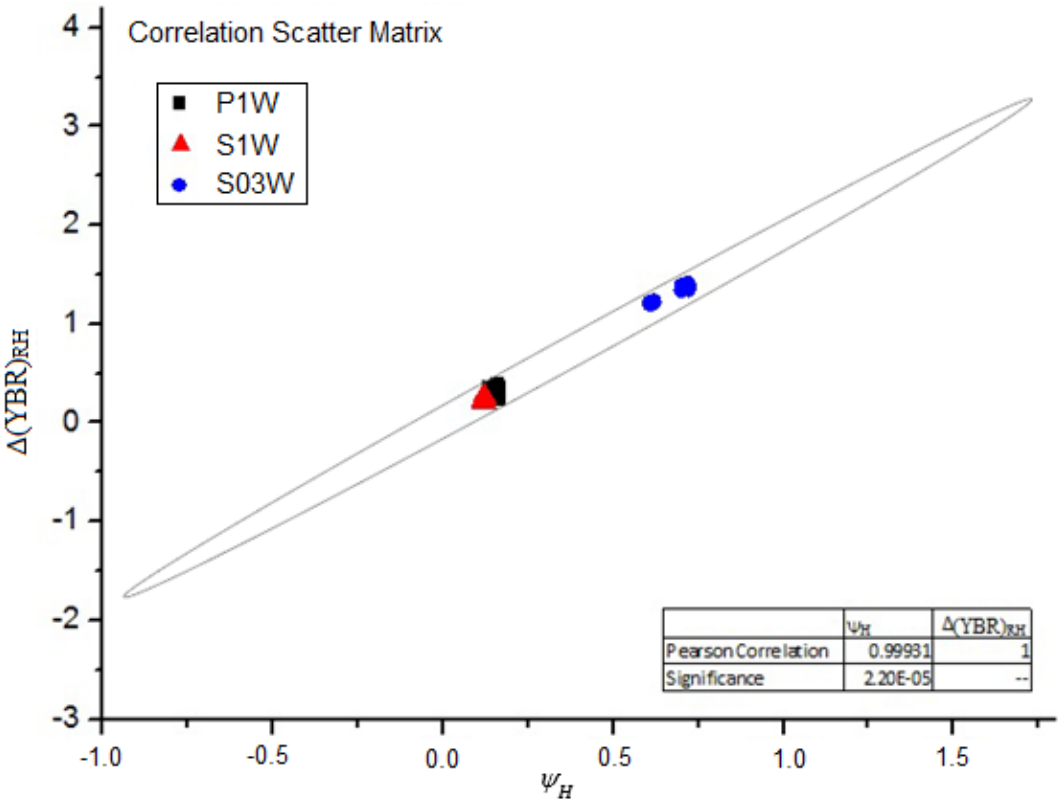

Fig. 6.3. Scatter matrix with confidence ellipse of ψ_H and $\Delta(\mathrm{YBR})_{\mathrm{RH}}$. Data points are computed from all the LED samples to demonstrate the distribution.

As a means of validation of the link between the lumen degradation and the change in colour, the photopic eye sensitivity function relationship with lumen output Φ(t) as prescribed by the International Commission on Illumination (CIE) [159] given by the base equation is used:

$$\Phi(t) = K_m \int_{380}^{780} \Phi_e(\lambda).V(\lambda).d\lambda \tag{6.13}$$

where the maximum spectral luminous efficacy normalization factor K_m = 683 lm/W, Φ_e the radiant flux derived from the SPD from wavelength 380 nm to 780 nm, and $V(\lambda)$ the spectral luminous efficiency function for photopic vision. Inserting the HBDM expression for $\Phi(t)$ from equation (6.7) into equation (6.13) gives:

$$Bexp\left(-\left[\frac{R_{stress}}{R_{use}}\right]^{\psi_H} \alpha_{use}\mathrm{t}\right) = K_m \int_{380}^{780} \Phi_e(\lambda).V(\lambda).d\lambda \tag{6.14}$$

Using the degradation values at the corresponding humidity levels from Table 6.1, then the value of ψ_H applying the human eye sensitivity function aspect may be computed from the radiant flux. It is observed from the experimental data that the minima or separation point between the yellow and blue spectra may be approximated at about 470 nm. To establish the relationship between the ψ_H in equation (6.14) and the YBR, equation (6.13) may be separated into two components representing the blue and yellow SPD peaks respectively:

$$\Phi(t) = K_m \int_{380}^{470} \Phi_e(\lambda).V(\lambda).d\lambda + K_m \int_{470}^{780} \Phi_e(\lambda).V(\lambda).d\lambda \tag{6.15}$$

So as to allow for the input of the discrete experimental values, equation (6.15) is approximated by numerical summation which may be described as:

$$\Phi(t) = K_m \sum_{i=380}^{i=470} \Phi_e(\lambda_i)V(\lambda_i)\delta(\lambda_i) + K_m \sum_{i=470}^{i=780} \Phi_e(\lambda_i)V(\lambda_i)\delta(\lambda_i) \quad (6.16)$$

As the YBR is derived from the deconvoluted SPD of the LED, the expression for YBR in equation (6.10) may be thus written as:

$$\text{YBR} = \frac{\sum_{i=380}^{i=470} \Phi_e(\lambda_i)\delta(\lambda_i)}{\sum_{i=470}^{i=780} \Phi_e(\lambda_i)\delta(\lambda_i)} \quad (6.17)$$

By substituting the radiant flux and spectral luminous efficiency function values for photopic vision at the respective relative humidity levels into equation (6.17), the change in YBR based on the photopic eye sensitivity function had shown to yield similar values for the different LED samples as in Table 6.3 with a variation of less than 6% for ψ_H and $\Delta(\text{YBR})_{\text{RH}}$. Although the universal applicability of the HBDM method can only be verified by applying the method to the field or experimental data at all scenarios, this approach has certain advantages over other data driven methodologies. The index ψ_{H} is simple to calculate and use and allows for both the prediction of relative moisture incursion and colour shift under specified humidity conditions.

In addition, both the parametric and physical investigation reported in Chapter 5 verify the HBDM colour predictions. The magnitude of the I-V and R_S changes correlate well to the degradation and YBR degradation data, and failure analysis of S03W show delamination and silver corrosion, which explains the package deterioration predicted, causing the pronounced degradation of the YBR.

6.3.1.3 Robustness of the HBDM

To demonstrate the robustness of the model, HBDM was applied to different LED samples used in a separate experiment. As mentioned earlier in the chapter introduction, humidity based degradation studies are few and far between, not to mention the dearth of comparative research providing experimental setup and conditions suitable for validity studies with the HBDM. Using data from one such research conducted by Tan et al [6], relevant parameters were extracted at 70% RH and 95% RH to be used in the HBDM. The lumen degradation data extracted was curve fitted as shown in Fig. 6.4 and the degradation rates α derived. Using R_{stress} = 95% RH and R_{use} = 70% RH, the humidity index ψ_H is then computed using equation (6.8) to give a value of 0.72, which indicates the relative amount of moisture incursion for the LED. Based on the positive association of ψ_H to the absolute value of ΔYBR_{RH} described in Section (6.3.1.2), ψ_H = 0.72 corresponds to predicted $|\Delta YBR_{RH}|$ = 1.44.

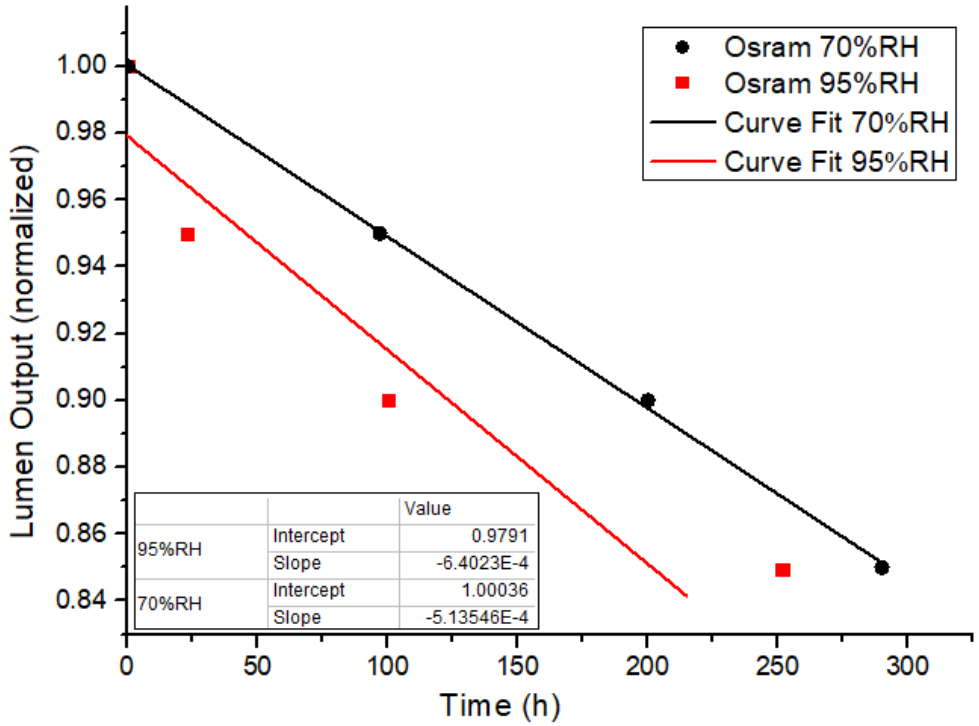

Fig. 6.4. Lumens degradation of Osram 1W LED at 70% RH and 95% RH [6]. Mean data provided by external source with slope of curve fit computed using procedure in Section (5.3.1).

To test the model, the YBR data points may be computed at different degradation points from the given data. As the HBDM predicts the overall change in YBR, the initial and final YBR reported at both RH values over the test period are utilized in this test. The overall $|\Delta YBR_{RH}|$ is measured to be 1.38 as shown in Table 6.4. This measured $\Delta(YBR)_{RH}$ differs from the HBDM prediction of 1.44 by less than 5%, which validates the correlation between humidity index ψ_H and colour change proposed by the HBDM.

To demonstrate these results, Fig. 6.5 is plotted with the initial and final measured YBR values used to compute the overall measured $|\Delta YBR_{RH}|$. Superimposed in the graph in red is the HBDM predicted ΔYBR_{RH} to illustrate how the HBDM predicted overall $|\Delta YBR_{RH}|$ varies with the measured values. The red line illustrates the predicted overall outcome over the entire period under test (based on the same R_{use} depicted as the baseline) and is not indicative of the trend, as the HBDM takes into account only the change in YBR over the entire period and not the interim values. It is also notable that although the duration of this experiment is considerably shorter than the duration the HBDM was developed for, the good correlation may be attributable to stabilization of lumen output and hence YBR early in the life cycle, allowing for comparable long term results.

Table 6.4. $\Delta(YBR)_{RH}$ HBDM prediction using Osram LEDs.

LED	**YBR Change over test period @base condition**		**YBR Change over test period @stress condition**		**Difference between RH $\Delta(YBR)_{RH}$ = (b) - (a)**	**HBDM predicted $\Delta(YBR)_{RH}$**	**Variation between predicted and measured**
	R_{use}	**$\Delta(YBR)_{RH}$ (a)**	R_{stress}	**$\Delta(YBR)_{RH}$ (b)**			
Osram 1W	70% RH	0.1	95% RH	1.48	1.38	1.44	4.10%

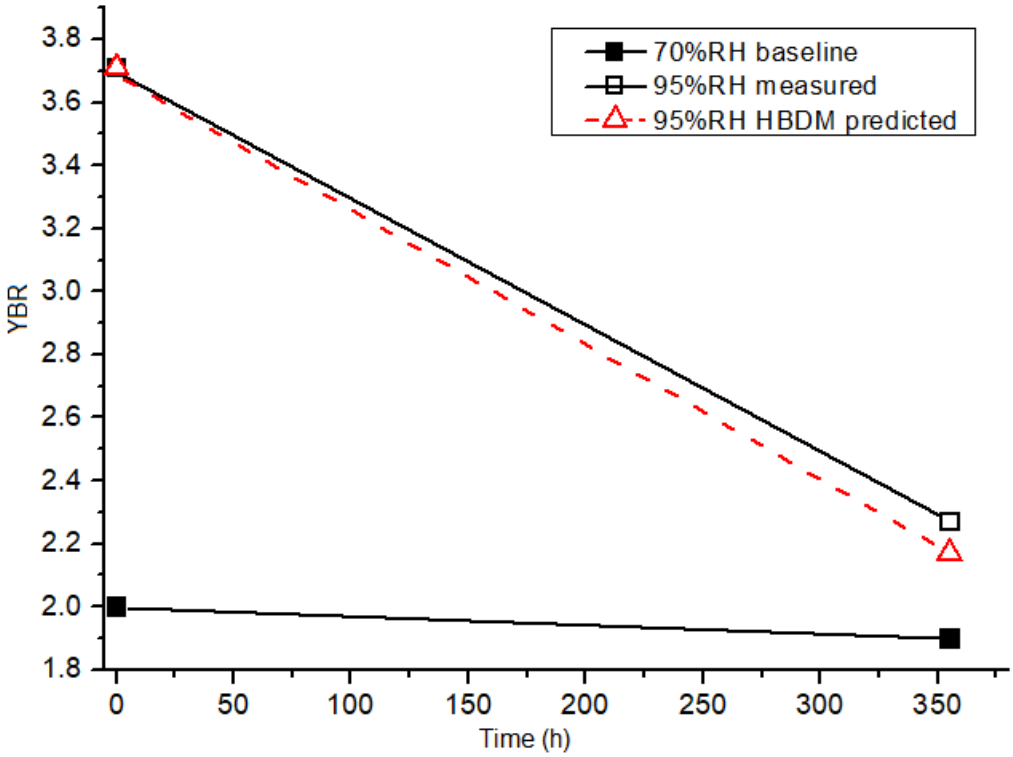

Fig. 6.5. Measured and HBDM predicted YBR shift for Osram 1W LED [6]. Solid lines represent the shift of the mean YBR data points provided by external source after 350 h.

Validation by means of data from external sources has proven to be difficult due to the lack of humidity based studies with relevant information. Additionally, data sheets typically do not publish data at more than one humidity level. Nevertheless, the results of this investigation show good correlation between the humidity index ψ_H and the colour change experienced in another research, which provides validation of the HBDM model's prognostication capability for different LEDs under different RH conditions.

Another validation of the HBDM is done through the analysis of commercial outdoor LEDs used for street illumination (Fig. 6.6). As part of a separate research project to understand the performance of LEDs in harsh environments, 20 LEDs each with a maximum rating of 30W were deployed under local outdoor conditions (average R_{stress} = 83% RH) with another 5 LEDs under indoor conditions (average R_{use} = 31% RH).

Fig. 6.6. Outdoor Street LEDs in customized enclosure deployed in local outdoor conditions. (Inset: Enclosure disassembled with LED displayed).

Similar to the 1W LEDs studied, the experimental setup described in Section (5.2) was used to extract the data used for the derivation of the required optical parameters. The lumen degradation data was curve fitted as shown in Fig. 6.7 and the degradation rates α derived. Using R_{stress} = 83% RH and R_{use} = 31% RH, ψ_H is then computed using equation (6.8) to give a value of 0.11. Based on the association of ψ_H to the absolute value of ΔYBR_{RH} described in Section (6.3.1.2), ψ_H = 0.11 corresponds to predicted $|\Delta YBR_{RH}|$ = 0.22.

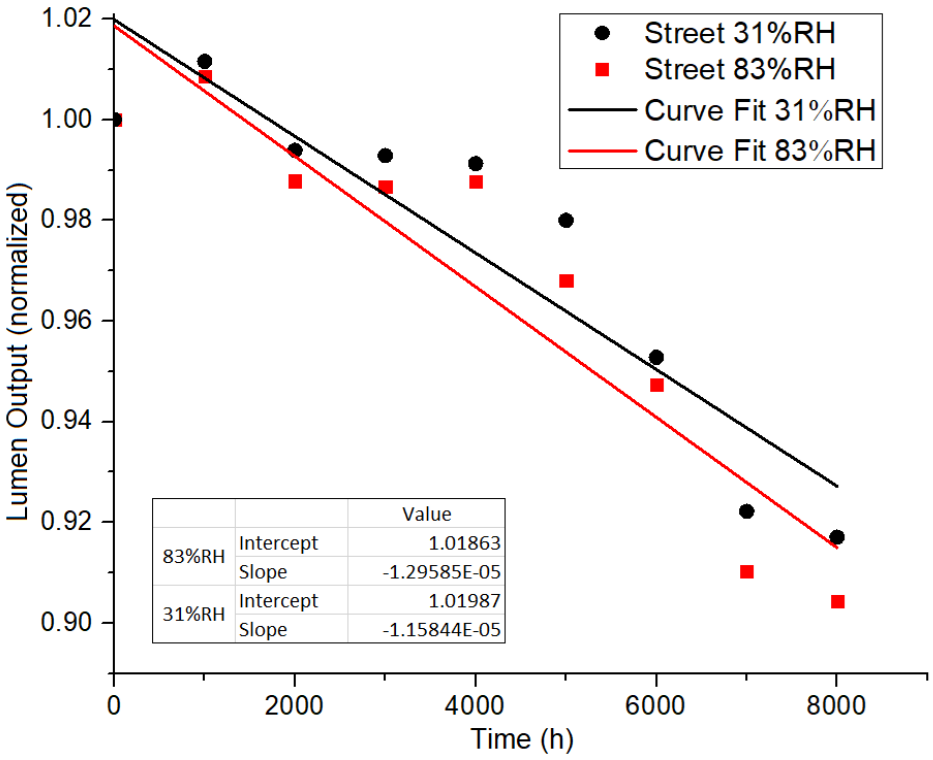

Fig. 6.7. Lumens degradation of Outdoor Street LED at 31% RH and 83% RH. Mean data provided by external source with slope of curve fit computed using procedure in Section (5.3.1).

The initial and final measured YBR at both RH values over 8000 h are used to compute the overall $|\Delta YBR_{RH}|$ as shown in Table 6.5. This measured $\Delta(YBR)_{RH}$ of 0.20 differs from the HBDM prediction of 0.22 by a fine margin of 0.02 or 9%, demonstrating that the HBDM is sufficiently robust to accommodate the variability of the outdoor street LED samples and suggests its effectiveness as a useful industrial prognostic tool.

As with the previous Osram data, to provide an illustrative comparison between the actual and HBDM prediction, the YBR starting and ending data points are plotted in Fig. 6.8 for the entire test period. Superimposed in the graph is the predicted overall difference in ΔYBR_{RH} between the RH levels to demonstrate the HBDM predicted $|\Delta YBR_{RH}|$ based on the same R_{use} baseline. Although HBDM was developed using comparatively lower power LEDs, the results with the

outdoor street LEDs bode well with the model. However, further research is needed to establish the validity of the HBDM with all LED species and power ratings.

Table 6.5. $\Delta(YBR)_{RH}$ HBDM prediction using Outdoor Street LEDs.

LED	YBR Change over test period @base condition		YBR Change over test period @stress condition		Difference between RH $\Delta(YBR)_{RH}$ = (b) - (a)	HBDM predicted $\Delta(YBR)_{RH}$	Variation between predicted and measured
	R_{use}	$\Delta(YBR)_{RH}$ (a)	R_{stress}	$\Delta(YBR)_{RH}$ (b)			
Street	31% RH	0.08	83% RH	0.28	0.20	0.22	9.0%

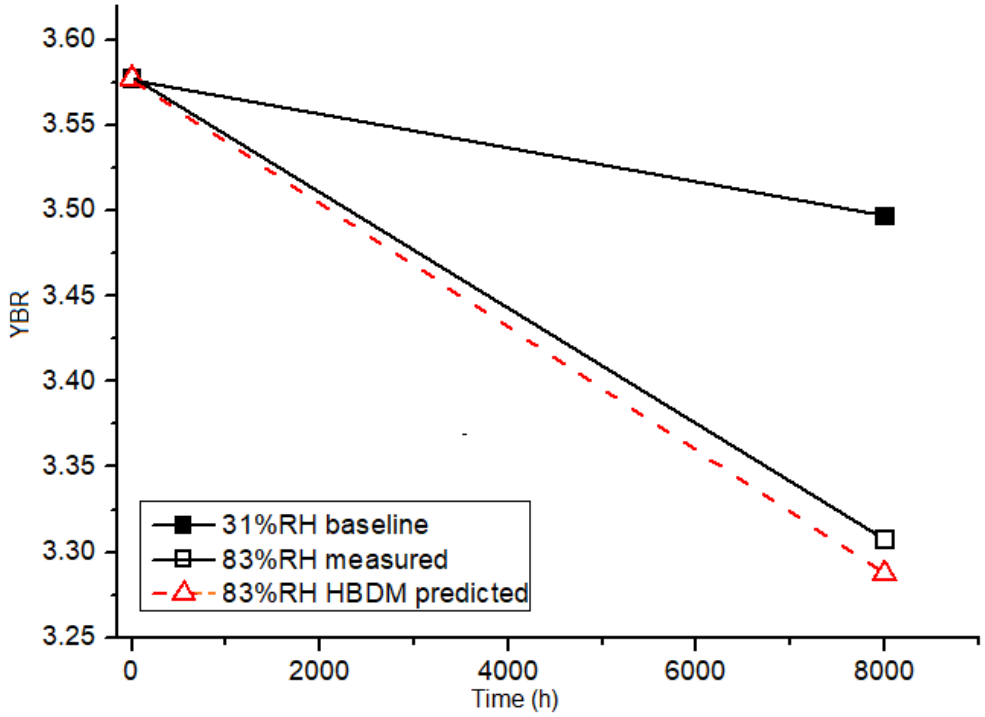

Fig. 6.8. Measured and HBDM predicted YBR shift for Outdoor Street LED. Solid lines represent the shift of the mean YBR data points after 8000 h.

6.3.1.4 Artificial Neural Network modeling of the HBDM

To further build on the HBDM, an artificial neural network model is developed to provide an efficient tool to predict the YBR changes based on the humidity degradation data. Based on the observations in Table 6.3, $\Delta(\text{YBR})_{RH} \approx 2\ \psi_H$ and an empirical expression to describe $\Delta(\text{YBR})_{RH}$ may be given as:

$$\Delta(\text{YBR})_{RH} = \frac{2log\left(\alpha_{stress}/\alpha_{use}\right)}{log\left(R_{stress}/R_{use}\right)} \tag{6.18}$$

The neural network to represent this relationship is represented in Fig 6.9 with one hidden layer and an output layer. To estimate $\Delta(\text{YBR})_{RH}$, 6 attributes are used as inputs to match up to the associated target output; LED type, R_{use}, R_{stress}, α_{use}, α_{stress}, ψ_H. The LED type is classified as 1, 2 or 3 for input as a quantifiable variable according to P1W = 1, S1W = 2, S03W = 3. A total of 60 LED samples initially (20 each from P1W, S1W and S03W described in Section (6.2.2) are used as input to the system). The input matrix thus has 6 rows for the 6 attributes and 60 columns corresponding to the LED samples. The network is designed by using the input quantities with known $\Delta(\text{YBR})_{RH}$ to train it to produce the target valuations.

If $x_1, x_2, \ldots x_6$ are the input signals into the hidden layer a^1, and z represents the product of the input signals and weight for the individual nodes plus the bias:

$$z = \sum_{i=1}^{6} x_i w_i^1 + b_i^1 \tag{6.19}$$

where w^1 and b^1 are the weights and bias terms respectively associated with the hidden layer. The activation function f_1 applied to the hidden layer is a *Tansig* hyperbolic transfer function centred at 0 with an output range between +1 and -1 given by:

$$f_1(z) = \frac{2}{[1 + exp(-2z)]} - 1 \tag{6.20}$$

The key advantage of the *Tansig* activation function besides its operation speed, is that negative and positive inputs are clearly mapped as negative and positive respectively [160]. The hidden layer output a^1 may then be represented as:

$$a^1 = f_1(z) \qquad (6.21)$$

The samples are divided into training, validation and test sets according to the following ratio: 70%, 15%, 15% corresponding to 42 for training (14 each of P1W, S1W and S03W), 9 for validation (3 each of P1W, S1W and S03W) and 9 for test (3 each of P1W, S1W and S03W) respectively.

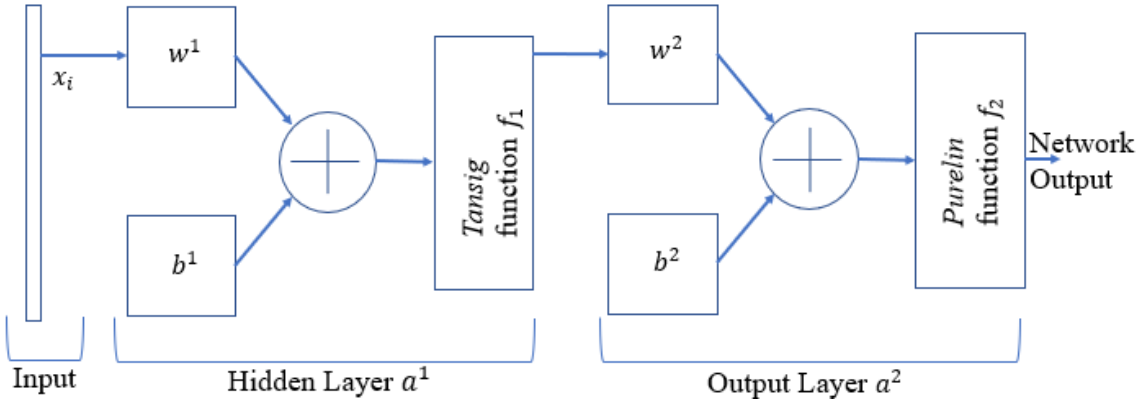

Fig. 6.9. Schematic overview of neural network setup used. *Tansig* activation function is applied to hidden layer while *Purelin* activation function is applied to the output layer. The final output of the network provides $\Delta(YBR)_{RH}$ prediction.

Using the output from the hidden layer, the final output a^2 may be represented as:

$$a^2 = f_2(a^1 w^2 + b^2) \qquad (6.22)$$

Where w^2 and b^2 are the weights and bias terms respectively associated with the output layer. The activation function f_2 applied to the output layer *Purelin*, is a linear transfer function which is a neutral transfer function which provides good representation of the input/output behaviour expected to be linear or close to linear [161]. The *Purelin* function converts the multiple input parameters to the network (described above) into a single output linear product $\Delta(YBR)_{RH}$ and is given by:

$$f_2(z) = z \tag{6.23}$$

MATLAB is used to synthesize the model. Network training on the training set continues as long as the network continues improving on the validation set. The test set is completely independent of the target results in the input data and was set to an initial pre-trained value of 0. The aim of the process is to adjust the weights to minimize the error between the actual and desired output for each neuron. The network is trained with the Levenberg-Marquardt backpropagation algorithm, which has been shown to have good results with fitting problems [162]. The results of 3 trial runs are shown in Table 6.6 with the parameters for the runs indicated in Table 6.7.

Table 6.6. Results of trial runs conducted using Levenberg-Marquardt backpropagation algorithm.

Input								
LED	1	1	2	2	2	3	3	3
R_{use}	10	10	10	10	10	10	10	10
R_{stress}	10	85	10	55	85	10	85	70
α_{use}	7.15E-6	7.15E-6	4.71E-6	4.71E-6	4.71E-6	1.80E-5	1.80E-5	1.80E-5
α_{stress}	7.15E-6	9.92E-6	4.71E-6	5.70E-6	6.20E-6	1.80E-5	6.47E-5	5.70E-5
ψ_H	0	0.15301	0	0.11176	0.12831	0	0.59804	0.59236
Expected								
$\Delta(YBR)_{RH}$	0	0.30602	0	0.22352	0.25662	0	1.19608	1.18472
Results								
Trial 1	0.00134	0.31022	0.00455	0.23890	0.24445	-0.0182	1.00562	0.92185
Trial 2	-0.0074	0.29991	0.00521	0.20556	0.22945	0.00693	1.27184	1.25999
Trial 3	0.00211	0.31211	0.00201	0.21438	0.24840	-0.0157	1.12185	1.12223

Table 6.7. Parameters of trial runs conducted.

	Trial 1	Trial 2	Trial 3
Best validation	2.62318E-05	1.1568E-01	1.0634-01
Epoch	9	6	3
No of neurons	10	50	48
R value (All Fittings)	0.856876	0.872823	0.895660
Weights	2	3	2
Bias	2	3	1
Algorithm	Levenberg-Marquardt	Levenberg-Marquardt	Levenberg-Marquardt

Performance is measured in terms of mean squared error and shown in log scale. It rapidly decreased as the network was trained and training stops once the validation performance reaches steady state. Fig. 6.10 shows the validation performance for trial 3 which illustrates the final network that performed best on the validation set.

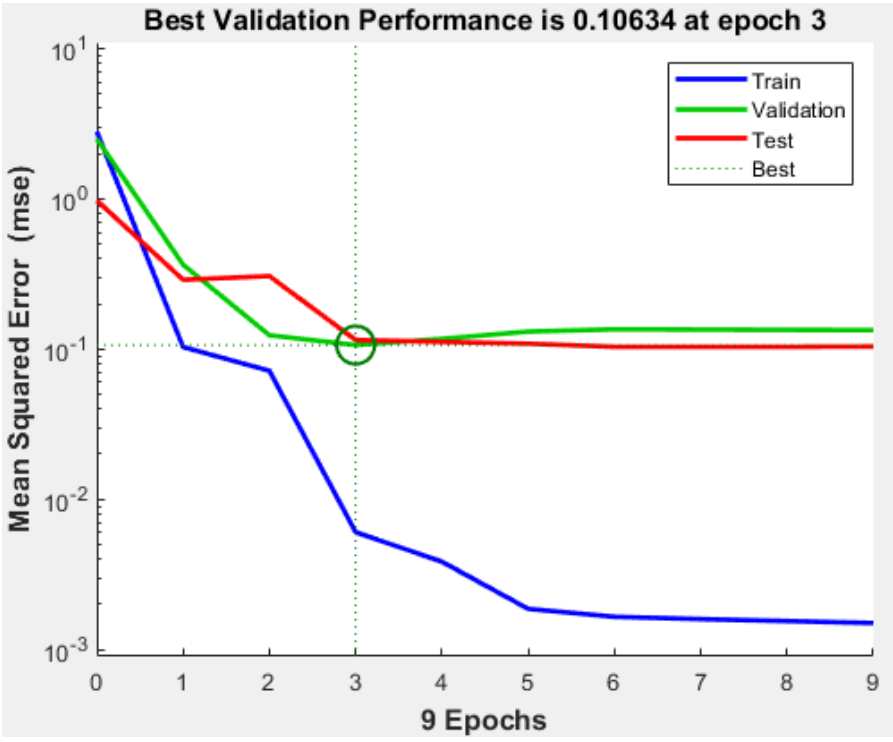

Fig. 6.10. Validation Performance plot at Epoch 3 for Trial 3.

A measure of how well the neural network has fit the data is the regression plot shown in Fig. 6.11, which is plotted across all training samples. The regression plot shows the actual network outputs plotted in terms of the associated target values. The linear fit to this output-target relationship closely intersects the bottom-left and top-right corners of the plot, implying that the network has learned to fit the data relatively well.

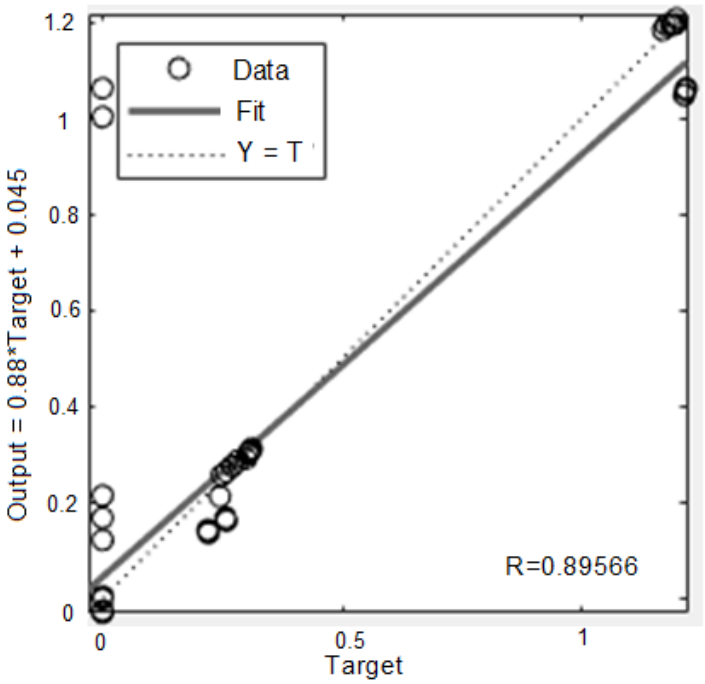

Fig. 6.11. Training Regression plot for Epoch 3 Validation stop. The solid line shows the linear regression between actual output data and targets for the 42 training data points, while the dotted line represents the ideal result (i.e. outputs = targets). The high R value indicates a good fit between the network output and the target values.

The results show that the ANN developed has good potential in simulating the HBDM given the right parametric inputs. With more samples to be used for training, the network can be fine-tuned to produce even better fit. Although this model uses 6 key parameters critical to humidity analysis derived from the HBDM, the model may be given better precision by inclusion of other important input attributes such as the chip design, material composition of the active layer, internal layer material configuration, etc. While the ANN model demonstrated accomplishes the task of HBDM prediction of YBR shift, its role may also be expanded in

practical applications to prognosticate degradation in other LED characteristics by the careful use of appropriate input attributes.

6.3.2 The Trivariate Distance Measure Approach (TDMA)

A Distance Measure approach is developed specifically for High Power LEDs due to the necessity to isolate outliers to improve reliability qualification. This approach is based on three variables and is more accurate than univariate analysis and other Distance Measure techniques as it takes into account the actual correlations and covariance of the selected features, and does not require any assumptions about the data distribution. The degradation rate, the colour shift and R_{th} change are the interdependent features specifically extracted for this method and are critical indicators of the physical state of the LED.

Anomaly identification based on single variables have setbacks, as this does not take into consideration the other variables. While one variable might indicate an anomaly, the LED might still be within the specified boundaries of the other variables, and overall be an acceptable operational unit. The difficulty is to define the constitution of an overall acceptable LED, and while there may be ambiguity in defining outliers in the overall context of LED health [163], one possibility is the use of a multivariate model with covariance or correlation between the variables based on preset boundaries or standards.

The TDMA uses the shifting from the expected norms of the combined variables in multivariate space to identify outliers based on the Mahalanobis Distance technique. The LED degradation rate α, the colour shift ΔYBR and the change in thermal resistance ΔR_{th} are the critical measurements used in this combined model. While any one of these on their own may be a useful standalone indicator of outlier LEDs, a combined multivariate approach to evaluate the collective deviation from these three correlated quantities would be more accurate in identifying outliers.

A data point can be a univariate outlier for any variable but not a multivariate outlier, and with complex dependencies between variables, the reverse may be true. Since the Mahalanobis Distance (MD) accounts for unequal variances as well as correlations between features, it will evaluate the distance by assigning different weights or importance factors to the features of data points [164], making MD a more sensitive measure than checking the dimensions individually. Unlike Euclidean distance, MD or Squared MD would take into account any correlation between the degradation rate α, the colour shift ΔYBR and the change in thermal resistance ΔR_{th} in computing the distance to a combined mean. The Squared Mahalanobis Distance D utilizes the square of the interpoint distance and is a generalized form of the MD. D accounts for the variance and covariance between the measures and may be defined as:

$$D = (\omega - \mu)^T S^{-1} (\omega - \mu) \tag{6.24}$$

where:

$$S^{-1} = \begin{bmatrix} cov(\omega_1, \omega_1) & cov(\omega_1, \omega_2) & cov(\omega_1, \omega_3) \\ cov(\omega_2, \omega_1) & cov(\omega_2, \omega_2) & cov(\omega_2, \omega_3) \\ cov(\omega_3, \omega_1) & cov(\omega_3, \omega_2) & cov(\omega_3, \omega_3) \end{bmatrix} \tag{6.25}$$

and D is the Squared Mahalanobis Distance or generalized squared interpoint distance, ω an observation from a set of observations with mean μ and S the covariance matrix for all the parameters. The criteria for an anomaly to be identified can be obtained from Physics of Failure (POF) models, historical databases, or expert knowledge. Depending on the specific requirement, the outlier boundary may be set as a multiple of the standard deviation, σ for each measure. Using S03W samples measured at 10% RH and at 85% RH, the univariate threshold values are computed for all the LEDs at μ, ($\mu + \sigma$) and ($\mu + 2\sigma$) and the corresponding Squared Mahalanobis Distance D computed as shown in Table 6.8.

Table 6.8. Squared Mahalanobis Distance D and univariate boundary computations at specific thresholds.

Thresholds	ΔYBR	ΔR_{th}	α	D
10% RH				
μ	0.337	1.053	1.76E-05	0
$(\mu + \sigma)$	0.341	1.116	1.77E-05	3.6497
$(\mu + 2\,\sigma)$	0.344	1.178	1.77E-05	14.5988
85% RH				
μ	1.559	8.799	6.48E-05	0
$(\mu + \sigma)$	1.645	11.581	6.82E-05	2.1372
$(\mu + 2\sigma)$	1.730	14.363	7.15E-05	8.5488

Table 6.9 shows the computed variables and corresponding D values for six S03W samples selected from the 20 S03W LEDs at different humidity settings in Section 6.2.2, with the darkened cells indicating the particular variable being out of the specific σ range for that measure. It can be seen that for samples B, C, E and F, although a variable is out of the specific σ range, the D values are still within the corresponding σ range established in Table 6.8. These LEDs are considered as within the Mahalanobis Distance multivariate boundary although they are univariate outliers. On the other hand, sample D has 2 variables outside 2σ. With $D > D_{(\mu + 2\sigma)}$, sample D is classified as a multivariate outlier. If the univariate threshold of μ at 2σ for this sample was used solely, the LED would have been considered acceptably within $D_{(\mu + 2\sigma)}$ specification instead of being considered an outlier placed beyond by the TDMA approach. In spite of the association between the variables, deviation from one variable norm while being within specification of another is possible due to the different rates of degradation of the variables, or different mechanisms dominating. Using all 20 S03W samples at each RH level described in Section (6.2.2), the relative positions of the LEDs in 3-D space were plotted using MATLAB in Fig. 6.12.

Table 6.9. Squared Mahalanobis Distance D and univariate computations for various samples at different RH conditions.

	ΔYBR	**ΔR_{th}**	***α***	***D***	**Univariate criterion**	**TDMA criterion**
10% RH						
Sample A	0.339	0.995	1.75E-05	1.367	Within 1σ	Within 1σ
Sample B	0.334	1.158	1.77E-05	3.148	Outlier 1σ (ΔR_{th})	Within 1σ
85% RH						
Sample C	1.539	11.765	6.43E-05	1.929	Outlier 1σ (ΔR_{th})	Within 1σ
Sample D	1.876	18.645	6.73E-05	17.719	Outlier 2σ (ΔYBR + ΔR_{th})	Outlier 2σ
Sample E	1.771	8.845	6.82E-05	8.169	Outlier 2σ (ΔYBR)	Within 2σ
Sample F	1.556	15.534	6.45E-05	8.025	Outlier 2σ (ΔR_{th})	Within 2σ

Failure analysis conducted (described in Section (5.3.4)) shows delamination in Sample D only. In addition, EDX elemental analysis reveal a considerable increase in elemental oxygen for Sample D compared to the other samples at the interface of the chip and the lead frame, shown as a darkened cell in Table 6.10. As discussed in in Section (5.3.4), the higher oxygen content in sample D indicates a higher chance of silver corrosion leading to severe colour deterioration compared to the other samples. These results justify the TDMA identification of sample D as an outlier.

Table 6.10. Weight by percentage of key elements for the LED samples.

Sample	Oxygen O weight %	Carbon C weight %	Silver Ag weight %
A	6.16	2.41	84.13
B	6.83	2.54	82.22
C	7.76	2.78	81.17
D	13.04	2.25	84.38
E	7.23	2.77	80.45
F	7.19	2.10	86.10

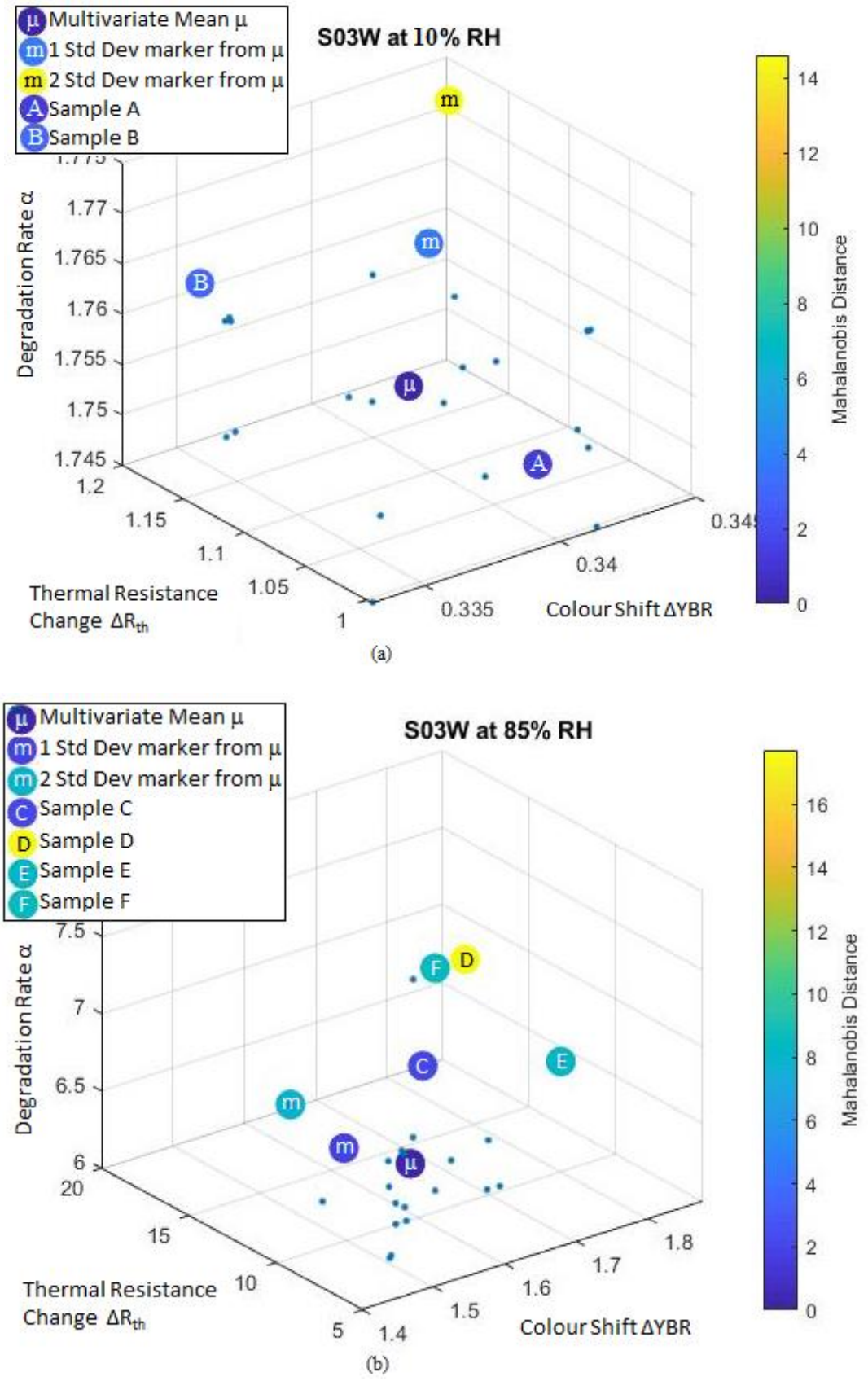

Fig. 6.12. 3-D diagram of computed TDMA data points at (a) 10% RH and (b) 85% RH. Data points shown are computed from all the 20 S03W LED samples at each RH level to demonstrate the distribution.

However it should be mentioned that while the Mahalanobis method performs well for identifying scattered outliers, it does not perform as accurately when the data set contains severely clustered outliers, due to masking and swamping effects [165]. The TDMA approach should be used in conjunction with a POF approach as part of a comprehensive prognostic tool for proper anomaly evaluation, with the sensitivity tweaked if necessary by adjusting the type or number of variables used. The TDMA provides indication of the physical state of the LED and utilized together with the HBDM, provides an effective tool in the overall LED health management process, especially for the LED manufacturing industry, where the combined methodology may be used to complement existing component and functional testing of LEDs to improve product reliability.

6.4. Summary

A new approach to indicate both the lumen and colour degradation of LEDs due to the effects of humidity is developed. A practical predictive method from the degradation behaviour is proposed to gauge the long-term moisture incursion by means of a humidity index ψ_H. This index shows good agreement with the absolute change in YBR with a positive association although a limitation of the model is that the direction of this change is not directly discernible. $\Delta(\mathrm{YBR})_{\mathrm{RH}}$ values extracted from experimental degradation data derived from separate independent external sources at different RH show close approximation to the HBDM predicted values. This provides validation of the HBDM's robustness for different LEDs under different RH conditions.

The HBDM is effective in indicating the extent of the impact of humidity and the relative YBR colour shift associated with this impact, demonstrating good accuracy with longer periods of moisture exposure. Physical analyses have indicated that P1W and S1W may exhibit chip deterioration while S03W exhibits phosphor or package decay by delamination and silver layer

corrosion. The results are in line with the HBDM in terms of lumen and YBR predictions. The HBDM is modeled by a feed forward network with six key attributes or indicators of LED degradation used to develop the HBDM, which shows good fitting results.

The HBDM alone does not however directly provide information on impending LED failures or improve reliability qualification. Accordingly, the study goes further to propose a new Trivariate Distance Measure Approach (TDMA) using three interrelated features which provide good indication of the state of the LED. The results demonstrate that this approach is a more effective gauge of anomalies than using the usual screen test of one or two variables. Used together with the HBDM, these two methods provide powerful prognostic tools in LED health management.

In the LED manufacturing binning process where LEDs may be categorized according to light output, the HBDM serves a cost-effective and rapid tool to sub-categorize according to colour output at various RH levels without the need for physical measurement. These binned LEDs may then subsequently be subject to the TDMA to ensure the overall reliability of each LED. On the other hand, if the integrity of the LED is important before a colour categorization exercise or experimentation (for example in laboratory research work), the TDMA may be performed prior to the HBDM to ensure that the work is performed on parametrically sound LEDs.

Chapter 7

Conclusions

This concluding chapter is divided primarily into 2 parts. In the first, the key findings are discussed with focus on how they impact academia and industry, while in the second, recommendations are proposed to either enhance the processes involved or proceed to the next stage of the research.

7.1. Concluding Remarks

This thesis presents research on both the thermal and reliability aspects of LEDs. The main stressors that induce heat accumulation in the LED, namely the drive current, the operating temperature and the relative humidity and their impact on the electrical-optical-thermal performance of the LED were analyzed in turn to uncover specific configurations and conditions upon which thermal management could be improved. In Chapter 3, anomalies involving temperature control affecting the LED self-heating which could affect subsequent measurements during EOT measurements were uncovered. Consequently, the proper temperature control procedures were determined to ensure accurate measurements. The universal use of temperature control in electrical sweep and transient thermal measurements in both industry and academia warrants immediate attention to these findings to prevent data reporting errors. As LEDs are commonly integrated into products downstream, the errors are magnified in the final device, potentially causing product failures due to component specification mismatch. In addition, LED data sheets and documentations reporting erroneous specifications may result in inaccurate LED choices for the consumer.

In Chapter 4, the effects of phosphor thickness and particle concentration on the optical efficiency and temperature rise on phosphor-coated LED packages were analyzed. A thicker

phosphor layer and a higher phosphor particle concentration will increase the amount of backscattering and back reflection of light from the phosphor layer. These light extraction losses not only reduce the optical efficiency of the light output but also cause heat accumulation in the phosphor layer, leading to higher LED T_j. The chromaticity shift and light extraction losses also depend on the uniformity of phosphor particles deposited over the LED surface. A non-uniform and sparse phosphor layer affects the Correlated Colour Temperature (CCT) and the spectral YBR due to the disproportionate contribution of light emission between the LED device and the phosphor layer. Furthermore, the YBR reduces with temperature due to higher Stoke's energy and light extraction losses in the phosphor layer. The thermal performance of a LED package however, is dependent on the die-bonding configurations (conventional and flip-chip). Due to the improved heat dissipation capabilities in flip-chip bonding, the temperature rise and R_{th} of the package was observed to reduce with temperature. By alleviating the heat accumulation in the package, flip-chip bonding can dissipate the heat generated in the GaN LED and phosphor layer effectively besides achieving more stable colorimetric properties such as CCT and YBR. The research provides a comprehensive investigation of the thermal impact by current and temperature stressors on different LED configurations, and also details the heat accumulation and dissipation profiles of such configurations by different packaging architectures. The analysis links the relationship between various LED configurations and thermal performance, a critical issue to industry in particular when selecting the right LED for specific application, while at the same time contributing important LED thermal management principles.

However, the T_j is also impacted by the long-term humidity effects which affect the temperature rise and R_{th}. In Chapter 5, the experiments also reveal photometric and colorimetric degradation at high humidity. The study indicates that the 1 W LEDs show accelerated chip failure compared to 0.3 W LED. It was observed however that the temperature

rise and R_{th} for the flip-chip bonded LEDs do not increase substantially as compared to the conventionally bonded LEDs. This is because the T_j can be reduced with a flip-chip die-bonding configuration where the heat generated in the LED chip is dissipated effectively onto the AlN substrate, thereby reducing the increase in temperature rise and R_{th}. The experimental results are supported by evaluation of the derivative structure functions. In addition, as the R_{th} of the LED package varies with different humidity levels, there is a need to specify the conditions of humidity in data sheets as LED manufacturers routinely specify a universal R_{th} value under a fixed operating condition [7, 32]. This information disclosure not only benefits system integrators and end-consumers, but also allows the manufacturers to align their LED package designs to cater to the relative humidity of the region of operation. As part of a government supported initiative, the findings in this phase of the research were communicated to relevant government agencies and research institutes providing the foundation for proper selection and management of lighting LEDs in open spaces in schools, parks and housing areas exposed to the environment humid conditions in Singapore. In addition, as part of the national Energy Efficiency program, the research played a key role in the institution of LEDs over fluorescent lighting in public infrastructure projects.

This increase in temperature rise is associated with both lumen degradation and colour shift, both of which are critical indicators of LED reliability. Using the lumen degradation data under varying conditions of relative humidity, the lumens maintenance of the LED is characterized using the TM-21 method, from which a humidity based degradation model (HBDM) is built. A practical estimation method from the degradation behaviour is developed to gauge the moisture incursion by means of a humidity index ψ_H. This index shows good agreement with the change in the colour shift YBR with a positive association. The HBDM provides a quantification of the extent of the impact of humidity on the LED. In addition, the results demonstrate that the model is capable of predicting the relative YBR colour shift associated

with the level of this impact, an important attribute used not only to determine the physical deterioration, but also to evaluate the suitability for particular industrial applications. Differentiating itself from other numerically complex data-driven methods, the HBDM is a novel yet simple model allowing for a direct and rapid reliability prognostication. The model is a unique practical approach to quantify the degree of moisture incursion and the corresponding colour shift, which is expected to provide an effective yet descriptive approach to indicating LED degradation due to humidity, distinguishing the mode or mechanism of failure. The index also easily translates to remaining lifetime, which provides the user with the linkage between the impact of humidity and the lifespan of different LEDs.

In the LED manufacturing industry, the humidity index developed allows for sub-binning according to the LED performance at different levels of relative humidity instead of being broadly based at a single relative humidity level, giving a higher level of reliability precision catering for markets in different areas of the world with different relative humidity levels. The index allows for stage checking in the binning process, providing a cost-effective means of benchmarking and ranking the quality of the binned LEDs, which would be useful particularly to LED system integrators. As the HBDM is derived from long-term LED degradation behaviour, it also provides the manufacturer insights on the long-term behaviour prognostication of the LED under specific humidity environments. Such information provided in testing documentation or datasheets allows both system integrators and consumers alike to understand the range of proper operation for different humidity conditions and make the correct LED selection. As the HBDM development was conducted with the consultation and support of LED manufacturers and integrators who incorporate the LEDs into their end products, the model has received endorsement for its concept, with the view to impending implementation with the refinements discussed later in the second part of this chapter.

To complement the HBDM lumen and colour stability predictive capability, the Trivariate Distance Measure Approach (TDMA) provides a reliable and accurate method to weed out outliers using the same humidity based data. The sensitivity of this flexible approach may be adjusted by changing the type or number of variables used. The TDMA provides indication of the physical state of the LED and utilized together with the HBDM, provides an effective tool in the overall LED thermal management process, especially for the LED manufacturing industry, where the methodology may be used to complement existing component and functional testing of LEDs to improve product reliability.

The work presented in this thesis is a detailed analysis of the impact of the temperature, current and humidity stressors on the EOT characteristics of the LED. Based on these studies, the HBDM and TDMA prognostic models were developed with the aim of providing academia and industry with tools to not only indicate the current physical condition of the LED exposed to long term humid environments, but also to predict and prevent future issues that might arise.

7.2. Recommendations for Future Work

The research presented paves the way for future work based on the following recommendations.

1. To overcome the issues of erroneous control of the self-heating in LEDs during measurement, it is proposed that an adaptive environmental temperature feedback control be developed to automatically detect and control the test temperature. Using the LED junction temperature as input, the system predictively controls the temperature setting or duty cycle to the correct value in response to the input. The system will provide industry and academia alike with an automated solution to ensure accurate measurement results. Fig 7.1 illustrates the proposed adaptive temperature feedback control system.

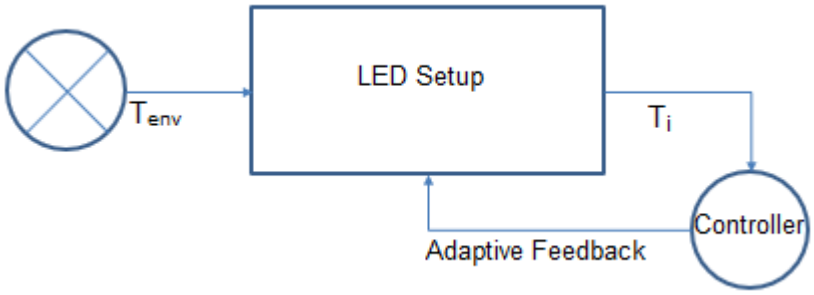

Fig. 7.1. Proposed adaptive temperature feedback control system. T_{env} is the control temperature of the TEC, and T_j the LED junction temperature.

2. Based on the test parameters used for the HBDM, it is proposed that a repository be setup consisting of a library of measurement results for LEDs of different brands, power levels and package configurations. The repository will provide an invaluable resource for academia and industry to tap on for further research and developmental work, and also a platform for expanding the database to improve the effectiveness of the HBDM and its associated ANN simulations. In addition, the repository augments the accuracy of the model with a larger sample size, reinforcing the user confidence.
3. By using a larger sample size through the proposed repository, it is proposed that a POF based outlier labelling process is conducted to further investigate any TDMA cases of false positives or false negatives arising, in particular any that might contradict the HDMA results. If necessary, outlier accommodation via robust statistical techniques may be designed to fine-tune the model.
4. To provide a single compact combined model encompassing the HBDM and TDMA, the ANN solution may be enhanced to provide outputs of moisture incursion, colour prediction and outlier detection, all inputs based on the same database created in the repository. This upgrade from an individualised system provides convenience to the user, while improving the functionality of the HBDM and TDMA through the effectiveness of the ANN and the use of repository. The resolution of the remodelled ANN may be improved through

experimentation with different activation functions, training algorithms, neuron numbers, etc. to optimize the result which provides a complete picture of the LED's humidity performance and current benchmarked physical status. In addition, to complete this proposed prognostication combined model, the suggested adaptive temperature feedback control system is implemented at the backend to ensure the integrity of the measurement results being input into the ANN. Fig. 7.2 illustrates the proposed combined model which incorporates the HBDM and TDMA.

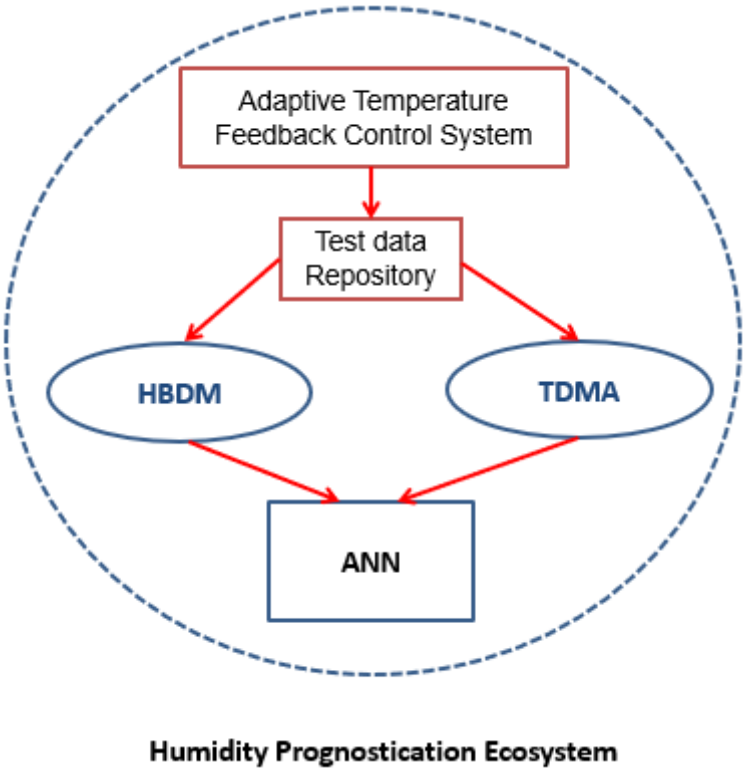

Fig. 7.2. Proposed compact combined model incorporating HBDM and TDMA.

References

[1] A. Poppe and C. J. M. Lasance, "On the Standardization of Thermal Characterization of LEDs," in *IEEE Semiconductor Thermal Measurement and Management Symposium*, 2009, pp. 151-158.

[2] J. Schanda, *Colorimetry: Understanding the CIE system*: John Wiley & Sons, 2007.

[3] N. T. Tran and F. G. Shi, "Studies of Phosphor Concentration and Thickness for Phosphor-Based White Light-Emitting-Diodes," *Journal of Lightwave Technology*, vol. 26, pp. 3556-3559, 2008.

[4] N. T. Tran, J. P. You, and F. G. Shi, "Effect of Phosphor Particle Size on Luminous Efficacy of Phosphor-Converted White LED," *Journal of Lightwave Technology*, vol. 27, pp. 5145-5150, 2009.

[5] J. Hu, L. Yang, and M. W. Shin, "Electrical, Optical and Thermal Degradation of High power GaN/InGaN Light-Emitting Diodes," *Journal of Physics D: Applied Physics*, vol. 41, p. 035107, 2008.

[6] C. M. Tan and P. Singh, "Time Evolution Degradation Physics in High Power White LEDs Under High Temperature-Humidity Conditions," *IEEE Transactions on Device and Materials Reliability*, vol. 14, pp. 742-750, 2014.

[7] Philips Lumileds. Luxeon Rebel Plus Datasheet [Online]. Available: https://www.lumileds.com/uploads/380/DS107-pdf

[8] "Life-Cycle Assessment of Energy and Environmental Impacts of LED Lighting Products," ed: U.S. Department of Energy, 2012.

[9] W. Guo, T. Ding, B. Cui, F. Yin, D. Cui, and W. Yan, "Thermal Resistance Analysis of High Power Light Emitting Diodes," in *IEEE Advances in Optoelectronics and Micro/Nano-Optics*, 2010, pp. 1-4.

[10] "Assessment of Solid-State Lighting, Phase 2," ed: Committee on Assessment of Solid-State Lighting, National Academies of Sciences, Engineering & Medicine, 2017.

[11] P. Singh and C. M. Tan, "A review on the humidity reliability of high power white light LEDs," *Microelectronics Reliability*, vol. 61, pp. 129-139, 6// 2016.

[12] C. Kim, J. Lee, J. Cho, D. Kim, and T. Seo, "Experimental Study of Humidity Control Methods in a Light-Emitting Diode (LED) Lighting Device," *Journal of Mechanical Science and Technology*, vol. 29, pp. 2501-2508, 2015.

[13] C. Qian, J. Fan, X. Fan, and G. Q. Zhang, "Advances in Reliability Testing and Standards Development for LED Packages and Systems," in *Solid State Lighting Reliability Part 2*, ed: Springer, 2018, pp. 77-114.

[14] M. Chang, D. Das, P. Varde, and M. Pecht, "Light Emitting Diodes Reliability Review," *Microelectronics Reliability*, vol. 52, pp. 762-782, 2012.

[15] P. Lall and H. Zhang, "LED Lumen Degradation and Remaining Life under Exposure to Temperature and Humidity," in *ASME International Mechanical Engineering Congress and Exposition*, 2013, p. A076.

[16] C. M. Tan, B. Chen, and M. Xiong, "Study of Humidity Reliability of High Power LEDs," in *IEEE Solid-State and Integrated Circuit Technology International Conference*, 2010, pp. 1592-1595.

[17] J. Sikorska, M. Hodkiewicz, and L. Ma, "Prognostic Modelling Options for Remaining Useful Life Estimation by Industry," *Mechanical Systems and Signal Processing*, vol. 25, pp. 1803-1836, 2011.

[18] United Nations Environment Programme, "Accelerating the Global Adoption of Energy Efficient Lighting," ed: UN Environment – Global Environment Facility, 2017.

[19] P. Lall and H. Zhang, "Assessment of Lumen Degradation and Remaining Life of Light-Emitting Diodes Using Physics-Based Indicators and Particle Filter," *Journal of Electronic Packaging,* vol. 137, pp. 021002-021002-10, 2015.

[20] I. Ashdown, S. Robinson, and M. Salsbury, *Binning and filtering: the six-color solution* vol. 6337: SPIE, 2006.

[21] S. W. Sanderson and K. L. Simons, "Light Emitting Diodes and the Lighting Revolution: The Emergence of a Solid-State LIghting Industry," *Research Policy,* vol. 43, pp. 1730-1746, 2014.

[22] J. Y. Tsao, J. J. Wierer, L. E. Rohwer, M. E. Coltrin, M. H. Crawford, J. A. Simmons, *et al.*, "Ultra-efficient solid-state lighting: Likely characteristics, economic benefits, technological approaches," in *III-Nitride Based Light Emitting Diodes and Applications*, ed: Springer, 2017, pp. 11-28.

[23] H. Masui, S. Nakamura, S. P. DenBaars, and U. K. Mishra, "Nonpolar and Semipolar III-Nitride Light-Emitting Diodes: Achievements and Challenges," *IEEE Transactions on Electron Devices,* vol. 57, pp. 88-100, 2010.

[24] E. F. Schubert, "Invited talk: Promises and challenges in light-emitting diodes for lighting applications," in *IEEE Workshop on Microelectronics and Electron Devices*, 2011, pp. 1-1.

[25] J. K. Kim and E. F. Schubert, "III-Nitride light-emitting diodes for solid state lighting revolution," in *2009 Asia Communications and Photonics conference and Exhibition (ACP),* 2009, pp. 1-2.

[26] V. Chandola, A. Banerjee, and V. Kumar, "Anomaly Detection: A survey," *ACM computing surveys (CSUR),* vol. 41, p. 15, 2009.

[27] Y. Ma, X. Yu, B. Xie, R. Hu, and X. Luo, "Analysis of Phosphor Heat Generation and Temperature Distribution in Remote-plate Phosphor-Converted Light-Emitting Diodes," in *Asian Conference on Thermal Sciences*, 2017, p. 00328.

[28] C. P. Wang, "Effects of Diode Voltage and Thermal Resistance on the Performance of Multichip LED Modules," *IEEE Transactions on Electron Devices*, vol. 63, pp. 390-393, 2016.

[29] E. Kolodeznyi, I. Ivukin, V. Serebryakova, V. Bougrov, and A. Romanov, "Thermal Analysis of Phosphor Containing Silicone Layer in High Power LEDs," *Materials Physics and Mechanics*, vol. 21, pp. 283-287, 2014.

[30] S. Maeng and S. Ko, "Thermal Characteristics for Chip on Metal Package of LED Lighting Module," *Materials Science in Semiconductor Processing*, vol. 38, pp. 357-361, 2015.

[31] S. Koh, H. Ye, M. Y. Mehr, J. Wei, W. D. V. Driel, L. B. Zhao, *et al.*, "Investigation of Color Shift of LEDs-based Lighting Products," in *IEEE International Conference onThermal, Mechanical and Multi-Physics Simulation and Experiments in Microelectronics and Microsystems*, 2014, pp. 1-5.

[32] X. Luo and R. Hu, "Calculation of the Phosphor Heat Generation in Phosphor-Converted Light-Emitting Diodes," *International Journal of Heat and Mass Transfer*, vol. 75, pp. 213-217, 2014.

[33] K. J. Chen, B. C. Lin, H. C. Chen, M. H. Shih, C. H. Wang, H. T. Kuo, *et al.*, "Effect of the Thermal Characteristics of Phosphor for the Conformal and Remote Structures in White Light-Emitting Diodes," *IEEE Photonics Journal*, vol. 5, pp. 8200508-8200508, 2013.

[34] S. Müller, T. Zahner, F. Singer, G. Schrag, and G. Wachutka, "Evaluation of Thermal Transient Characterization Methodologies for High-Power LED Applications," *Microelectronics Journal*, vol. 44, pp. 1005-1010, 2013.

[35] H. Alexander, S. Maximilian, E. Liu, and E. Gordon, "Transient thermal analysis as measurement method for IC package structural integrity," *Chinese Physics B,* vol. 24, p. 068105, 2015.

[36] L. Brown, "Building an Energy-Efficient Global Economy," in *World on the edge: how to prevent environmental and economic collapse*, ed: Routledge, 2012, pp. 100-101.

[37] Y. Wang, K. Wang, Z. Han, Z. Yin, C. Zhou, F. Du, *et al.*, "High Color Rendering Index Trichromatic White and Red LEDs Prepared from Silane-functionalized Carbon Dots," *Journal of Materials Chemistry C,* vol. 5, pp. 9629-9637, 2017.

[38] N. T. Tran, C. G. Campbell, and F. G. Shi, "Study of Particle Size Effects on an Optical Fber Sensor Response Examined with Monte Carlo Simulation," *Applied Optics,* vol. 45, pp. 7557-7566, 2006.

[39] Z. Liu, S. Liu, K. Wang, and X. Luo, "Studies on Optical Consistency of White LEDs Affected by Phosphor Thickness and Concentration Using Optical Simulation," *IEEE Transactions on Components and Packaging Technologies,* vol. 33, pp. 680-687, 2010.

[40] M. Huang and L. Yang, "Heat Generation by the Phosphor Layer of Hgh-Power White LED Emitters," *IEEE Photonics Technology Letters,* vol. 25, pp. 1317-1320, 2013.

[41] M. Dal Lago, M. Meneghini, N. Trivellin, G. Mura, M. Vanzi, G. Meneghesso, *et al.*, "Phosphors for LED-based Lght Sources: Thermal Properties and Reliability Issues," *Microelectronics Reliability,* vol. 52, pp. 2164-2167, 2012.

[42] X. Luo, X. Fu, F. Chen, and H. Zheng, "Phosphor Self-Heating in Phosphor Converted Light Emitting Diode Packaging," *International Journal of Heat and Mass Transfer,* vol. 58, pp. 276-281, 2013.

[43] Y. Bohan, N. T. Tran, Y. Jiun-Pyng, and F. G. Shi, "Can Junction Temperature Alone Characterize Thermal Performance of White LED Emitters?," *IEEE Photonics Technology Letters,* vol. 23, pp. 555-557, 2011.

[44] X. Shen, D. Zhang, X. Fan, G. Hu, X. Bian, and L. Yang, "Fabrication and Characterization of YAG:Ce Phosphor Films for White LED Applications," *Journal of Materials Science: Materials in Electronics,* vol. 27, pp. 976-981, 2016.

[45] M. Y. Tsai, C. Y. Tang, C. H. Wang, Y. Y. Tsai, and C. H. Chen, "Investigation on Some Parameters Affecting Optical Degradation of LED Packages During High-Temperature Aging," *IEEE Transactions on Device and Materials Reliability,* vol. 15, pp. 335-341, 2015.

[46] X. Tao, H. Chen, S. N. Li, and S. R. Hui, "A New Noncontact Method for the Prediction of Both Internal Thermal Resistance and Junction Temperature of White Light-Emitting Diodes," *IEEE Transactions on Power Electronics,* vol. 27, pp. 2184-2192, 2012.

[47] L. Yang, J. Hu, L. Kim, and M. W. Shin, "Variation of Thermal Resistance with Input Power in LEDs," *Physica Status Solidi (c),* vol. 3, pp. 2187-2190, 2006.

[48] M. Ha and S. Graham, "Development of a Thermal Resistance Model for Chip-On-board Packaging of High Power LED Arrays," *Microelectronics Reliability,* vol. 52, pp. 836-844, 2012.

[49] X. Luo, Z. Mao, J. Yang, and S. Liu, "Engineering Method for Predicting Junction Temperatures of High-Power Lght-Emitting Diodes," *IET Optoelectronics,* vol. 6, pp. 230-236, 2012.

[50] T. K. Law, F. Lim, Y. Li, K. K. G. Yeong, G. K. E. Sng, M. V. Uvarajan, *et al.*, "Implications of Phosphor Coating on the Thermal Characteristics of Phosphor-

Converted White LEDs," *IEEE Transactions on Device and Materials Reliability,* vol. 16, pp. 576-582, 2016.

[51] M. W. Jeong, S. W. Jeon, S. H. Lee, and Y. Kim, "Effective heat dissipation and geometric optimization in an LED module with aluminum nitride (AlN) insulation plate," *Applied Thermal Engineering,* vol. 76, pp. 212-219, 2015.

[52] J. Hu, L. Yang, L. Kim, and M. W. Shin, "The Ageing Mechanism of High-Power InGaN/GaN Lght-Emitting Diodes Under Electrical Stresses," *Semiconductor Science and Technology,* vol. 22, p. 1249, 2007.

[53] S. W. Lee, D. C. Oh, H. Goto, J. S. Ha, H. J. Lee, T. Hanada, *et al.*, "Origin of forward leakage current in GaN-based light-emitting devices," *Applied Physics Letters,* vol. 89, p. 132117, 2006.

[54] J. Singh, *Semiconductor Optoelectronics: Physics and Technology*: McGraw-Hill, 1995.

[55] S.-L. Chuang, A. Ishibashi, S. Kijima, N. Nakayama, M. Ukita, and S. Taniguchi, "Kinetic model for degradation of light-emitting diodes," *IEEE Journal of Quantum Electronics,* vol. 33, pp. 970-979, 1997.

[56] J. Huang, D. S. Golubović, S. Koh, D. Yang, X. Li, X. Fan, *et al.*, "Optical degradation mechanisms of mid-power white-light LEDs in LM-80-08 tests," *Microelectronics Reliability,* vol. 55, pp. 2654-2662, 2015.

[57] L. Xiaobing, W. Bulong, and L. Sheng, "Effects of Moist Environments on LED Module Reliability," *IEEE Transactions on Device and Materials Reliability,* vol. 10, pp. 182-186, 2010.

[58] C. M. Tan, B. K. E. Chen, G. Xu, and Y. Liu, "Analysis of Humidity Effects on the Degradation of High-Power White LEDs," *Microelectronics Reliability,* vol. 49, pp. 1226-1230, 2009.

[59] J. Hu, L. Yang, and M. W. Shin, "Mechanism and Thermal Efect of Delamination in Lght-Emitting Diode Packages," *Microelectronics Journal,* vol. 38, pp. 157-163, 2007.

[60] J. Hu, L. Yang, and M. W. Shin, "Thermal Effects of Moisture inducing Delamination in Light-Emitting Diode Packages," in *IEEE Electronic Components and Technology Conference* 2006, pp. 635516-635516-9.

[61] P. Lall, Z. Hao, and L. Davis, "A Comparison of Temperature and Humidity Effects on Phosphor Converted LED Package and the Prediction of Remaining Useful Life with State Estimation," in *IEEE Intersociety Conference on Thermal and Thermomechanical Phenomena in Electronic Systems* 2016, pp. 207-217.

[62] G. Hantos, J. Hegedüs, M. Rencz, and A. Poppe, "Aging Tendencies of Power Leds under Different Humidity Conditions During Thermal Reliability Testing," in *IEEE International Workshop on Thermal Investigations of ICs and Systems* 2015, pp. 1-4.

[63] M. Pecht, *Prognostics and health management of electronics*: Wiley Online Library, 2008.

[64] T. Sutharssan, S. Stoyanov, C. Bailey, and Y. Rosunally, "Prognostics and health monitoring of high power LED," *Micromachines,* vol. 3, pp. 78-100, 2012.

[65] "IES TM-21-11-Projecting long term lumen maintenance of LED light sources," ed: Illuminating Engineering Society of North America, 2011.

[66] B. Sun, X. Jiang, K. Yung, J. Fan, and M. Pecht, "A Review of Prognostics Techniques for High-Power White LEDs," *IEEE Transactions in Power Electronics,* vol. 32, pp. 6338-6362, 2017.

[67] C. J. Lu and W. O. Meeker, "Using Degradation Measures to Estimate a Time-to-Failure Distribution," *Technometrics,* vol. 35, pp. 161-174, 1993.

[68] J. Fan, K. Yung, and M. Pecht, "Lifetime Estimation of High-Power White LED Using Degradation-Data-Driven Method," *IEEE Transactions on Device and Materials Reliability,* vol. 12, pp. 470-477, 2012.

[69] J. Fan, K. Yung, and M. Pecht, "Comparison of Statistical Models for the Lumen Lifetime Distribution of High Power White LEDs," in *IEEE Conference on Prognostics and System Health Management* 2012, pp. 1-7.

[70] J. Huang, D. S. Golubović, S. Koh, D. Yang, X. Li, X. Fan, *et al.*, "Degradation modeling of mid-power white-light LEDs by using Wiener process," *Optics Express,* vol. 23, pp. A966-A978, 2015.

[71] T. Tsai, C. Lin, Y. Sung, P. Chou, C. Chen, and Y. Lio, "Inference from Lumen Degradation data under Wiener Diffusion Process," *IEEE Transactions on Reliability,* vol. 61, pp. 710-718, 2012.

[72] H. Hao, C. Su, and C. Li, "LED Lighting System Reliability Modeling and Inference via Random Effects Gamma process and Copula function," *International Journal of Photoenergy,* vol. 2015, p. 243648, 2015.

[73] H. Langseth and L. Portinale, "Bayesian networks in reliability," *Reliability Engineering & System Safety,* vol. 92, pp. 92-108, 2007.

[74] P. Lall, J. Wei, and P. Sakalaukus, "Bayesian Models for Life Prediction and Fault-Mode Classification in Solid State Lamps," in *IEEE International Conference onThermal, Mechanical and Multi-Physics Simulation and Experiments in Microelectronics and Microsystems,* 2015, pp. 1-13.

[75] J. Fan, K. Yung, and M. Pecht, "Prognostics of Chromaticity State for Phosphor-converted White Light Emitting Diodes using an Unscented Kalman Filter Approach," *IEEE Transactions on Device and Materials Reliability,* vol. 14, pp. 564-573, 2014.

[76] J. Fan, K. Yung, and M. Pecht, "Predicting Long-Term Lumen Maintenance life of LED Light Sources using a Particle Filter-Based Prognostic Approach," *Expert Systems with Applications,* vol. 42, pp. 2411-2420, 2015.

[77] M. S. Kan, A. C. Tan, and J. Mathew, "A review on prognostic techniques for non-stationary and non-linear rotating systems," *Mechanical Systems and Signal Processing,* vol. 62, pp. 1-20, 2015.

[78] A. Usynin, "Model-fitting approaches to reliability assessment and prognostic problems," *Journal of Pattern Recognition Research,* vol. 1, pp. 32-36, 2006.

[79] P. Rijwani and S. Jain, "Enhanced software effort estimation using multi layered feed forward artificial neural network technique," *Procedia Computer Science,* vol. 89, pp. 307-312, 2016.

[80] B. Widrow, D. E. Rumelhart, and M. A. Lehr, "Neural networks: applications in industry, business and science," *Communications of the Association for Computing Machinery,* vol. 37, pp. 93-106, 1994.

[81] T. Sutharssan, "Prognostics and health management of light emitting diodes," University of Greenwich, 2012.

[82] C. M. Tan and P. Singh, "A review on Degradation Physics of High Power LEDs in Outdoor Applications," in *IEEE International Symposium on the Physical and Failure Analysis of Integrated Circuits,* 2016, pp. 383-386.

[83] Q. Chen, X. Luo, Q. Chen, K. Wang, S. Liu, and J. Li, "Research on Lumen Depreciation Related to LED Packages by In-situ Measurement Method," *Microelectronics Reliability,* vol. 55, pp. 2269-2275, 2015.

[84] M. Buffolo, C. De Santi, M. Meneghini, D. Rigon, G. Meneghesso, and E. Zanoni, "Long-term degradation mechanisms of mid-power LEDs for lighting applications," *Microelectronics Reliability,* vol. 55, pp. 1754-1758, 2015.

[85] M. Royer, R. Tuttle, S. Rosenfeld, and N. Miller, "Color Maintenance of LEDs in Laboratory and Field Applications," ed: U.S. Department of Energy, 2013.

[86] N. Narendran, J. D. Bullough, N. Maliyagoda, and A. Bierman, "What is Useful Life for White Light LEDs?," *Journal of the Illuminating Engineering Society,* vol. 30, pp. 57-67, 2001.

[87] N. Narendran, L. Deng, R. M. Pysar, Y. Gu, and H. Yu, "Performance Characteristics of High-Power Light-Emitting Diodes," in *SPIE Optical Science and Technology*, 2004, p. 9.

[88] A. Padmasali and S. Kini, "LED life prediction based on lumen depreciation and colour shift," *Lighting Research & Technology,* vol. 49, pp. 84-99, 2017.

[89] C. Qian, J. Fan, X. Fan, and G. Zhang, "Prediction of lumen depreciation and color shift for phosphor-converted white light-emitting diodes based on a spectral power distribution analysis method," *IEEE Access,* vol. 5, pp. 24054-24061, 2017.

[90] C. Weng, "Advanced Thermal Enhancement and Management of LED Packages," *International Communications in Heat and Mass Transfer,* vol. 36, pp. 245-248, 2009.

[91] T. K. Law, F. Lim, Y. Li, X. Puan, G. K. E. Sng, and J. W. Ronnie Teo, "Effect of Packaging Architecture on the Optical and Thermal Performances of High-Power Light Emitting Diodes," *ASME Journal of Electronic Packaging,* vol. 139, pp. 0310031-0310035, 2017.

[92] C. Wang, D. Lin, C. Lee, M. Tsai, G. Chen, H. Kuo, *et al.*, "Efficiency and droop improvement in GaN-based high-voltage light-emitting diodes," *IEEE Electron Device Letters,* vol. 32, pp. 1098-1100, 2011.

[93] D. Zakheim, G. Itkinson, M. Kukushkin, L. Markov, O. Osipov, A. Pavluchenko, *et al.*, "High power blue AlGaInN LED chips with two-level metallization," *physica status solidi (c),* vol. 12, pp. 381-384, 2015.

[94] C. J. M. Lasance and A. Poppe, "Challenges in LED Thermal Characterisation," in *IEEE International Conference on Thermal, Mechanical and Multi-Physics simulation and Experiments in Microelectronics and Microsystems*, 2009, pp. 1-11.

[95] A. Poppe and C. Lasance, "Standardization of LED Thermal Characterization," in *Thermal Management for LED Applications*, ed: Springer, 2014.

[96] Y. Xi, J. Xi, T. Gessmann, J. Shah, J. Kim, E. Schubert, *et al.*, "Junction and Carrier Temperature Measurements in Deep-Ultraviolet Light-Emitting Diodes using Three Different Methods," *Applied Physics Letters,* vol. 86, pp. 031907-031907-3, 2005.

[97] "IES LM-80-08-Approved method for measuring lumen maintenance or LED light sources," ed: Illuminating Engineering Society of North America, 2008.

[98] J. Wang, C. Fang, Y. Wu, W. Chen, D. Kuo, P. Fan, *et al.*, "The Effect of Junction Temperature on the Optoelectrical Properties of InGaN/GaN Multiple Quantum Well Light-Emitting Diodes," *Journal of Luminescence,* vol. 132, pp. 429-433, 2012.

[99] S. P. DenBaars, D. Feezell, K. Kelchner, S. Pimputkar, C.-C. Pan, C.-C. Yen, *et al.*, "Development of gallium-nitride-based light-emitting diodes (LEDs) and laser diodes for energy-efficient lighting and displays," *Acta Materialia,* vol. 61, pp. 945-951, 2013.

[100] H. T. Chen, X. H. Tao, and S. Y. R. Hui, "Estimation of Optical Power and Heat-Dissipation Coefficient for the Photo-Electro-Thermal Theory for LED Systems," *IEEE Transactions on Power Electronics,*, vol. 27, pp. 2176-2183, 2012.

[101] X. Luo, R. Hu, S. Liu, and K. Wang, "Heat and Fluid flow in High-Power LED Packaging and Applications," *Progress in Energy and Combustion Science,* vol. 56, pp. 1-32, 2016.

[102] J. Iveland, L. Martinelli, J. Peretti, J. S. Speck, and C. Weisbuch, "Direct measurement of Auger electrons emitted from a semiconductor light-emitting diode under electrical

injection: identification of the dominant mechanism for efficiency droop," *Physical review letters*, vol. 110, p. 177406, 2013.

[103] M. Pecht and M. Chang, "Failure Mechanisms and Reliability Issues in LEDs," in *Solid State Lighting Reliability: Components to Systems*, ed: Springer, 2013.

[104] "JESD51-51 Implementation of the Electrical Test Method for the Measurement of Real Thermal Resistance and Impedance of Light-Emitting Diodes with Exposed Cooling," ed: Joint Electron Device Engineering Council JEDEC, 2012.

[105] M. Arik, S. Weaver, C. Becker, M. Hsing, and A. Srivastava, "Effects of Localized Heat Generations Due to the Color Conversion in Phosphor Particles and Layers of High Brightness Light Emitting Diodes," in *ASME International Electronic Packaging Technical Conference*, 2003, pp. 611-619.

[106] C. C. Lin and R. Liu, "Advances in Phosphors for Light-emitting Diodes," *Journal of Physical Chemistry Letters*, vol. 2, pp. 1268-1277, 2011.

[107] L. Chen, C. Lin, C. Yeh, and R. Liu, "Light Converting Inorganic Phosphors for White Light-Emitting Diodes," *Materials*, vol. 3, pp. 2172-2195, 2010.

[108] V. Bachmann, C. Ronda, and A. Meijerink, "Temperature Quenching of Yellow Ce3+ Luminescence in YAG: Ce," *Chemistry of Materials*, vol. 21, pp. 2077-2084, 2009.

[109] Q. Zhang, F. Jiao, Z. Chen, L. Xu, S. Wang, and S. Liu, "Effect of temperature and moisture on the luminescence properties of silicone filled with YAG phosphor," *Journal of Semiconductors*, vol. 32, p. 012002, 2011.

[110] Seoul Semiconductor Z series Datasheet [Online]. Available: http://www.seoulsemicon.com/upload2/SZ5M.pdf

[111] J. Paasschens, S. Harmsma, and R. Van der Toorn, "Dependence of Thermal Resistance on Ambient and Actual Temperature," in *Bipolar/BiCMOS Circuits and Technology*, 2004, pp. 96-99.

[112] A. Poppe, G. Molnár, and T. Temesvölgyi, "Temperature Dependent Thermal Resistance in Power LED Assemblies and a Way to Cope With It," in *IEEE Semiconductor Thermal Measurement and Management Symposium*, 2010, pp. 283-288.

[113] S. Kuo, C. Liu, M. Dai, C. Yu, H. Chien, and C. Hsu, "Characteristics of Thermal Resistance for High Power LEDs," in *IEEE Electronics Packaging Technology Conference*, 2008, pp. 149-154.

[114] M. H. Crawford, "LEDs for Solid-State Lighting: Performance Challenges and Recent Advances," *IEEE Journal of Selected Topics in Quantum Electronics*, vol. 15, pp. 1028-1040, 2009.

[115] G. Ryu and H. Ryu, "Analysis of the Temperature Dependence of Phosphor Conversion Efficiency in White Light-Emitting Diodes," *Journal of the Optical Society of Korea*, vol. 19, pp. 311-316, 2015.

[116] H. P. T. Nguyen, M. Djavid, and Z. Mi, "Nonradiative Recombination Mechanism in Phosphor-Free GaN-Based Nanowire White Light Emitting Diodes and the effect of Ammonium Sulfide Surface Passivation," *ECS Transactions*, vol. 53, pp. 93-100, 2013.

[117] S. Shionoya, W. M. Yen, and H. Yamamoto, *Phosphor handbook*: CRC press, 2006.

[118] K. H. Chan, J. S. M. Peiris, S. Y. Lam, L. L. M. Poon, K. Y. Yuen, and W. H. Seto, "The Effects of Temperature and Relative Humidity on the Viability of the SARS Coronavirus," *Advances in Virology*, vol. 2011, 2011.

[119] S. Zhou, Z. Qin, C. Bin, and S. Liu, "Evaluation of GaN-based Blue Light Emitting Diodes based on Temperature/humidity Accelerated tests," in *IEEE Electronic Packaging Technology & High Density Packaging*, 2010, pp. 930-934.

[120] R. Lenk and C. Lenk, *Practical lighting design with LEDs*: John Wiley & Sons, 2017.

[121] T. K. Law and F. Lim, "A Practical Degradation Based Method to Predict Long-Term Moisture Incursion and Color Change in High Power LEDs," *IEEE Photonics Journal*, vol. 10, pp. 1-14, 2018.

[122] P. Singh and C. M. Tan, "Degradation Physics of High Power LEDs in Outdoor Environment and the Role of Phosphor in the Degradation Process," *Nature Scientific Reports*, vol. 6, p. 24052, 2016.

[123] C. M. Tan, B. Chen, Y. Y. Foo, R. Y. Chan, G. Xu, and Y. J. Liu, "Humidity Effect on the Degradation of Packaged Ultra-bright White LEDs," in *IEEE Electronics Packaging Technology Conference*, 2008, pp. 923-928.

[124] B. M. Song and B. Han, "Analytical/Experimental Hybrid Approach Based on Spectral Power Distribution for Quantitative Degradation Analysis of Phosphor Converted LED," *IEEE Transactions on Device and Materials Reliability*, vol. 14, pp. 365-374, 2014.

[125] S. Yang and C. Lu, "Influence of Doping and Coating on the Photoluminescence Properties of Yttrium Aluminum Garnet Phosphors," *Journal of The Electrochemical Society*, vol. 154, pp. J397-J401, 2007.

[126] R. Mueller-Mach, G. O. Mueller, M. R. Krames, and T. Trottier, "High-power phosphor-converted light-emitting diodes based on III-nitrides," *IEEE Journal of Selected Topics in Quantum Electronics*, vol. 8, pp. 339-345, 2002.

[127] G. Meneghesso, M. Meneghini, and E. Zanoni, "Recent results on the degradation of white LEDs for lighting," *Journal of Physics D: Applied Physics*, vol. 43, p. 354007, 2010.

[128] M. Meneghini, L. Trevisanello, C. Sanna, G. Mura, M. Vanzi, G. Meneghesso, *et al.*, "High temperature electro-optical degradation of InGaN/GaN HBLEDs," *Microelectronics Reliability*, vol. 47, pp. 1625-1629, 2007.

[129] M. Meneghini, L.-R. Trevisanello, G. Meneghesso, and E. Zanoni, "A review on the reliability of GaN-based LEDs," *IEEE Transactions on Device and Materials Reliability,* vol. 8, pp. 323-331, 2008.

[130] A. Uddin, A. C. Wei, and T. G. Andersson, "Study of Degradation Mechanism of Blue Light Emitting Diodes," *Thin Solid Films,* vol. 483, pp. 378-381, 2005.

[131] G. Lu, S. Yang, and Y. Huang, "Analysis on Failure Modes and Mechanisms of LED," in *IEEE International Conference on Reliability, Maintainability and Safety*, 2009, pp. 1237-1241.

[132] G. Meneghesso, S. Levada, R. Pierobon, F. Rampazzo, E. Zanoni, A. Cavallini, *et al.*, "Degradation mechanisms of GaN-based LEDs after accelerated DC current aging," in *Digest. International Electron Devices Meeting*, 2002, pp. 103-106.

[133] G. Meneghesso, S. Levada, E. Zanoni, G. Salviati, N. Armani, F. Rossi, *et al.*, "Failure Mechanisms of GaN-based LEDs Related with Instabilities in Doping Profile and Deep Levels," in *IEEE International Reliability Physics Symposium*, 2004, pp. 474-478.

[134] X. Cao, P. Sandvik, S. LeBoeuf, and S. Arthur, "Defect generation in InGaN/GaN light-emitting diodes under forward and reverse electrical stresses," *Microelectronics Reliability,* vol. 43, pp. 1987-1991, 2003.

[135] K. Yung, H. Liem, H. Choy, and W. Lun, "Degradation Mechanism Beyond Device Self-Heating in High Power Light-Emitting Diodes," *Journal of Applied Physics,* vol. 109, p. 094509, 2011.

[136] M. Meneghini, A. Tazzoli, G. Mura, G. Meneghesso, and E. Zanoni, "A Review on the Physical Mechanisms That Limit the Reliability of GaN-Based LEDs," *IEEE Transactions on Electron Devices,* vol. 57, pp. 108-118, 2010.

[137] M. Meneghini, L. Trevisanello, S. Levada, G. Meneghesso, G. Tamiazzo, E. Zanoni, *et al.*, "Failure Mechanisms of Gallium Nitride LEDs Related with Passivation," in *Digest. International Electron Devices Meeting*, 2005, p. 1012.

[138] M. J. Cristea, "Capacitance-Voltage Profiling Techniques for Characterization of Semiconductor Materials and Devices," *Emerging Trends in Electrical, Electronics & Instrumentation Engineering*, vol. 1, p. 29, 2014.

[139] M. Meneghini, G. Meneghesso, and E. Zanoni, "Electrical Properties, Reliability Issues, and ESD Robustness of InGaN-Based LEDs," in *III-Nitride Based Light Emitting Diodes and Applications*, ed: Springer, 2013, pp. 197-229.

[140] Y. Xia, E. Williams, Y. Park, I. Yilmaz, J. Shah, E. Schubert, *et al.*, "Discrete steps in the capacitance-voltage characteristics of GaInN/GaN light emitting diode structures," *Materials Research Society Online Proceedings Library Archive*, vol. 831, 2004.

[141] G. Meneghesso, M. Meneghini, S. Levada, E. Zanoni, A. D. M. Cavallini, A. Castaldini, *et al.*, "Study of short-term instabilities of InGaN/GaN light-emitting diodes by means of capacitance-voltage measurements and deep-level transient spectroscopy," in *SPIE Optical Science and Technology*, 2004, p. 9.

[142] Y. Luo, "Structure Function Based Thermal Resistance & Thermal Capacitance Measurement for Electronic System," in *IEEE Components, Packaging and Manufacturing Technology Symposium*, 2010, pp. 1-5.

[143] V. Szekely and T. Van Bien, "Fine structure of heat flow path in semiconductor devices: a measurement and identification method," *Solid-State Electronics*, vol. 31, pp. 1363-1368, 1988.

[144] T. Liuxi, L. Jia, W. Kai, and L. Sheng, "Effects of Defects on the Thermal and Optical Performance of High-Brightness Light-Emitting Diodes," *IEEE Transactions on Electronics Packaging Manufacturing*, vol. 32, pp. 233-240, 2009.

[145] P. Singh and C. M. Tan, "Uncover the Degradation Science of Silicone Under the Combined Temperature and Humidity Conditions," *IEEE Access*, vol. 6, pp. 1302-1311, 2018.

[146] Z. Chen, D. Liang, G. Ma, G. Frankel, H. Allen, and R. Kelly, "Influence of UV irradiation and ozone on atmospheric corrosion of bare silver," *Corrosion Engineering, Science and Technology*, vol. 45, pp. 169-180, 2010.

[147] R. Perkins, B. Tilak, B. Conway, and H. Kozlowska, "Impedance and formation characteristics of electrolytically generated silver oxides—II. photo-effects," *Electrochimica Acta*, vol. 17, pp. 1471-1489, 1972.

[148] M. Zheludkevich, A. Gusakov, A. Voropaev, A. Vecher, E. Kozyrski, and S. Raspopov, "Oxidation of silver by atomic oxygen," *Oxidation of metals*, vol. 61, pp. 39-48, 2004.

[149] J. P. Allen, D. O. Scanlon, and G. W. Watson, "Electronic structures of silver oxides," *Physical Review B*, vol. 84, p. 115141, 2011.

[150] Q. Zhang, F. Jiao, Z. Chen, L. Xu, S. Wang, and S. Liu, "Effect of temperature and moisture on the luminescence properties of silicone filled with YAG phosphor," *Journal of Semiconductors*, vol. 32, 2011.

[151] X. Luo, J. Fan, M. Zhang, C. Qian, X. Fan, and G. Zhang, "Degradation mechanism analysis for phosphor/silicone composites aged under high temperature and high humidity condition," in *IEEE International Conference on Electronic Packaging Technology* 2017, pp. 1331-1336.

[152] I. Cho, G. Anoop, D. Suh, S. Lee, and J. Yoo, "On the stability and reliability of Sr 1-x Ba x Si 2 O 2 N 2: Eu 2+ phosphors for white LED applications," *Optical Materials Express*, vol. 2, pp. 1292-1305, 2012.

[153] G. J. McLachlan, "Mahalanobis distance," *Resonance*, vol. 4, pp. 20-26, 1999.

[154] S. Ishizaki, H. Kimura, and M. Sugimoto, "Lifetime Estimation of High Power White LEDs," *Journal of Light & Visual Environment,* vol. 31, pp. 11-18, 2007.

[155] Ö. Hallberg and D. S. Peck, "Recent humidity accelerations, a base for testing standards," *Quality and Reliability Engineering International,* vol. 7, pp. 169-180, 1991.

[156] B. Song and B. Han, "Spectral Power Distribution Deconvolution Scheme for Phosphor-Converted White Light-Emitting Diode using Multiple Gaussian Functions," *Applied Optics,* vol. 52, pp. 1016-1024, 2013.

[157] P. Sedgwick, "Pearson's Correlation Coefficient," *British Medical Journal,* vol. 345, p. e4483, 2012.

[158] British Medical Journal. *Correlation and Regression*. Available: https://www.bmj.com/about-bmj/resources-readers/publications/statistics-square-one/11-correlation-and-regression

[159] "CIE 2^0 Spectral Luminous Efficiency Function for Photopic Vision," vol. CIE 086-1990, ed: International Commision on Illumination, 1988.

[160] M. Dorofki, A. H. Elshafie, O. Jaafar, O. A. Karim, and S. Mastura, "Comparison of Artificial Neural Network Transfer Functions Abilities To Simulate Extreme Runoff Data," in *International Conference on Environment, Energy and Biotechnology* 2012, pp. 39-44.

[161] G. Rutka, "Neural network models for Internet traffic prediction," *Elektronika ir Elektrotechnika,* vol. 68, pp. 55-58, 2006.

[162] Semantic Scholar. *The Levenberg-Marquardt Algorithm*. Available: https://www.semanticscholar.org/paper/The-Levenberg-Marquardt-Algorithm-Ranganathan/1e0078d36080d288dc240877fdb33f54ef5028c6?citationIntent=methodology#citing-papers

[163] N. M. Vichare and M. G. Pecht, "Prognostics and Health Management of Electronics," *IEEE Transactions on Components and Packaging Technologies,* vol. 29, pp. 222-229, 2006.

[164] S. Xiang, F. Nie, and C. Zhang, "Learning a Mahalanobis distance metric for data clustering and classification," *Pattern Recognition,* vol. 41, pp. 3600-3612, 2008.

[165] E. Acuña and C. Rodriguez, "On Detection of Outliers and their Effect in Supervised Classification," University of Puerto Rico at Mayaguez, 2004.